Investigation into microstructural and mechanical properties of a Ti-6Al-4V hybrid manufactured component

K Beyl

orcid.org/ 0000-0002-2859-5873

Dissertation accepted in fulfilment of the requirements for the degree *Master of Engineering in Mechanical Engineering* at the North West University

Supervisor:	Mr CP Kloppers
Co-Supervisor:	Dr K Mutombo

Graduation:	May 2020
Student number:	25744097

ABSTRACT

Keywords: *Investment Cast, Additive Manufacture, Hybrid Manufacture, Tensile Properties, Hardness, Heat-Treatment, Fractography, Ti-6Al-4V alloy, microstructures*

Hybrid manufacturing, as a combination of investment cast and additive manufacturing, is investigated in this study. Hybrid manufacturing acts as a potential manufacturing process for Ti6Al4V components.

The project investigates the effect of different surface preparations, cooling mediums and high-temperature applications, on the diffusion zone of a hybrid manufactured component. The microstructures and mechanical properties obtained from the various testing conditions are compared to wrought, investment cast and additive manufactured properties. The microstructures and tensile fractures were characterized using light optical microscopy, stereo microscopy, microhardness and Scanning Electron Microscopy (SEM) to investigate the microstructural morphology and the structural hardness variation.

Six different surface preparations were applied to Ti6Al4V investment cast rods prior to additive manufacturing. Smooth surfaces led to better diffusion as opposed to a rougher surface. Plain just-cut surface preparation was concluded as the most suitable surface preparation technique. Hybrid manufacturing revealed three different regions; investment cast region, diffusion zone region and the additive manufactured region. The microstructures of the investment cast and additive manufactured region compared well with the microstructures of investment cast and additive manufacturing specimens, respectively. The diffusion zone resulted in acicular α' martensitic morphology. The fractures of hybrid manufactured specimens with sufficient bonding fractured in the investment cast region and showed similar tensile properties to the investment cast specimens. Additive manufactured specimens proved to have higher yield strength, ultimate tensile strength, hardness and strain hardening exponent, compared to the investment cast, wrought and hybrid manufactured specimens.

A temperature of 1050 °C was used for 2 hours to solution-treat hybrid manufactured specimens, followed by different cooling mediums; air cooling, water quenching and furnace cooling. It was found that the hardness of the water quenched specimen indicated a more homogeneous structure across the different regions of the hybrid manufactured specimen while also producing a higher hardness compared to the non-heat treated hybrid manufactured specimen.

The investigation of high-temperature applications was done by furnace tensile testing hybrid manufactured specimens at 400 °C, 600 °C and 800 °C. The investigation concluded that the

yield strength, ultimate tensile strength and strain hardening exponent decrease with an increase in the furnace tensile test temperature. The ductility was found to increase with temperature.

ACKNOWLEDGEMENTS

I wish to especially thank my CSIR supervisor, Dr Kalenda Mutombo, for his guidance, support and training during the course of this study. I would also like to thank Dr Sagren Govender for his time and guidance in formulating this study. Thank you to my supervisor at the North-West University, CP Kloppers for his continued support throughout this study.

I would like to thank the CSIR for funding this project, and the light metals team for all their support. Thank you to the National Laser Centre (NLC) and Nana Arthur for their time and advice on additive manufacturing, Pierre Rossouw for providing material and his expertise in investment casting, Marius Grobler for machining and Chris McDuling for his expertise and mentoring in the mechanical testing laboratory.

To my family, friends and colleagues, without you, it could not have been possible. Thank you all.

"Yours, O Lord, is the greatness, the power, the glory, the victory, and the majesty. Everything in the heavens and on earth is yours, O Lord, and this is your kingdom. We adore you as the one who is over all things." - 1 Chronicles 29:11

TABLE OF CONTENTS

ABSTRACT ..... **I**

ACKNOWLEDGEMENTS ..... **III**

CHAPTER 1. INTRODUCTION **1**

1.1 Background information **1**

1.2 Problem statement **2**

1.3 Aim and objectives **2**

CHAPTER 2. LITERATURE REVIEW **4**

2.1 Ti6Al4V Alloy **4**

2.2 Heat-treatments **4**

2.3 Investment Cast **6**

2.4 Additive manufacturing **8**

2.5 Hybrid manufacturing **10**

2.6 Hardness and tensile properties **12**

2.7 Fractography **13**

CHAPTER 3. METHODOLOGY **16**

3.1 Research design **16**

3.2 Materials Ti6Al4V alloy **18**

3.3 Manufacturing and machining of specimens **19**

3.3.1 Wrought specimens 19

3.3.2 Investment cast 19

3.3.3 Additive manufacturing 20

3.4 Hybrid manufacturing 22

3.5 Surface preparation techniques 23

3.6 Heat-treatments 24

3.7 Tensile testing 25

3.8 Metallographic analysis 27

3.9 Fractography 27

CHAPTER 4. RESULTS 29

4.1 Microstructural characterization 29

4.1.1 Wrought 30

4.1.2 Investment cast 30

4.1.3 Additive manufacturing 31

4.1.4 Hybrid manufacturing 32

4.1.5 Surface preparations 36

4.1.6 Heat-treatments of Ti6Al4V 40

4.1.7 Furnace tensile tested 45

4.2 Room temperature tensile properties 49

4.2.1 Wrought, Investment cast and Additive manufacturing 49

4.2.2 Hybrid manufacture 51

4.2.3 High-temperature tensile properties 53

4.3 Fractography 55

4.3.1 Wrought, Investment cast, Additive manufacture 55

4.3.2 Hybrid manufacture 57

4.3.3 Furnace tensile tested 62

CHAPTER 5. DISCUSSION 65

5.1 Microstructural evolution 65

5.2 Tensile properties 67

5.3 Fractography 68

CHAPTER 6. CONCLUSIONS 70

6.1 Conclusion 70

CHAPTER 7. FUTURE RESEARCH 72

BIBLIOGRAPHY 73

LIST OF TABLES

Table 1. Additive manufacturing processes for Titanium alloys [32] 9

Table 2. Tensile properties and microstructural characterization of additive manufactured, investment cast and wrought Ti6Al4V alloy 17

Table 3. Influence of prior surface preparations on microstructural defects of hybrid manufactured Ti6Al4V components 17

Table 4. Effect of cooling medium on the microstructure and hardness of Ti6Al4V hybrid manufactured components 18

Table 5. Investigation of the tensile and microstructural behaviour of Ti6Al4V hybrid manufactured components at elevated temperatures 18

Table 6. Chemical composition of the as-received wrought Ti6Al4V bar (wt. %) 19

Table 7. Chemical composition of Ti6Al4V investment casting (wt. %) 20

Table 8. SEM/ EDS analysis of some single particles of atomized Ti4Al4V powder 21

Table 9. Process summary of each specimen. 25

Table 10. Subgroup variables for tensile testing 26

Table 11. EDS analysis of a Ti6Al4V sample 29

Table 12. Grain size, lath thickness and percentage α-and-β for different manufacturing processes of Ti6Al4V 32

Table 13. Grain size, lath size and volume fraction of α and β-phase in IC, DZ and FC regions for the solution-treated HM and AC, WQ and FC Ti6Al4V specimens 45

Table 14. Grain size, lath size and volume fraction of α and β-phase for HM Ti6Al4V tensile tested at 400, 600 and 800°C 49

Table 15. Ti6Al4V strain hardening exponents and strength coefficients for various manufacturing processes 50

Table 16. Hybrid manufactured Ti6Al4V strain hardening exponents and strength coefficients for various surface preparations 52

Table 17. Hybrid manufactured Ti6Al4V strain hardening exponents and strength coefficients for various furnace tensile testing temperatures 54

Table 18. EDS analysis of different fracture modes in the ablation 2 surface preparation HM Ti6Al4V tensile specimen 62

LIST OF FIGURES

Figure 1. Ternary phase diagram for Ti6Al4V [13] 5

Figure 2. Continuous cooling transformation diagram for Ti6Al4V 6

Figure 3. Ti6Al4V microstructural formation after cooling[4] 6

Figure 4. (a)Single-stage air compressor rotor. (b) Single-stage air compressor rotor indicating the different sections to be investment cast and additive manufactured (red = IC, grey = AM) 12

Figure 5. Different types of fractures. (a) Extreme necking with a highly ductile fracture. (b) Somewhat necking and moderate ductility. (c) No necking with brittle fracture. [43] 14

Figure 6. (a) Fine equiaxed dimples. (b) transcrystalline cleavage. (c) Fatigue fracture. (d) intergranular fracture.[24] 14

Figure 7. Ductile fracture: (a) necking. (b) microvoid formation. (c) coalescence of microvoids (d) crack propagation. (e) final fracture at max shear [43] 15

Figure 8. Research design subgroups 16

Figure 9. (a) Wrought bar shipment container from Baoti. (b) the as-received wrought bar. 19

Figure 10. (a) Wax tree pattern for rods. (b) Ceramic mould after burnout. (c) Ti6Al4V mould after shell removal. (d) Ti6Al4V investment cast rods. (e) Investment cast tensile specimens 20

Figure 11. (a) Spherical Ti6Al4V atomized powder, and (b) electron microscopy/ EDS analysis on some single particles. 21

Figure 12. (a) Optomec LENS™ 850-R system [48], and (b) additive manufactured tensile specimens. 22

Figure 13. (a) Quarter investment cast rods. (b) Aluminium frame for holding IC parts (c) hybrid manufactured rod Ti6Al4V 23

Figure 14. Surface preparations (a) polished (b) chemical mill (c) sandblast (d) just-cut..... 24

Figure 15. (a) Hybrid manufactured ti6Al4V specimen and (b) wired-cut hybrid manufactured sample..... 24

Figure 16. Experimental cooling rates on hybrid manufactured specimens..... 25

Figure 17. a) Schematic of ASTM EM04 standard tensile specimen and (b) machined wrought tensile specimens..... 26

Figure 18. (a) Tensile specimen prepared for analysis, (b) a mounted cross-section of a tensile specimen in a SEM sample holder, and (c) fractured tensile surface setup to analyse the fracture surface using SEM. 28

Figure 19. Electron microscopy EDS analysis on different phases of a Ti6Al4V sample..... 29

Figure 20. (a) Stereo microscope image, and (b) optical microscope image of wrought Ti6Al4V alloy..... 30

Figure 21. (a) Stereo microscope image, and (b) optical microscope image of investment cast Ti6Al4V alloy 31

Figure 22. (a) Stereo microscope image, and (b) optical microscope image of additive manufactured Ti6Al4V alloy 31

Figure 23. Stereo micrograph of a hybrid manufactured Ti6Al4V alloy 32

Figure 24. (a) Stereo microscope image, and (b) optical microscope image of the diffusion zone of a hybrid manufactured Ti6Al4V alloy 33

Figure 25. SEM micrographs of the different zones of a hybrid manufactured Ti6Al4V alloy specimen. (a) Investment cast zone. (b) Diffusion zone. (c) Additive manufactured zone 33

Figure 26. EDS line scanning analysis of the diffusion zone of the Ti6Al4V hybrid manufactured specimen..... 34

Figure 27. Average Vickers micro-hardness with standard deviation error bars of specimens manufactured with additive manufacturing, investment cast, wrought and hybrid manufacturing 35

Figure 28. Hardness profiles of wrought, investment cast, additive manufactured and hybrid manufactured Ti6Al4V specimens. 36

Figure 29. Hybrid manufactured Ti6Al4V using different surface preparation techniques; (a) ablation, (b) as-cast, (c) chemical milling, (d) just-cut, (e) polishing, (f) sandblasting. 36

Figure 30. Optical micrographs of the diffusion zone of hybrid manufactured Ti6Al4V with different surface preparation techniques; (a) ablation, (b) as-cast, (c) chemical milling, (d) just-cut, (e) polishing, (f) sandblasting 37

Figure 31. Diffusion zone thickness measurements of hybrid manufactured Ti6Al4V alloy specimens with different surface preparations 38

Figure 32. Defects, in the diffusion zone of HM specimens, resulting from (a) as-cast surface, (b) ablation, (c) sandblasting and (d) chemical milling techniques 39

Figure 33. Vickers microhardness profile of HM Ti6Al4V showing the effect of ablation, chemical milling, sandblasting techniques, as cast and just-cut free surface 40

Figure 34. Diffusion zones of hybrid manufactured Ti6A4V specimens in (a) non-heat treated, (b) air-cooled, (c) water quenched, and (d) furnace cooled after solution treatment 41

Figure 35. IC, DZ and AM regions of the hybrid manufactured Ti6Al4V after solution-treatment and (a)-(c) air-cooled, (d)-(f) water quench, and (g)-(i) furnace cooled. 42

Figure 36. Average Vickers microhardness with standard deviation error bars of the non-heat treated, solution-treated and air-cooled (AC), water quenched (QW) and furnace cooled (FC) hybrid manufactured Ti6Al4V 43

Figure 37. Hardness profiles of Ti6Al4V hybrid manufactured in IC, DZ and AM regions after solution-treated and air-cooled, water quenched and furnace cooled. 44

Figure 38. Vickers microhardness indents in the diffusion zone of hybrid manufactured specimens (a) Reference, (b) solution-treated and water quenched, (c) solution-treated and air-cooled, (d) solution-treated and furnace cooled 44

Figure 39. Tensile specimens of HM Ti6Al4V tested at (a) room temperature, (b) 400°C, (c) 600°C, and (d) 800°C 45

Figure 40. IC, DZ and AM regions of hybrid manufactured Ti6Al4V specimens tensile tested at (a)-(c) 400°C, (d)-(f) 600°C, and (g)-(i) 800°C. 47

Figure 41. Average Vickers micro-hardness of fractured specimens tensile tested at different elevated temperatures with standard deviation error bars 48

Figure 42. Hardness profiles of fractured Ti6Al4V alloy specimens tensile tested at different elevated temperatures 48

Figure 43. Engineering stress-strain curve for tensile tested Ti6Al4V alloy specimens manufactured with different processes 50

Figure 44. Hardening curves for tensile tested Ti6Al4V alloy specimens manufactured with different processes 51

Figure 45. Engineering stress-strain curve for tensile tested hybrid manufactured Ti6Al4V alloy specimens with different surface preparations 52

Figure 46. Hardening curves for tensile tested hybrid manufactured Ti6Al4V alloy specimens with different surface preparations 53

Figure 47. Engineering stress-strain curve for hybrid manufactured Ti6Al4V alloy specimens furnace tensile tested at different elevated temperatures 54

Figure 48. Hardening curves for hybrid manufactured Ti6Al4V alloy specimens furnace tensile tested at different elevated temperatures 55

Figure 49. Stereo micrographs of cross-sectioned tensile tested specimens manufactured by (a) wrought, (b) IC, and (c) AM processes 55

Figure 50. SEM micrographs showing cross-sectioned fracture regions of tensile tested specimens (a) wrought, (b) IC, and (c) AM tensile test specimens 56

Figure 51. The fracture surfaces of (a) wrought, (b) IC, and (c) AM Ti6Al4V 56

Figure 52. Fracture surfaces of a)-c) Wrought, d)-f) IC and g)-i) AM Ti6Al4V tensile specimens 57

Figure 53. Stereo micrographs of cross-sectioned tensile tested specimens with surface preparations (a)-(c) Ablation, and (d)-(f) just-cut 58

Figure 54. Stereo micrographs of cross-sectioned fracture regions of tensile tested specimens with surface preparations (a)-(c) Ablation, and (d)-(f) just-cut 59

Figure 55. Stereo micrographs showing the fractured surfaces of hybrid manufactured and tensile tested specimens, the specimens were prepared with (a)-(c) Ablation, and (d)-(f) Just-cut, prior to additive manufacturing 60

Figure 56. Fracture surfaces of Ti6Al4V hybrid manufactured specimens with (a)-(c) Ablation, and (d)-(f) just-cut surface preparations prior to additive manufacturing 60

Figure 57. Two fracture modes found in a single specimen prepared with Ablation 61

Figure 58. EDS analysis of different fracture modes in the same specimen..... 62

Figure 59. Stereo micrographs of furnace tensile tested specimens at (a) 400°C, (b) 600°C, and (c) 800°C. Cross-sectioned furnace tensile tested specimens at (d) 400°C, (e) 600°C, and (f) 800°C. 63

Figure 60. Optical micrographs of cross-sectioned fracture regions of furnace tensile tested specimens at (a) 400°C, (b) 600°C, and (c) 800°C. 63

Figure 61. Stereo micrographs showing the fractured surfaces of hybrid manufactured and tensile tested specimens, the specimens were prepared with (a)-(c) Ablation, and (d)-(f) Just-cut, prior to additive manufacturing 64

Figure 62. Fracture surfaces of Ti6Al4V hybrid manufactured specimens with (a)-(c) Ablation, and (d)-(f) just-cut surface preparations prior to additive manufacturing 64

Figure 63. Single track of additive manufacturing onto an investment casted rod 72

LIST OF ABBREVIATIONS

%EL	Percentage Elongation
AC	Air Cool
AM	Additive Manufacture
ASTM	American Society for Testing and Materials
CAD	Computer Aided Design
CIRP	International Academy for Production Engineering
DED	Directed Energy Deposition
EBD	Electron Bed Deposition
EDS	Electron Diffraction Spectrometry
EIGA	Electrode Inert Gas Atomisation
FC	Furnace Cool
HIP	Hot Isostatic Pressing
HM	Hybrid Manufacture
LENS	Laser Engineered Net Shaping
OM	Optical Microscope
PBF	Powder Bed Fusion
P/M	Powder Metallurgy
SEM	Scanning Electron Microscope
UTS	Ultimate Tensile Strength
WQ	Water Quench
YS	Yield Strength

CHAPTER 1. INTRODUCTION

The introduction chapter will explain precisely what the study holds and the reasoning behind it. Background on the topic is provided to give an insight on current developing in the field. The background information leads to the problem statement, aims and objectives which is then followed by a brief overview of the proceeding chapters.

1.1 Background information

The continuous growth in the development industry is generating a need for hybrid manufacturing (HM); a combination of manufacturing processes which combines the advantages of each process [1].

The CSIR's investment cast facilities are well developed, while the additive manufacturing cluster made some significant advances in recent decades. With both manufacturing processes having individual setbacks, the logical next step in improving manufacturing is to combine the processes to try and eliminate the disadvantages. Consequently, the hybrid manufacturing that will be investigated will integrate investment casting with additive manufacturing.

Titanium alloys have found many uses in aerospace, medical, chemical plants and sporting equipment, this is because of its high strength to weight ratio and corrosion-resistant properties. The Ti6Al4V alloy is commonly used in these industries for complex components, currently often manufactured with investment casting (IC) [2]. The IC process can be controlled, thus we can intentionally alter the component's mechanical properties to a certain extent [3]. Due to the lower oxygen level in the grade 23 Ti6Al4V alloy, it is used in the additive manufacturing (AM) industries as well [4]. Laser Engineered Net Shaping (LENS), an AM method has become a strong competitor in the production of metal components due to its ability to create near-net-shape products in less time. The process is cost-effective, has excellent material utilisation and gives an appealing fine microstructure [5], [6]. Each manufacturing method has its own advantages and shortcomings.

The Ti6Al4V alloy's microstructure is particularly sensitive to the manufacturing process and thermal history [5]. Thus, it is vital to study the effect of hybrid manufacturing on the microstructure of the alloy to understand and predict the mechanical properties of a hybrid manufactured component.

1.2 Problem statement

Hybrid manufacturing is a new process which is not well understood especially in terms of manufacturing process parameters and generated mechanical properties. The major concern of hybrid manufacturing is the presence of a diffusion zone between the investment casting and additive manufactured region and an inhomogeneous microstructure which consequently have a negative impact on mechanical properties.

Previous research done on hybrid manufacturing includes a study examining the microstructures, hardness and tensile properties of TC11 titanium alloys. The study combined additive manufacturing with typical β forged TC11. The forged TC11 was sandblasted prior to additive manufacturing. The study revealed that three different regions exist; laser additive manufactured region, heat-affected zone and a wrought region. The laser additive manufactured, and heat-affected zone formed a basketweave structure, the wrought had a lamellar microstructure while the transition region formed coarse fork-like primary α and fine β. The study concluded that good mechanical properties were achieved, with a tensile strength of 1033 MPa, elongation of 6.8%. The tensile specimen fractured in the wrought region, indicating that the bonding region was stronger than the substrate [7]. No other research on hybrid manufacturing has been done to date.

1.3 Aim and objectives

The aim of the study is to evaluate the effect of the surface preparation technique on the microstructure and tensile properties of a hybrid manufactured Ti6Al4V component.

Thus, the study has the following major objectives:

- To establish a surface preparation technique to ensure good diffusion during HM, consequently, the study looks at the diffusion zone between manufacturing processes,
- To design a correct heat-treatment process to produce a hybrid manufacture Ti6Al4V component with homogenous structure i.e. free of diffusion zone between investment cast and additive manufactured region.
- To evaluate the tensile properties of the hybrid manufactured Ti6Al4V component at room and elevated temperatures in order to understand the behaviour of these components in normal and aggressive environments.
- To establish the tensile properties and microstructural characterization of additive manufactured, investment cast and wrought Ti6Al4V alloys
- To study the influence of prior surface preparations on microstructural defects of hybrid manufactured Ti6Al4V components

To accurately attend to all objectives, a literature study follows, which covers the main topics concerning the objectives. The literature chapter provides more insight into the various facets of the project. The literature chapter is followed by the methods chapter which explains how the literature was used to produce results. The methods chapter aims at explaining the procedures followed, in such a manner as to repeat the study and acquire the same results. The results obtained by using the methods are presented and described in the 4th chapter. The results are followed by a discussion chapter where the results are analysed and discussed. Conclusions made from the discussion of the results are then presented in the conclusion chapter, followed by a section on recommendations for future research.

CHAPTER 2. LITERATURE REVIEW

In this chapter, the literature on aspects associated with the problem statement are discussed. Essential information on the material used and its current manufacturing processes are discussed, leading into literature on hybrid manufacturing along with its main variables and operating conditions.

2.1 Ti6Al4V Alloy

The Ti6Al4V alloy, consists of the primary alloying elements; 6% Aluminium and 4% Vanadium, with traces of oxygen and nitrogen. The alloy is made up of primary and secondary α-phase (HPC), and a small amount widely spread β-phase (bcc) [5]. Because it is an (α + β) alloy, it allows evolution of microstructures through heat-treatments in order to improve the mechanical properties through heat treatments [8]. Different heat treatments can give different combinations of microstructures and mechanical properties. By knowing the outcome of different heat treatments, a treatment cycle can be designed to optimise the mechanical properties.

Titanium exists in multiple crystallographic forms, these forms are defined by transition temperatures, the temperature at which the crystallographic form changes is called the crystallographic transformation temperature (or β-transus temperature), it is also the lowest equilibrium temperature for 100% β-phase [9]. Thus, if the temperature would rise above the β-transus the structure of the alloy would change and the phase would become bcc. The Ti6Al4V β-transus temperatures is in the range of 950.2°C to 996°C for wrought [8], investment casting [10] and additive manufacturing [11].

The microstructural evolution of the titanium alloy has a great influence on the mechanical properties. The microstructure is usually described by the size and morphology of α and β phases. The morphologies most often found in titanium alloys are lamellar microstructures developed by cooling from the β phase, and equiaxed microstructure formed during the recrystallisation process [4]. The microstructural evolution occurs during the manufacturing process's thermal changes.

Developing properties of Ti6Al4V depends on the refinement of grains when cooled from the β-phase or the α-β phase, and the decomposition of martensite by low-temperature ageing formed by quenching. In the α-phase, the grain refinement and shape limit the microstructure changes.

2.2 Heat-treatments

The Ti6Al4V alloy's performance is greatly dependent on the proportion, morphology, size and shape of α and β phases. The microstructures and mechanical properties of two-phase titanium alloy can be enhanced with the correct heat treatment process [12]. The heat-treatment process

can produce the desired combination of strength ductility and machinability while reducing residual stresses.

The diagram given in Figure 1 is a ternary phase diagram for the Ti6Al4V alloy, which indicates that the β-transus temperature is around 1000°C. A solution treatment temperature often used is 1050°C to ensure a stable β phase is achieved before cooling [4], [13].

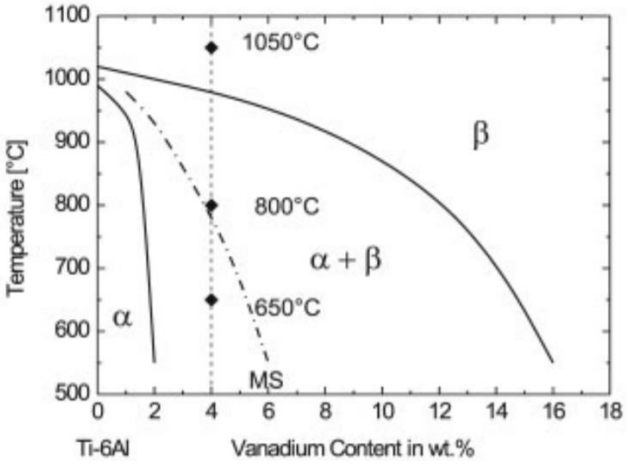

Figure 1. Ternary phase diagram for Ti6Al4V [13]

Solution treatment above the β-transus temperature strengthens the material at the expense of ductility and toughness [14]. On the contrary, numerous studies have indicated that the cooling rate after solution treatment above the β-transus can influence the properties and thus provide a sought after balance of mechanical properties [15], [16], [17]. Previous research found that the cooling rate has more of an impact on the microstructures as compared to the solution treatment temperature [18], [19]. If strength is sought after, the cooling rate is the main variable [20]. The three main routes for different cooling rates are; air cooling, water quenching and furnace cooling.

The continuous cooling transformation (CCT) diagram (Figure 2) indicates that the cooling rate from a solution treatment above the β-transus can control the formation of various microstructures. Cooling curves for air cooling, water quenching and furnace cooling are roughly drawn on the graph to indicate the different temperature drops.

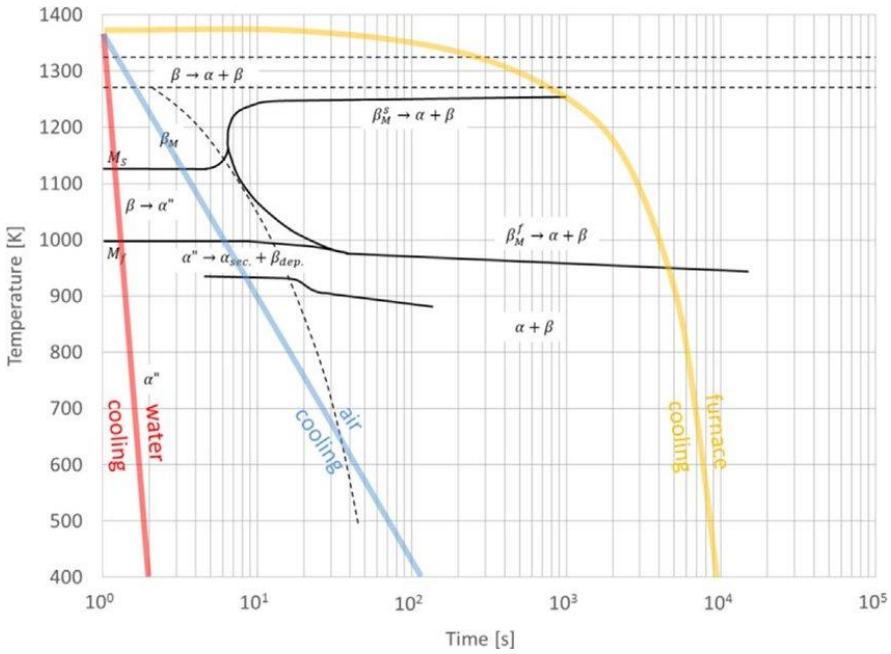

Figure 2. Continuous cooling transformation diagram for Ti6Al4V

Depending on the cooling rate the microstructure can either be fine lamellar, coarse lamellar or a martensitic transformation of the β phase seen as fine needle-like microstructures. An example of the microstructures can be seen in Figure 3. Literature found that reducing the cooling rate will result in larger grains [12], [18].and an increase in the amount of primary α phase [20]. Previous studies also concluded that a decrease in cooling rate will result in lower hardness and tensile strength but higher ductility [18], [19], [20].

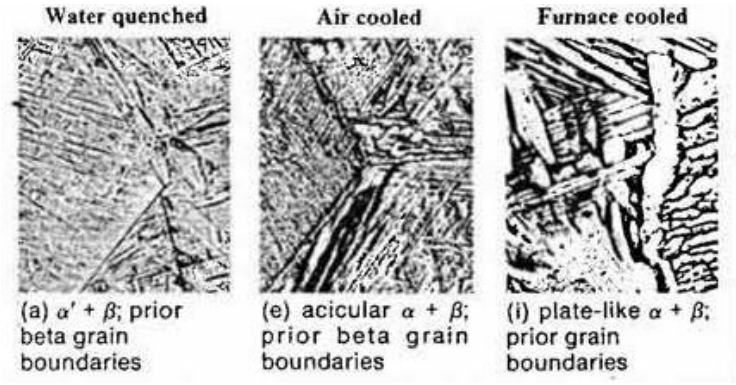

Figure 3. Ti6Al4V microstructural formation after cooling[4]

2.3 Investment Cast

The investment casting process is a metal shaping process offering great material utilisation, with lower production costs compared to machining or forging. The process starts with the desired

component formed with wax, which is then coated with a ceramic slurry to create a shell, the wax is then burned out leaving a cavity for the molten titanium metal to be poured in. After solidification the shell is broken off, revealing the as-cast titanium component.

Casting is a delicate process; any variable can influence the quality of the casting. To design a part for casting the design constrains should be studied along with common defects that occur during casting. The advantages of investment casting include; smooth surface finishes, high dimensional accuracy, complex parts, no parting lines and most importantly the metallurgical properties can be controlled allowing single crystal structure to be formed. Common defects that arise in investment casting of titanium are defects like gas porosities, shrinkage, cold shuts and misruns these defects can be limited or even eliminated by designing the casting accordingly.

Titanium castings are widely used in industries that require high precision, high strength complex parts. Industries such as aerospace and medical are industries that benefit from titanium casting, it also include marine, chemical plants and oil fields [4], [13], [21]–[27]. Titanium castings are also used as heat barriers, due to its low conductivity. Casting is the most fully developed net-shape manufacturing process. The casting technique used in this study is investment casting also known as lost-wax casting which is an expendable-mould, expendable-pattern casting process [28].

When designing for casting, the following are important [28]:

- Avoid sharp corners/angles or fillets
- Design uniform cross-sections and wall thickness throughout the part
- Use small cores
- Avoid large flat areas
- Use ribs or support structures where large material was removed
- Design for shrinkage
- Add a draft
- Dimensional tolerance should be accounted for
- Design for machine finishes, features include a flat surface for drilling holes, small dimple for a drill starting point and added features so that it can be clamped if necessary

The downside of investment casting is the initial cost. Expensive machinery is required and creating wax patterns are time-consuming and labour intensive. Designing new wax models should be minimised, thus IC is not a suitable manufacturing process for a production line of unique products.

Investment cast components are typically HIP'ed (Hot Isostatic Pressing) afterwards. HIP uses heated gas and high pressure to create a forming and densification process. Unlike mechanical

pressing where pressure is applied from one or two sides, isostatic pressure is applied uniformly on all sides of the object eliminating porosity while maintaining its net shape [29].

The microstructures of Ti6Al4V during investment casting is formed when the molten metal solidifies within the ceramic mould. The main structure of an as-cast component consists mainly of an α-plate colony, with a small amount of β which can be seen at the grain boundaries [30].
The solidification temperature for pure titanium is 1668°C, the solidification starts by forming β-titanium (bcc structure). When the titanium cools from 882°C an allotropic transformation happens, the β-phase transforms to (α+β) -phase by forming hcp structures (α-titanium) along the β grain boundaries. Future slow cooling results in colonies of α-platelets [3].

2.4 Additive manufacturing

Additive manufacturing (AM) or sometimes referred to as 3D printing is the process of taking a 3D CAD model and slicing it layer by layer creating a trail to follow one layer at a time. AM uses Powder Metallurgy (P/M), which is considered as a cost-effective process to produce complex near-net-shape titanium products. Electrode Inert Gas Atomisation (EIGA) is used to create metallic powder from a solid, EIGA is done by induction melting of a rotating electrode and atomised by inert gas [31]. According to ASTM standards metal AM can be divided into Powder Bed Fusion (PBF) and Directed Energy Deposition (DED) [32], while each of these categories are made up of several technologies as referred to by different manufacturing companies as seen in Table 1.

Table 1. Additive manufacturing processes for Titanium alloys [32]

Additive Manufacturing Technologies		
Technologies to process titanium and its alloys		
Category	**Processing technology**	**Method**
Directed Energy Deposition (DED)	Direct Metal Deposition (DMD)	This method uses a laser with metal powder for depositing and melting using a closed-loop process
	Laser Engineered Net Shaping (LENS)	This method uses a laser with metal powder for depositing and melting
	Direct Manufacturing (DM)	This method uses a metal wire and an electron beam for depositing and melting
	Shaped Metal Deposition or Wire and Arc Additive Manufacturing (WAAM)	This method uses a metal wire and electric arc for depositing and melting
Powder Bed Fusion (PBF)	Selective Laser Sintering (SLS), also referred to as Laser Melting (LM), Direct Metal Laser Sintering (DMLS), or LaserCUSING	This method uses metal powder and laser for bonding and sintering
	Electron Beam Melting (EBM)	This method uses metal powder and an electron beam for bonding and melting

This study will focus on Laser Engineered Net Shaping (LENS) as the AM process to be used. LENS is a Directed Energy Deposition (DED) process. The DED process is done in a concealed chamber, where an inert gas is fed into the chamber to decrease the oxygen level. The DED process is initiated by placing a small existing metal piece into the chamber as a starting point for the laser to focus on. The laser creates an area of melted metal, the part can now be created by feeding metal into the melted area under the laser. The metal can be a powder, fed through a coaxial nozzle (for laser) or it can be a thin metal wire (for electron beam). The nozzle follows the trail set out by the layering of the CAD model, as the nozzle moves, the area of melted metal behind it solidifies.

To design a part for AM the design constraints should be studied along with common defects that occur during printing. The advantages of AM include; near-net-shape manufacturing, custom designs on-demand, high dimensional accuracy, can be used for extremely complex components. Common defects that arise in AM of titanium alloys are defects like rough surface finish, porosities, unmelted powder particles, poor joining between layers, residual stresses, cracking and warpage.

When designing for AM, the following are important:

- Create a strong base, or use an appropriate substrate
- Grain direction
- Overhangs or holes need support material
- Wall thickness
- Tolerances
- Time-consuming for large areas

If the design considerations are followed AM can produce components with a complex internal structure thus, creating a shell and core structure. Less material can be used in areas with less stress, resulting in strong lightweight components. However, AM is extremely time-consuming, and will not be a viable option for creating large products.

The Laser Engineered Net Shaping (LENS) process produces a change in microstructure from the initial equiaxed (α + β) microstructure to a mixed acicular α in β matrix, this is because of the high cooling rate. A study conducted by A. Bagheri, N. Shamsaei and S.M Thompson on the microstructures of Ti6Al4V fabricated by LENS revealed that the microstructures are predominantly columnar. Containing large prior-β columnar grains and showed that the prior-β grain boundaries were parallel to the build direction and continuous across the different boundaries [5]. This agreed with the conference paper; Microstructure Evolution, Tensile Properties, and Fatigue Damage Mechanisms in Ti-6Al-4V Alloys Fabricated by Two Additive Manufacturing Techniques literature, where dominant columnar β grains were found due to the substrate's heat extraction [33]. Furthermore, between the layers, the microstructures consist of α-basketweave laths with β-grain boundaries. The layer itself shows large colonies of acicular α. The LENS process adds heat cycles with every layer of material, thus each layer is affected by the deposition of the next layer. The cooling rate affects the formation, and high cooling rates can lead to the formation of martensite.

2.5 Hybrid manufacturing

Current manufacturing processes such as forging, machining, casting, powder metallurgy and additive manufacturing each have their own setbacks, usually as a consequence of its technical constraints. Thus making it unsuitable for certain sizes or geometries [34]. Investment casting is an extremely time consuming and expensive process for custom or personalised products such as biomedical implants, sporting equipment or atypical fittings. While additive manufacturing has the advantage of custom products in less time, it is still restricted due to its long-running hours for large products and small chamber size.

In 2010 the CIRP (International Academy for Production Engineering) proposed an open and narrow definition [35]:

> Open definition: A hybrid manufacturing process combines two or more established manufacturing processes into a newly combined set-up whereby the advantages of each discrete process can be exploited synergistically.
>
> Narrow definition: Hybrid processes comprise a simultaneous acting of different (chemical, physical, controlled) processing principles on the same processing zone.

By combining two established manufacturing processes such as investment casting and additive manufacturing, we can avoid some crucial drawbacks of each of the processes. In the hybrid manufacturing process, investment cast will typically be used to create the larger part of the component, thus the base of the component which will have a set geometry. Consequently, the fixed geometry will minimise the design of new wax patterns. Additive manufacturing will then build material onto the casted part to complete the component. The AM section of the component will typically consist of the unique structures desired. By only adding the custom sections to the component using AM the running time for the whole component will drastically decrease.

An example where hybrid manufacturing can be used to aid in the manufacturing of components is given in Figure 4, where a single-stage air compressor rotor is illustrated. Currently the component is manufactured with intricate machining. The blades are too thin for molten metal to accurately flow into the cavities during investment casting, the component can, however, be AM, but will be very time consuming and expensive. To reduce the cost and time the component can be HM. The red indicates the section to be cast while the grey indicates sections to be AM (Figure 4 (b)). The HM offers additional advantages, such as the ability to manufacture for failure, if we know which section of a HM component is more prone to failure we can manufacture the component to fail in the least destructive or expensive section of the component. Hybrid manufactured products can be used in the medical industry as implants, for example an elbow implant. The implant can be a titanium prosthetic component that replaces the elbow joint bones. The artificial elbow joint consists of two stems which are assembled with a hinge allowing the elbow to bend [36]. The basis of the stems and hinge can be produced via investment casting, while the top section of the stems depending on the patient's size can be AM with a bone-like-porous structure.

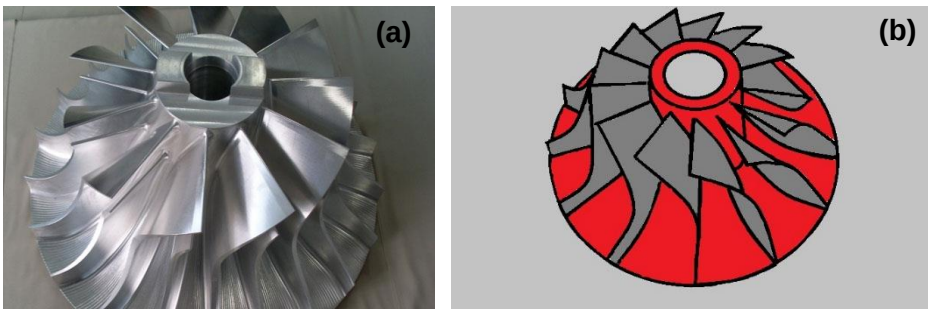

Figure 4. (a)Single-stage air compressor rotor. (b) Single-stage air compressor rotor indicating the different sections to be investment cast and additive manufactured (red = IC, grey = AM)

Surface pre-treatments are applied to titanium castings prior to additive manufacturing, this is done to remove the alpha-case layer and avoid subsequent microstructural defects. The α-case is an oxygen-enriched layer caused by titanium alloys exposed to air above 540°C, this leads to the casting free surface being hard and brittle [37]. An α-case layer can usually be found on the outer surface of IC components. It is common practice to remove this brittle layer by either chemical or mechanical methods.

A study investigating the effect of different surface pre-treatments on laser welding of Ti6Al4V [38] revealed that the surface pre-treatments influenced the microstructure and microhardness of the welds while the strength in tensile tests remained the same as the reference samples without weldments. The study showed that the fusion zone's microstructures of sandblasting, ground and chemical cleaned surface preparations formed acicular α' martensite. While painted black marker gave plate-like martensite with a higher density of dark acicular particles and the microstructure of graphite-based coating gave small dark elongated zones in the martensitic microstructure [38]. Another study looked at different surface preparations for laser penetration into cast titanium. The study concluded that air abrasion is the preferred surface preparation method with a deep laser weld penetration, while a mirror-finished surface led to a shallow laser weld penetration and thus a weaker weldment [39]. Although laser welding is a completely different process as to hybrid manufacturing, there are a few similarities. Similarities such as the existence of a diffusion zone and a heat-affected zone, both obtained from a melting pool with temperatures above the β-transus and a high cooling rate. From these studies it is evident that the surface preparation technique is an important aspect of the process.

2.6 Hardness and tensile properties

The microstructure of Ti6Al4V influences the tensile properties, hardness and fracture modes of Ti6Al4V components. Depending on the manufacturing processes, Ti6Al4V can be of equiaxed, lamellar or martensitic microstructures. The martensitic microstructure has higher yield strength,

ultimate tensile strength and hardness. While lamellar structures have a higher ductility and resistance to crack propagation.

When grain sizes decrease, the number of grains in the same area increase, thus causing an increase in the number of grain boundaries. Grain boundaries are obstacles to crack propagation causing entanglement and resulting in increased material strength [40]. The Hall-Petch equation (1) indicates that smaller grain sizes promote higher Yield strength (YS) and ultimate strength (UTS) [41], [42]

$$\boldsymbol{\sigma_y = \sigma_0 + \frac{K_y}{\sqrt{d}}} \quad \textbf{(1)}$$

where parameter $\boldsymbol{\sigma_y}$ is the yield strength, $\boldsymbol{\sigma_0}$ material constant, $\boldsymbol{K_y}$ strengthening coefficient and $\boldsymbol{d}$ the diameter of the average grain.

2.7 Fractography

A fracture takes place in two steps; crack initiation and crack propagation. A fracture is either classified as ductile or brittle depending on the material's ability to withstand plastic deformation. As seen in Figure 5, ductile fractures indicate extensive plastic deformation (necking) before fracture while brittle fractures indicate no necking. Ductility depends on the stress state, strain rate and the temperature of the material. The extent of ductility can be measured by percentage elongation and percentage area reduction [43]. Fracture can occur either by cutting through grains (transgranular) or following grain boundaries (intergranular)[24], [44], [43].

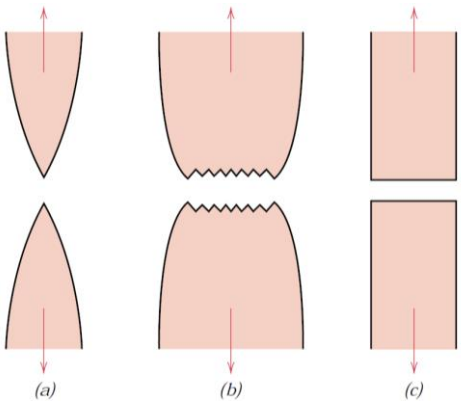

Figure 5. Different types of fractures. (a) Extreme necking with a highly ductile fracture. (b) Somewhat necking and moderate ductility. (c) No necking with brittle fracture.
[43]

The four principal fracture modes are dimples, cleavage, fatigue (striation lines) and intergranular. SEM micrographs examples for each principle fracture mode are shown in Figure 6.

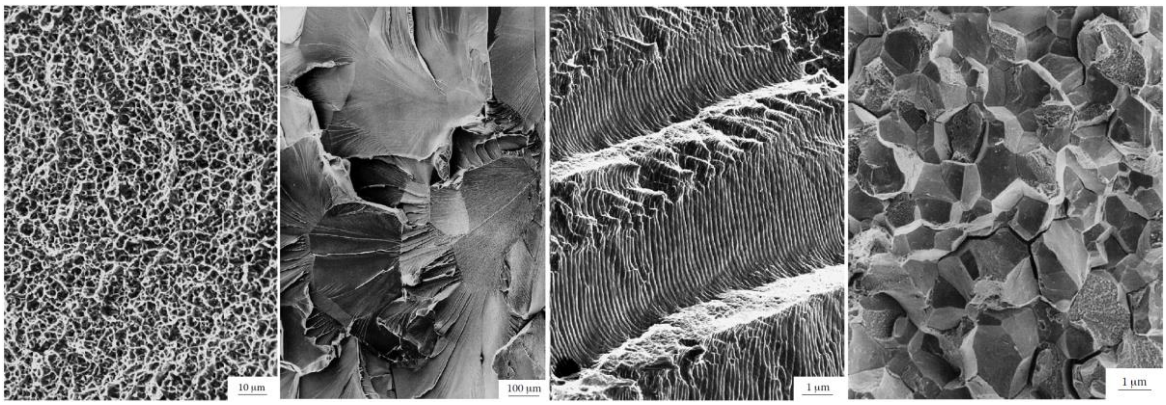

Figure 6. (a) Fine equiaxed dimples. (b) transcrystalline cleavage. (c) Fatigue fracture. (d) intergranular fracture.[24]

Previous research indicates that the Ti6Al4V alloy's fracture mode usually consists of dimples and cleavage fracture modes [45], [46], [47]. Dimple rupture occurs when a coalescence of microvoids are formed under an increasing load. The dimple rupture of a tensile specimen starts with minor necking, then openings between grain boundaries or defects forming microvoids. A coalescence of the microvoids are formed, then crack propagation occurs until final fracture. A schematic diagram of a dimple rupture is shown in Figure 7.

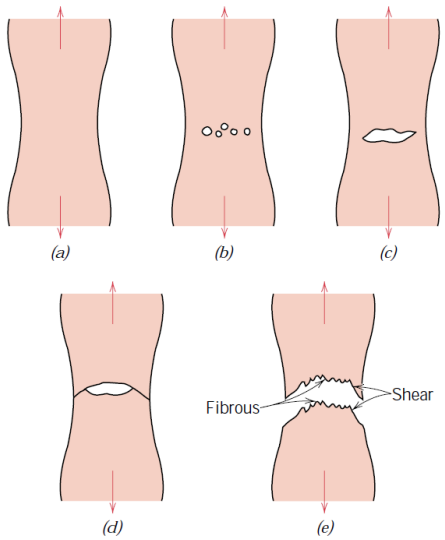

Figure 7. Ductile fracture: (a) necking. (b) microvoid formation. (c) coalescence of microvoids (d) crack propagation. (e) final fracture at max shear [43]

The cleavage fracture is a low-energy fracture, usually taking place on well-defined crystallographic planes [24]. The cleavage fracture does not necessarily indicate ductility, but rather the fracture mechanism. The surface of a cleavage fracture is rarely featureless, the features usually found on cleavage planes include, river markings, feature markings herringbone structure, tongues, Wallner lines and the most common in Ti6Al4V alloys the quasi-cleavage features. The quasi-cleavage feature is a combination of dimples and cleavage facets.

A review on the material, its traditional manufacturing processes and mechanical testing methods provided insight into how a hybrid manufactured component can be analysed. The literature led to the main variables and operating conditions. The methods used to analyse the variables and operating conditions are discussed in the next chapter.

CHAPTER 3. METHODOLOGY

The experimental procedure is designed in such a manner as to evaluate the effect of surface preparation techniques on the microstructure, diffusion zone and microstructure generated and consequently the hardness and tensile properties of the hybrid manufactured (HM) Ti6Al4V component. This chapter aims at providing sufficient experimental design details, analysis techniques and data processing method. The layout includes information on the materials and manufacturing processes, and a research design section to explain the overall approach. A detailed description of the experimental hybrid manufacturing is then presented to ensure that the non-standard process is clear and comprehensive. Followed by surface preparations of HM and the heat-treatments used. Lastly, the methods used for hardness measurement and tensile testing, and analysis methods are described.

3.1 Research design

The objectives of this project require four individual studies, with this in mind the research design will be divided into four subgroups. A diagram of the subgroups is given in Figure 8 followed by a brief description of each method used for this study. The various methods mentioned in each subgroup study is fully described in the proceeding sections of this chapter.

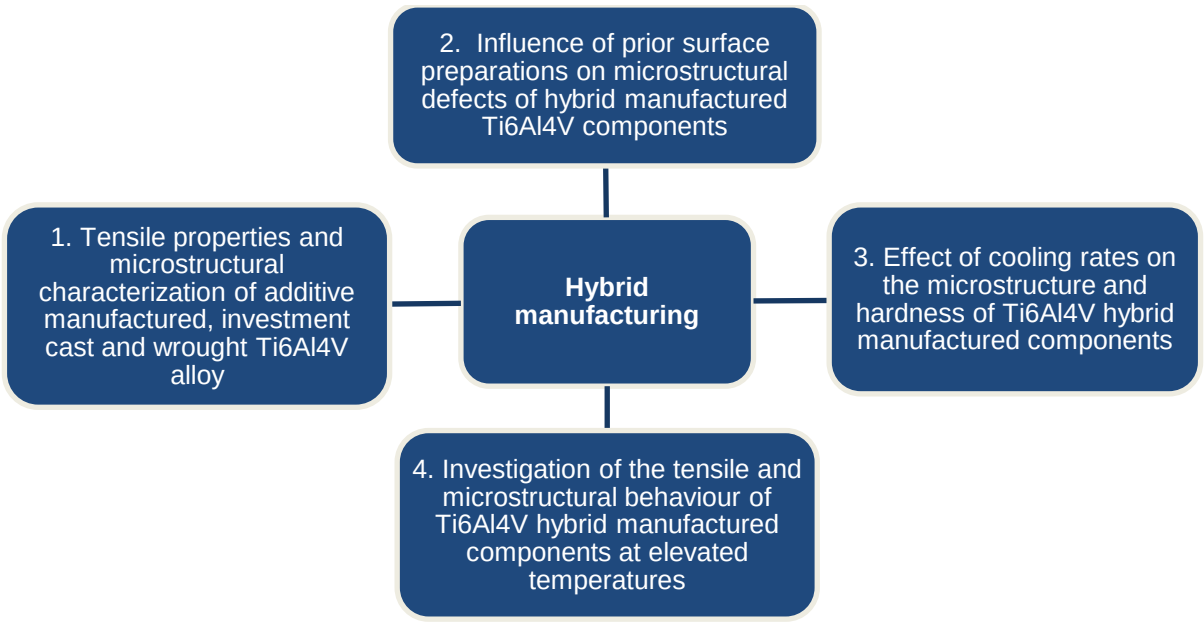

Figure 8. Research design subgroups

Table 2 gives a summary of the number of specimens that was used and the major variable for this subgroup study. The microstructural characterization and tensile properties of additive manufactured, investment cast and wrought Ti6Al4V alloy study was done by manufacturing three

rods of each manufacturing process. The nine specimens were tensile tested and evaluated by metallurgical analysis and fractography.

Table 2. Tensile properties and microstructural characterization of additive manufactured, investment cast and wrought Ti6Al4V alloy

Subgroup	Number of specimens	Manufacturing process	Mechanical test
1	3	Wrought	Tensile test @ room temperature
	3	Investment casting	
	3	Additive manufacturing	

A summary of specimens used for subgroup study 2 is given in Table 3. The influence of prior surface preparations on microstructural defects of hybrid manufactured Ti6Al4V components was determined by manufacturing six samples using hybrid manufacturing. Each investment cast (IC) sample was given a different surface preparation prior to additive manufacturing (AM). The two best surface preparation techniques were determined through metallurgical analysis (referred to as surface preparation A & B). An additional six hybrid manufactured specimens were manufactured for tensile testing. The first three specimens received surface preparation A and the following three surface preparation B. These six specimens were tensile tested and evaluated with metallurgical analysis and fractography, to make a recommendation of which surface preparation to use for subgroup studies 3 and 4. A summary of specimens used for subgroup study 2 is given in Table 3.

Table 3. Influence of prior surface preparations on microstructural defects of hybrid manufactured Ti6Al4V components

Subgroup	Number of specimens	Manufacturing process	Surface preparation
2	1	Hybrid manufacturing	As-Cast
	1		Polishing
	1		Just-cut
	1		Sandblasting
	1		Ablation
	1		Chemical milling
	3		Surface preparation A
	3		Surface preparation B

To study the effect of cooling rates on the microstructure and hardness of Ti6Al4V hybrid manufactured components a hybrid manufactured specimen was wire cut it into quarters. Each quarter was heat-treated and cooled at different cooling rates. The effects were studied using metallurgical analysis. Table 4 indicates the specimens used for this study and the variable.

Table 4. Effect of cooling medium on the microstructure and hardness of Ti6Al4V hybrid manufactured components

Subgroup	Number of specimens	Manufacturing process	Cooling medium
3	1/4	Hybrid manufacturing	Non-heat treated
	1/4		Air cooling
	1/4		Water quench
	1/4		Furnace cooling

Table 5 gives a summary of the specimens used for testing. The tensile and microstructural behaviour of Ti6Al4V hybrid manufactured components at elevated temperatures were investigated by manufacturing nine specimens using the hybrid manufacturing process. The specimens were divided into three groups, each group was tensile tested at a different temperature (400°C, 600°C and 800°C). The differences were compared using metallurgical analysis and fractography.

Table 5. Investigation of the tensile and microstructural behaviour of Ti6Al4V hybrid manufactured components at elevated temperatures

Subgroup	Number of specimens	Manufacturing process	Tensile test
4	3	Hybrid manufacturing	Tensile test @ 400°C
	3		Tensile test @ 600°C
	3		Tensile test @ 800°C

3.2 Materials Ti6Al4V alloy

To compare different variables, the Ti6Al4V alloy material used should remain constant. Consequently, for the entire study wrought commercial grade 23 Ti6Al4V ELI alloy bars bought from Baoti in China (Figure 9) was used. The Titanium alloy was received as wrought bars with a 74 mm diameter. The chemical composition of the as-received bar is given in Table 6.

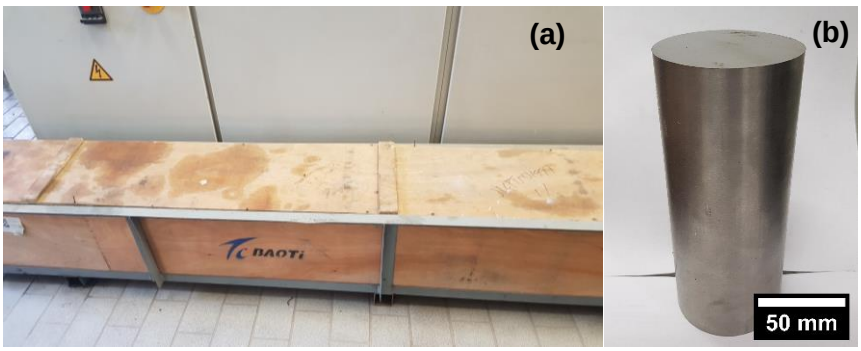

Figure 9. (a) Wrought bar shipment container from Baoti. (b) the as-received wrought bar.

Table 6. Chemical composition of the as-received wrought Ti6Al4V bar (wt. %)

Al	V	Fe	Y	C	H	N	O	Other	Ti
6.75	4.5	0.30	≤0.005	≤0.08	≤0.0125	≤0.05	≤0.2	≤0.4	Bal

3.3 Manufacturing and machining of specimens

The first objective that was tested was the tensile properties and microstructural characterization of wrought, investment cast and additive manufactured Ti6Al4V alloy. This section will explain how each of these manufacturing processes was done to create the specimens for testing and evaluation.

3.3.1 Wrought specimens

Wrought specimens for tensile testing were machined from an as-received wrought bar cut-off with 74 mm diameter and 200 mm length, next rods were wired-cut EDM (Electrical Discharge Machining) from the cut-off bar. The rods were heat-treated at 1050°C for 30 minutes then furnace cooled using a vacuum furnace to generate colony lamellar structure.

3.3.2 Investment cast

The investment cast (IC) process started with a wax tree pattern for eight rods of 212 mm length and 15 mm diameter (Figure 10 (a)) which was dipped into two alternating ceramic slurries, colloidal ZrO2 and stuccoing with ZrO2 stucco (Figure 10 (b)). The mould was dried for 24 hours at room temperature. The wax was burned-out at 200°C and 8 bars pressure using a Leeds and Bradford Boiler (LBBC) Steam Boilerclave® for 15 minutes and then fired for two hours at 800°C. A piece of as-received Ti6Al4V wrought bar (Figure 9 (a)) was melted using an induction melting furnace, the molten alloy was poured into the ceramic shell and left to solidify. The shell was broken off revealing the runners, sprue and rods (Figure 10 (c)). The IC rods were cut-off from the runners and sprue (Figure 10 (d)) and hot isostatically pressed (HIPed) to reduce any porosity.

The tensile specimens were machined from the HIPed IC rods (Figure 10 (e)). The chemical composition of the Ti6Al4V IC rods is given in Table 7.

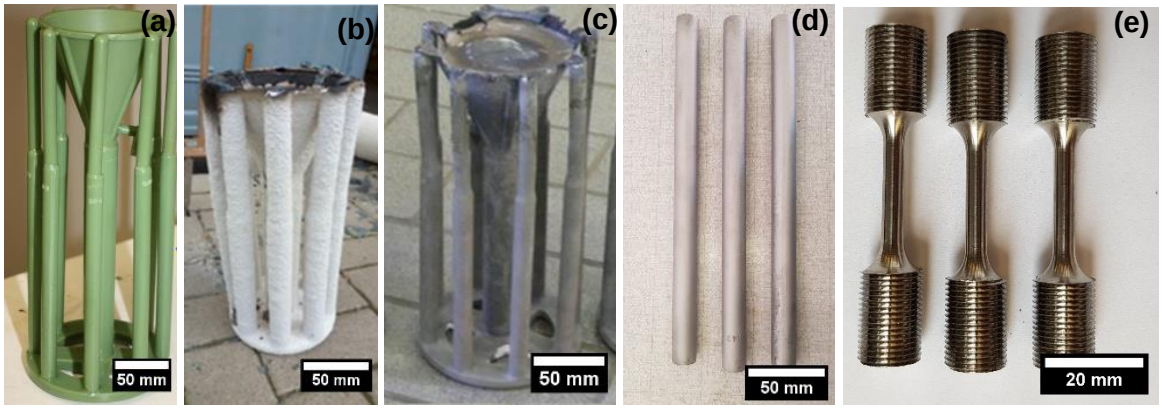

Figure 10. (a) Wax tree pattern for rods. (b) Ceramic mould after burnout. (c) Ti6Al4V mould after shell removal. (d) Ti6Al4V investment cast rods. (e) Investment cast tensile specimens

Table 7. Chemical composition of Ti6Al4V investment casting (wt. %)

Al	V	Fe	Y	C	Cr	Mo	Ni	S	Sn	Cu	Zr	Ti
6.76	4.51	0.12	ppm≤7	0.018	0.12	0.009	0.007	≤0.005	ppm≤50	0.021	ppm≤100	Bal

3.3.3 Additive manufacturing

The additive manufacturing used for this study is Laser Engineered Net Shaping (LENS) which uses powder. To ensure that we use the same Ti6Al4V alloy chemistry as in the previous manufacturing processes, the as-received wrought bars was atomised to produce spherical Ti6Al4V powder. Therefore, two as-received wrought Ti6Al4V alloy bars (Figure 9 (a)) were supplied for atomisation to TLS (Technik GmbH & Co. Spezialpulver) an international supplier of titanium powder in Germany. Electrode Inert Gas Atomisation (EIGA) was used to produce spherical powder for additive manufacturing. EIGA is done by induction melting of a rotating electrode and atomised by inert gas [31]. The spherical atomized Ti6Al4V powder (Figure 11) and Energy Dispersive X-ray Spectrometer (EDS) analysis of some single particles of the atomized Ti6Al4V powder is given in Table 8. The powder produced is spherical with a large range of particle sizes.

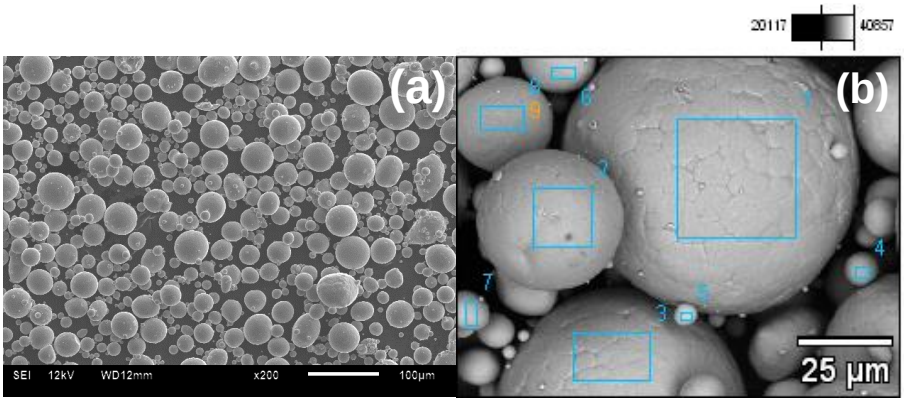

Figure 11. (a) Spherical Ti6Al4V atomized powder, and (b) electron microscopy/ EDS analysis on some single particles.

Table 8. SEM/ EDS analysis of some single particles of atomized Ti4Al4V powder

Element	Al-K	Ti-K	V-K
Atomized Ti6Al4V _pt1	5.5	90.1	4.4
Atomized Ti6Al4V _pt2	5.5	90.1	4.3
Atomized Ti6Al4V _pt3	4.7	89.6	5.6
Atomized Ti6Al4V _pt4	4.3	91.5	4.2
Atomized Ti6Al4V _pt5	1.3	93.5	5.1
Atomized Ti6Al4V _pt6	3.5	92.6	4.0
Atomized Ti6Al4V _pt7	4.4	91.0	4.6
Atomized Ti6Al4V _pt8	6.1	89.5	4.4
Atomized Ti6Al4V _pt9	5.8	90.2	3.8

The atomised powder was used on the Optomec LENS™ 850-R system (Figure 12) to laser print Ti6Al4V rods. The Optomec LENS^{TM} used a 1 kW IPG high energy fibre laser and three co-axial powder nozzles which are set at 8 ± 2 mm from the substrate (stand-off distance). The substrate was a 5 mm thick Grade 5 titanium plate which was sandblasted and cleaned with acetone to remove any surface contamination. The chamber was filled with argon gas to reduce oxidation, the gas also played the role of quenching medium as it was fed at room temperature. An energy density range of 180 J/mm^3 to 315 J/mm^3 was used to 3D print the Ti6Al4V rods. Figure 12 (b) illustrates the AM rods after machining for tensile testing.

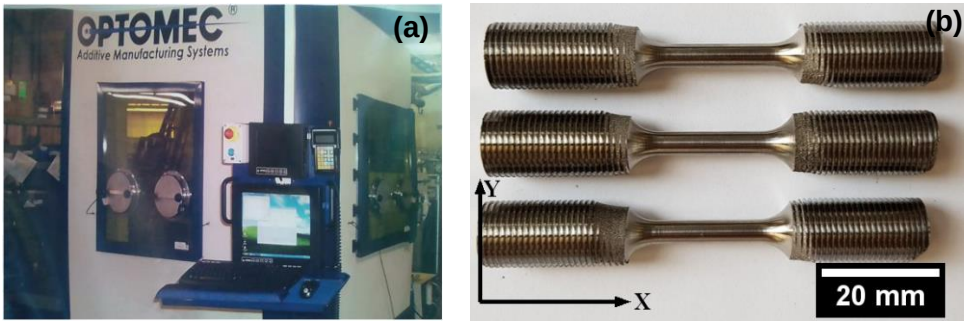

Figure 12. (a) Optomec LENS™ 850-R system [48]**, and (b) additive manufactured tensile specimens.**

3.4 Hybrid manufacturing

The hybrid manufacturing (HM) process developed combines the two aforementioned manufacturing processes; investment cast (IC) and additive manufacture (AM). The basis of HM is to 3D print material onto IC components. For this study, IC rods were used and AM laser printed material onto the rods in a symmetrical manner to extend the overall length of the rod/specimen.

HM specimens were used for subgroup studies 2(surface preparations), 3 (heat-treatments) and 4 (furnace tensile testing).

The rods manufactured with IC (Figure 10 (d)), as described previously, acts as the first section of the HM specimen. The IC rods was first sectioned into quarters (52 mm in length and 15 mm diameter) using a Rusch HBS 250 bandsaw at 35 m/min and AFROX torch coolant. The quarter IC rods (Figure 13 (a)) then underwent surface preparations to remove the oxide layer and any contaminations, more details on surface preparations are given in section 3.5. Since the IC rod takes the place of the normally used substrate in the additive manufacturing (AM) chamber, the heat dissipation is affected. An aluminium frame (Figure 13 (b)) was developed for the purpose of transferring heat away from the IC rod. The frame also allows for two IC rods to be placed inside the chamber simultaneously, reducing the operating time. The Al frame with two IC rods in place was then clamped into the AM chamber and the same LENS process, as described above (Section 3.3.3), was executed onto the IC rods. Thus, the second section of the HM specimen was printed onto the IC rod to complete the HM specimen (Figure 13 (c)).

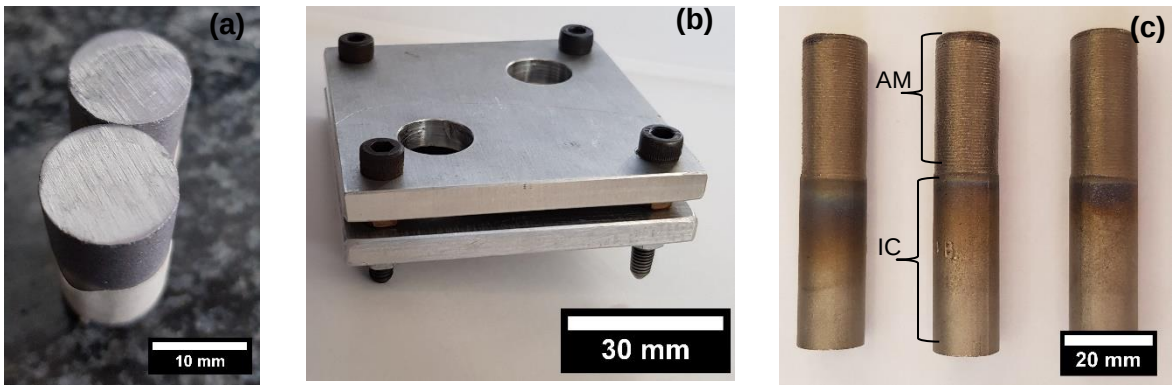

Figure 13. (a) Quarter investment cast rods. (b) Aluminium frame for holding IC parts (c) hybrid manufactured rod Ti6Al4V

3.5 Surface preparation techniques

To determine the influence of surface preparation of the IC rods before laser printing material onto it, five different surface preparation techniques were chosen along with an *as-cast* rod for reference. The surface preparations used was *ablation*, *just-cut, sandblasting, polishing* and *chemical milling* along with the *as-cast* rod acting as a reference. Each surface preparation technique was applied to one of the IC rods after it was sectioned into quarters. By sectioning it into quarters the α-case or oxide layer was already removed, the succeeding surface preparations were then used to test the diffusion bonding between IC and AM.

The *as-cast* rod was untouched and the α-case still intact. The *just-cut* surface preparation was achieved through the sectioning of the rods into quarters. The *ablation* surface preparation was done by irradiating the surface with a laser beam to remove material and thus any contaminations on the top layer. The *sandblasting* technique was chosen as it would roughen the surface while also removing any contaminations. The *sandblasting* technique is in direct contrast to the *polished* surface. The *polished* surface involved grounding and polishing the sample to a mirror finish. The *chemical mill* surface preparation was done by treating the rod's surface with Kroll's reagent for 20 seconds. An illustration of various surface preparations on IC rods is given in Figure 14.

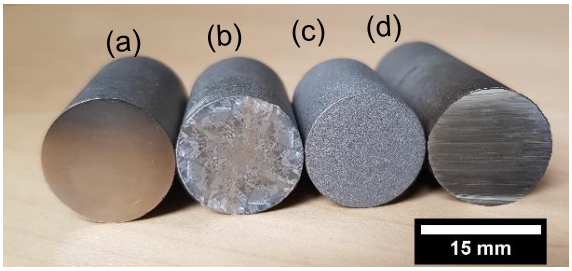

Figure 14. Surface preparations (a) polished (b) chemical mill (c) sandblast (d) just-cut

3.6 Heat-treatments

The heat-treatment chosen was a solution treatment above the β-transus at 1050°C, to transform the phase to a complete β-phase prior to cooling to room temperature.

The HM specimen (Figure 15 (a)) was wired-cut into quarters ((Figure 15 (a)). One quarter was used as a received HM. The rest were solution treated at 1050°C for 2 hours to ensure complete transformation of α-phase to β-phase.

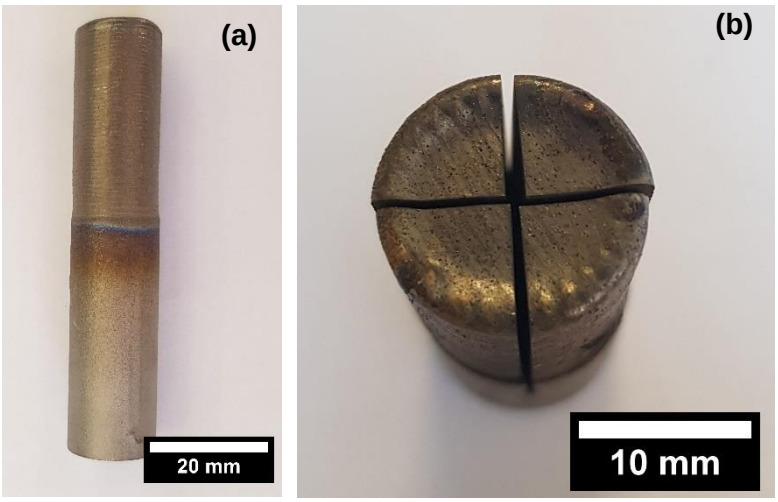

Figure 15. (a) Hybrid manufactured ti6Al4V specimen and (b) wired-cut hybrid manufactured sample.

The heat-treatment was done using a muffle furnace. After the 2 hours on holding time the first specimen was removed and water quenched, the transition from the furnace to water was as fast as possible. The second specimen was then removed and placed onto a ceramic plate and left to cool in air. The third specimen was left in the furnace to cool within the furnace. A graph indicating the temperature change over time for each specimen is given in Figure 16. The graph can be divided into three phases. The first phase heats up the furnace from room temperature to holding temperature, the second phase holds that temperature for two hours and the third phase is the cooling phase. The temperature of the first two phases are recorded with a build in

thermostat. Phase three indicates the different cooling rates. Table 9 gives a summary of the process for each specimen.

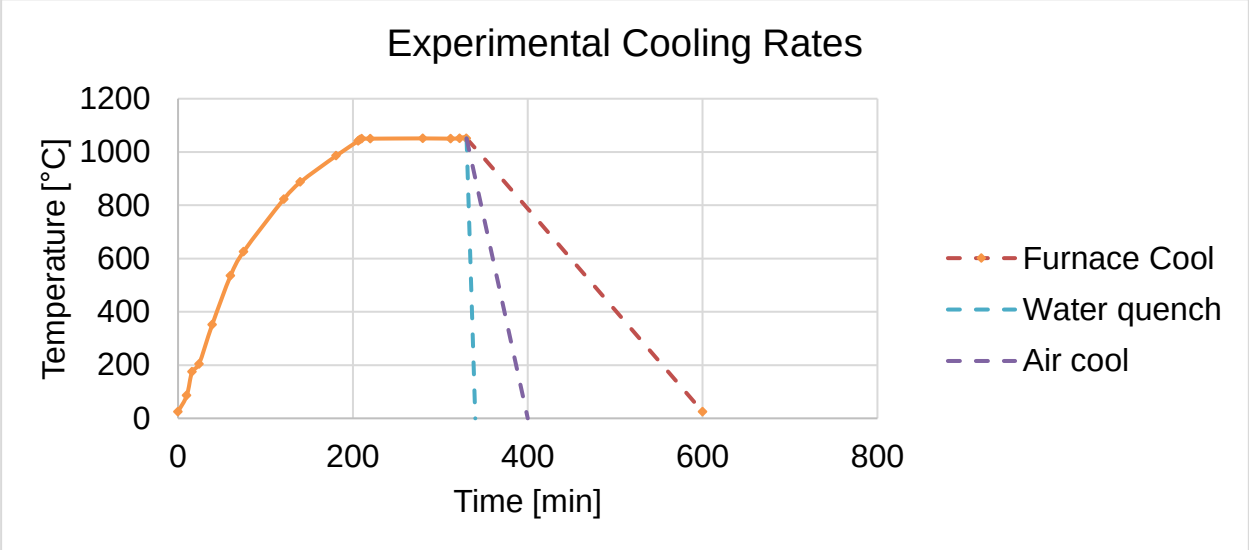

Figure 16. Experimental cooling rates on hybrid manufactured specimens.

Table 9. Process summary of each specimen.

	Process	Temp	Time	Cooling medium
1	Solution treatment	1050ºC	2 hrs	Furnace cool (FC)
2	Solution treatment	1050ºC	2 hrs	Air cooling (AC)
3	Solution treatment	1050ºC	2 hrs	Water quench (WQ)

3.7 Tensile testing

Two types of tensile testing were chosen to compare the mechanical properties of different manufacturing processes against hybrid manufacturing. Standard room temperature tensile testing and hot tensile testing (HTT). All specimens were machined on a CNC lathe to ASTM E 8M-04 standards, a detailed drawing is given in Figure 17.

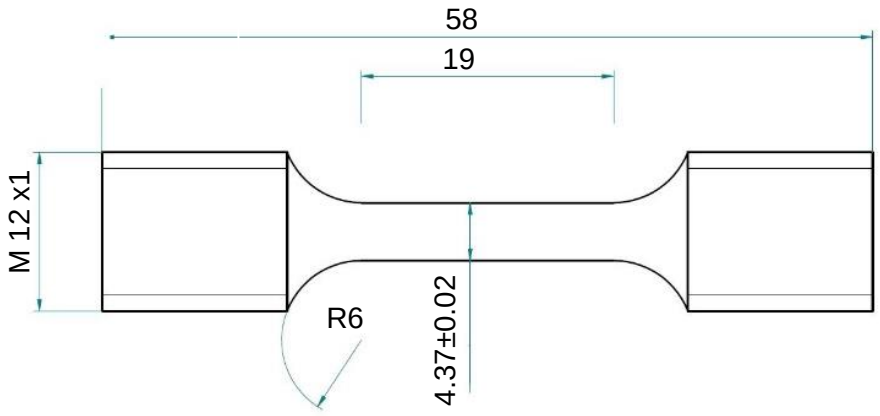

Figure 17. a) Schematic of ASTM EM04 standard tensile specimen and (b) machined wrought tensile specimens

Tensile tests were carried out using a servo-hydraulic fluid-controlled machine (Instron™ 1342). For subgroup study 1 a total of nine specimens was tensile tested, to compare the difference in manufacturing processes. Subgroup study 2 used six specimens to test the effect of two different surface preparations of HM specimens. All specimens were pulled at 0.25mm/min.

The furnace tensile tests used a furnace clamped around the specimen's area, with a thermocouple attached to the specimen. Wool was used around the furnace to ensure minimum heat loss. The Instron™ also makes use of a chiller to cool down the wedge grips and stop any heat from reaching the crosshead or any electrical parts of the machine. After the tensile specimen and furnace were set in place the furnace was switched on. When the furnace's temperature was stable at the desired temperature on the thermocouple the tensile test commenced. Subgroup study 4 pulled three specimens at 400°C, three at 600°C and three at 800°C all using a pulling rate of 0.25mm/min.

Initial length, area, continuous load and extension values were captured, and the stress-strain curves drawn for all three subgroup studies. Table 10 provides a summary tensile tests for each subgroup and its main variable being compared or tested.

Table 10. Subgroup variables for tensile testing

Subgroup study	Variable	Tensile testing head speed, mm/min	Tensile test temperature
1	Manufacturing process	0.25	Room temperature
2	Surface preparation		Room temperature
4	Tensile testing temperature		400°C 600°C 800°C

The true stress-strain curves were drawn and the strain hardening exponent and rate were determined from the yield point and area reduction using the Hollomon equation (2).

$$\boldsymbol{\sigma = K(\varepsilon)^n} \quad \textbf{(2)}$$

with $\boldsymbol{\sigma}$ as true-stress, $\boldsymbol{K}$ as the strength coefficient, $\boldsymbol{\varepsilon}$ as the true-strain and $\boldsymbol{n}$ as the hardening exponent. The strain-hardening rate equation was calculated from the derivative of the true stress-strain curve between the yield strength and ultimate tensile strength. The strain hardening rate was plotted against the true strain and the analysed. The stress needed to increase the strain beyond the proportional limit in a ductile material continues to rise beyond the proportional limit; the material requires an ever-increasing stress to continue straining, a mechanism termed strain hardening [49].

3.8 Metallographic analysis

Specimens were cut, mount and ground then polished and etched using Kroll's reagent (2 ml HF: 6 ml HNO_3: 92 ml H_2O) to reveal the microstructure. The microstructure analysis was performed using a Leica DMI5000M Optical Microscope (OM) and Scanning Electron Microscope (SEM) equipped with energy-dispersive X-ray spectroscopy (EDX). Both secondary images and backscatter images were collected.

Microstructures were quantified using an image processing program (ImageJ). The grain sizes were measured using the line intercept method. The α and β phases were determined using the SEM's spectral imaging at high magnification, by identifying black and white areas and scanning them separately. The volume fraction of alpha-phase (α-phase) and beta-phase (β-phase) were measured using the segmentation method.

An automatic Vickers micro-hardness tester FM-700 was used to measure the change in hardness to investigate the structural homogeneity. Indentations were made using a load of 300 g for a dwell time of 15 seconds.

3.9 Fractography

Tensile fractures were studied using the Leica MZ16 Stereo-microscope and Scanning Electron Microscopy (SEM) to reveal the fracture mode. Tensile specimens were prepared for fractography by cutting-off the grip sections (Figure 18 (a)) and mounting the larger sections of the specimens. Fractography analysis was performed on the fractured tensile specimens' polished cross-sections (Figure 18 (b)) and on fracture surfaces (Figure 18 (c)).

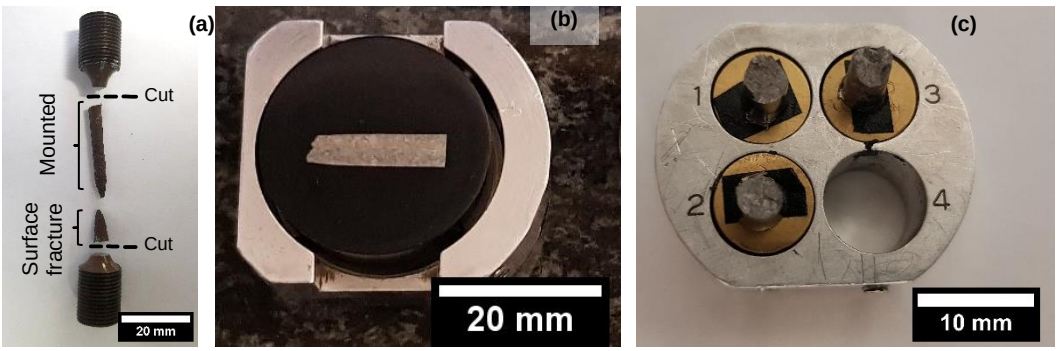

Figure 18. (a) Tensile specimen prepared for analysis, (b) a mounted cross-section of a tensile specimen in a SEM sample holder, and (c) fractured tensile surface setup to analyse the fracture surface using SEM.

Fractures were analysed by observing the initial point of fracture, microvoids, crack propagation, secondary cracks and the fracture modes and features.

CHAPTER 4. RESULTS

In the previous chapter, the methods to generate results were discussed, in this chapter, the results obtained from those methods are presented. The results include microstructural analysis, hardness measurements, tensile properties and fractographic analysis results obtained from the four subgroup studies. These results are chosen to better understand hybrid manufacturing and the influence of its major variables and operating conditions.

4.1 Microstructural characterization

The Energy Dispersive X-ray Spectrometer (EDS) analysis results for the different phases of the Ti6Al4V material is given in Figure 19 and Table 11. The light (white) areas show higher Vanadium weight percentage, while the dark (black) areas show an increase in Aluminium weight percentage.

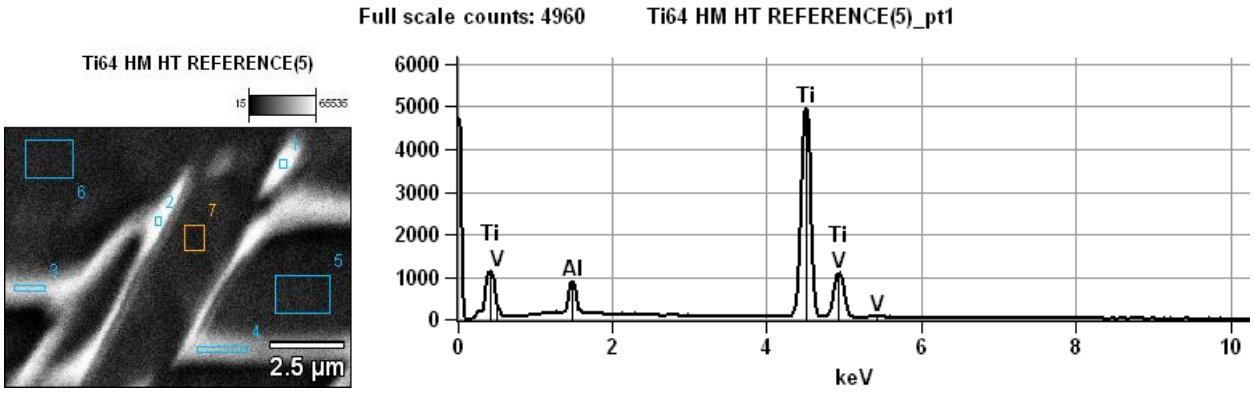

Figure 19. Electron microscopy EDS analysis on different phases of a Ti6Al4V sample

Table 11. EDS analysis of a Ti6Al4V sample

	Al-K	Ti-K	V-K
Ti6Al4V REFERENCE_pt1	3.76	84.93	10.31
Ti6Al4V REFERENCE_pt2	3.43	84.19	12.38
Ti6Al4V REFERENCE_pt3	2.87	81.37	14.92
Ti6Al4V REFERENCE_pt4	4.34	87.47	8.19
Ti6Al4V REFERENCE_pt5	5.73	94.27	
Ti6Al4V REFERENCE_pt7	5.74	94.26	

4.1.1 Wrought

The stereo and optical micrographs of the wrought Ti6Al4V alloy is shown in Figure 20 (a) and (b), respectively. The microstructure consisted of small equiaxed grains, with various colonies of α -phase and transformed β-phase inside the grains. The grains are separated by an α-phase network, and the colonies consist of very fine plate-like α -phase lamellae.

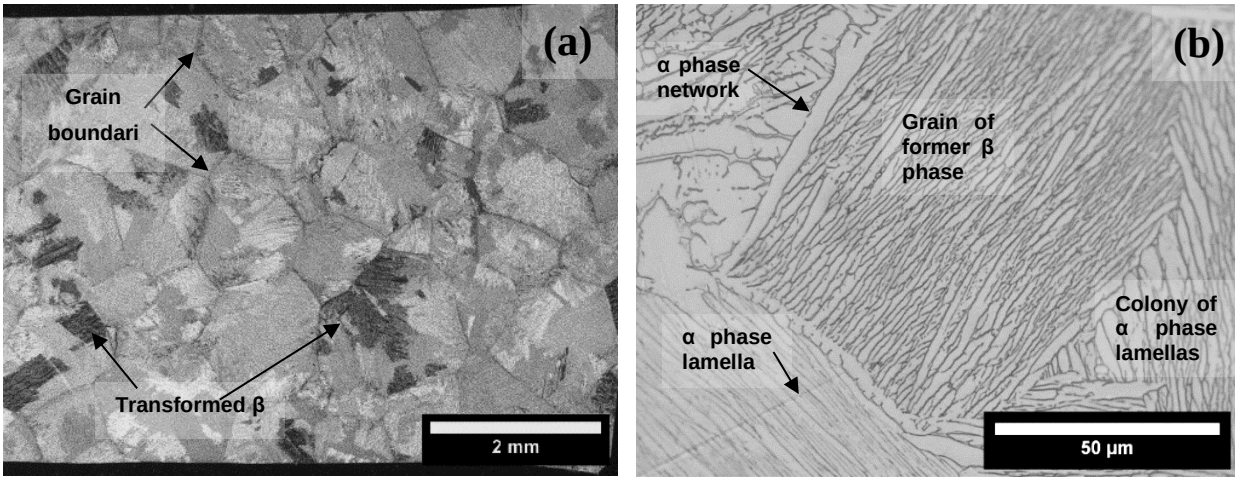

Figure 20. (a) Stereo microscope image, and (b) optical microscope image of wrought Ti6Al4V alloy

4.1.2 Investment cast

The microstructure of the investment cast (IC) Ti6Al4V alloy is presented in Figure 21. The microstructure obtained from IC shows large equiaxed grains with α grain boundaries. Coarse α/β-lamellae colonies in various directions are observed within the grain.

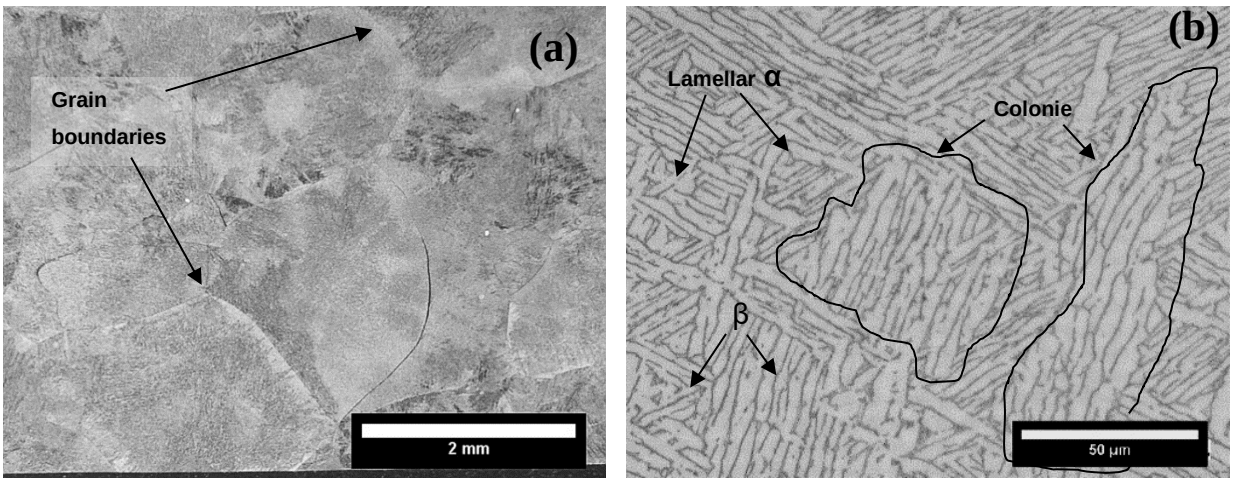

Figure 21. (a) Stereo microscope image, and (b) optical microscope image of investment cast Ti6Al4V alloy

4.1.3 Additive manufacturing

The layer bands and grains of the additive manufactured (AM) Ti6Al4V alloy's microstructure are revealed in Figure 22 (a). Long columnar grains are observed growing in the building direction across multiple layer bands. The micrograph in Figure 22 (b) revealed a typical Widmanstätten structure of α' martensitic laths with prior β-grain boundaries.

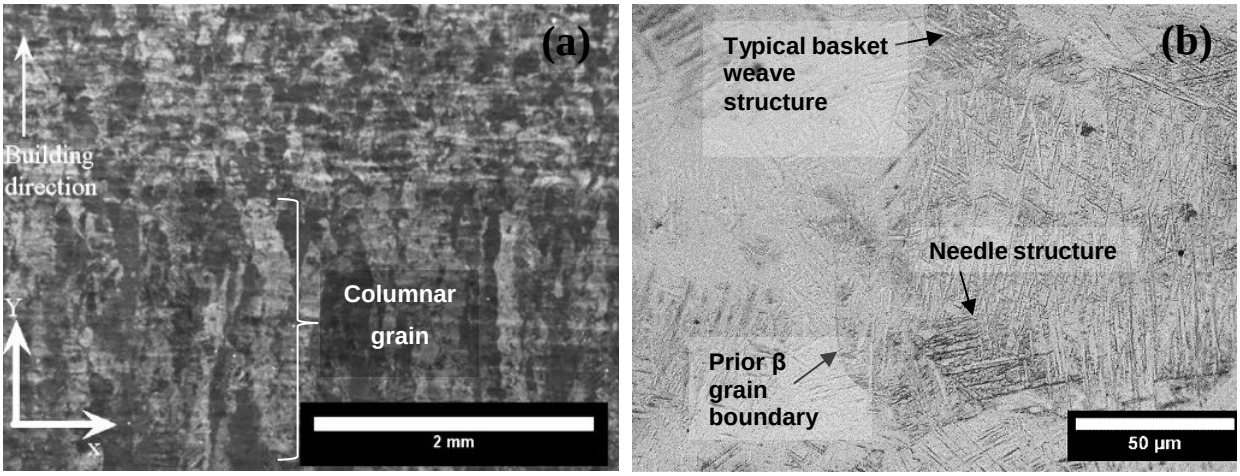

Figure 22. (a) Stereo microscope image, and (b) optical microscope image of additive manufactured Ti6Al4V alloy

The microstructural quantification results for different manufacturing processes of Ti6A4V is presented in Table 12. The grain sizes and lath thicknesses are larger for the IC microstructure compared to the wrought Ti6Al4V's microstructure. The AM martensitic needles were too thin to measure, while the overall size of the columnar grains was much smaller than the equiaxed IC and wrought grains. The average percentage of α-and β-phase remains constant and not affected by the manufacturing process used.

Table 12. Grain size, lath thickness and percentage α-and-β for different manufacturing processes of Ti6Al4V

Manufacturing process	Grain size (μm/grain)	laths size (μm)	Average %	
			α	β
Wrought	551.1	2.02	65.0585	34.9415
Investment Cast	1109.2	3.02	64.273	35.727
Additive manufacturing	146.7	*	65.214	34.786

4.1.4 Hybrid manufacturing

The three different regions of a hybrid manufactured (HM) Ti6Al4V alloy are shown in Figure 23. The additive manufacturing (AM), diffusion zone (DZ) and investment cast (IC) regions are indicated. In the AM region, the layer bands are visible, and the building direction indicated. The DZ was identified as the layer band between the AM and IC regions. The IC region appeared darker, while some large grains can still be observed.

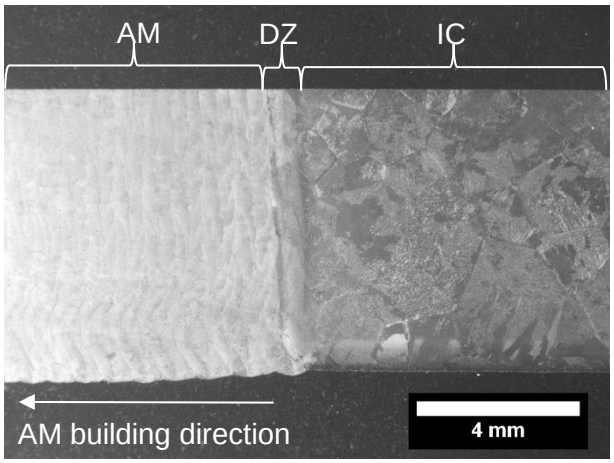

Figure 23. Stereo micrograph of a hybrid manufactured Ti6Al4V alloy

The DZ, shown in Figure 24, is the area of interest for HM. Figure 24 (a) showed a clear distinguished line between the AM and IC regions. The microstructure of this line can be seen in Figure 24 (b) as an acicular α' martensitic morphology.

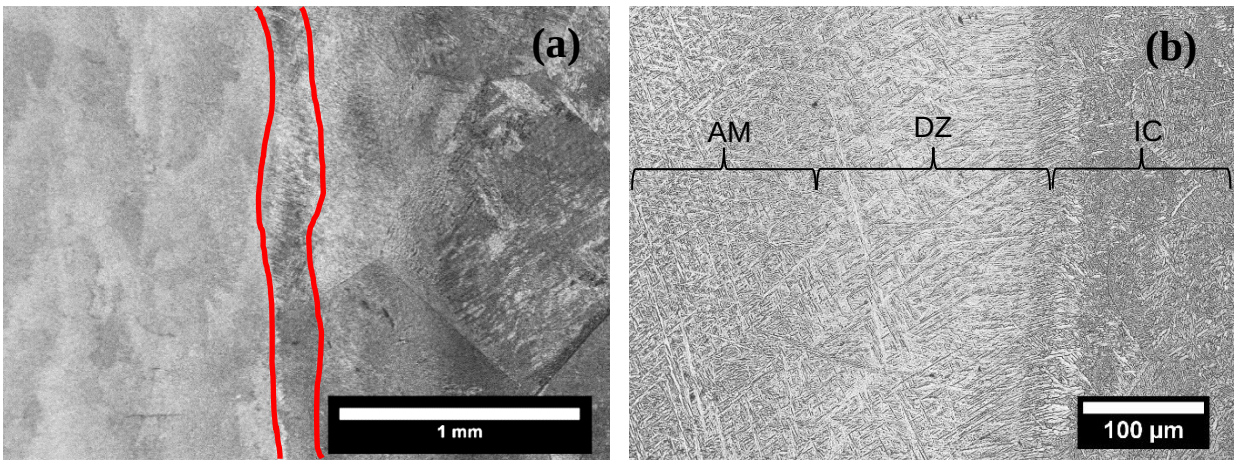

Figure 24. (a) Stereo microscope image, and (b) optical microscope image of the diffusion zone of a hybrid manufactured Ti6Al4V alloy

The SEM (Scanning Electron Microscope) micrographs of the different regions of HM Ti6Al4V alloy specimens are shown in Figure 25. The IC region (Figure 25 (a)) shows α/β lamellae. The DZ (Figure 25 (b)) shows a parallel needle structure of an α' martensitic morphology. The AM structure (Figure 25 (c)) shows an α' martensitic basketweave structure, and a prior β columnar grain boundary can be seen.

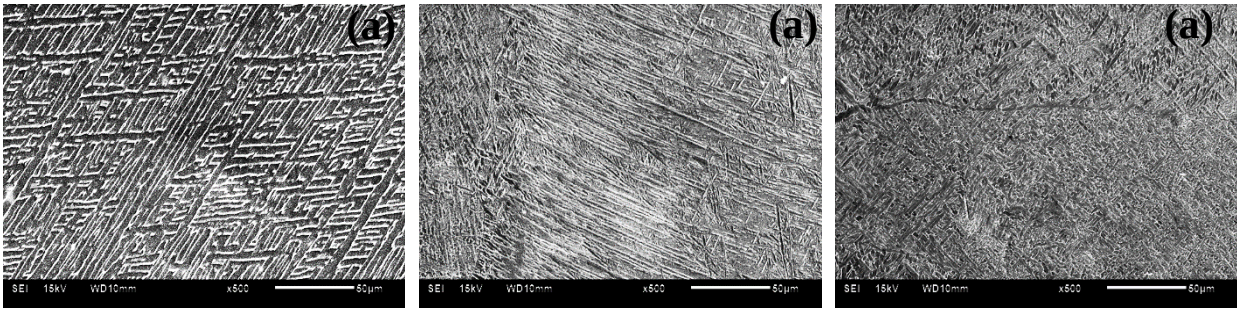

Figure 25. SEM micrographs of the different zones of a hybrid manufactured Ti6Al4V alloy specimen. (a) Investment cast zone. (b) Diffusion zone. (c) Additive manufactured zone

The SEM-EDS line scanning analysis results for the DZ of a HM specimen is presented in Figure 26. The results indicate no chemical segregation across the three different regions of the HM specimen.

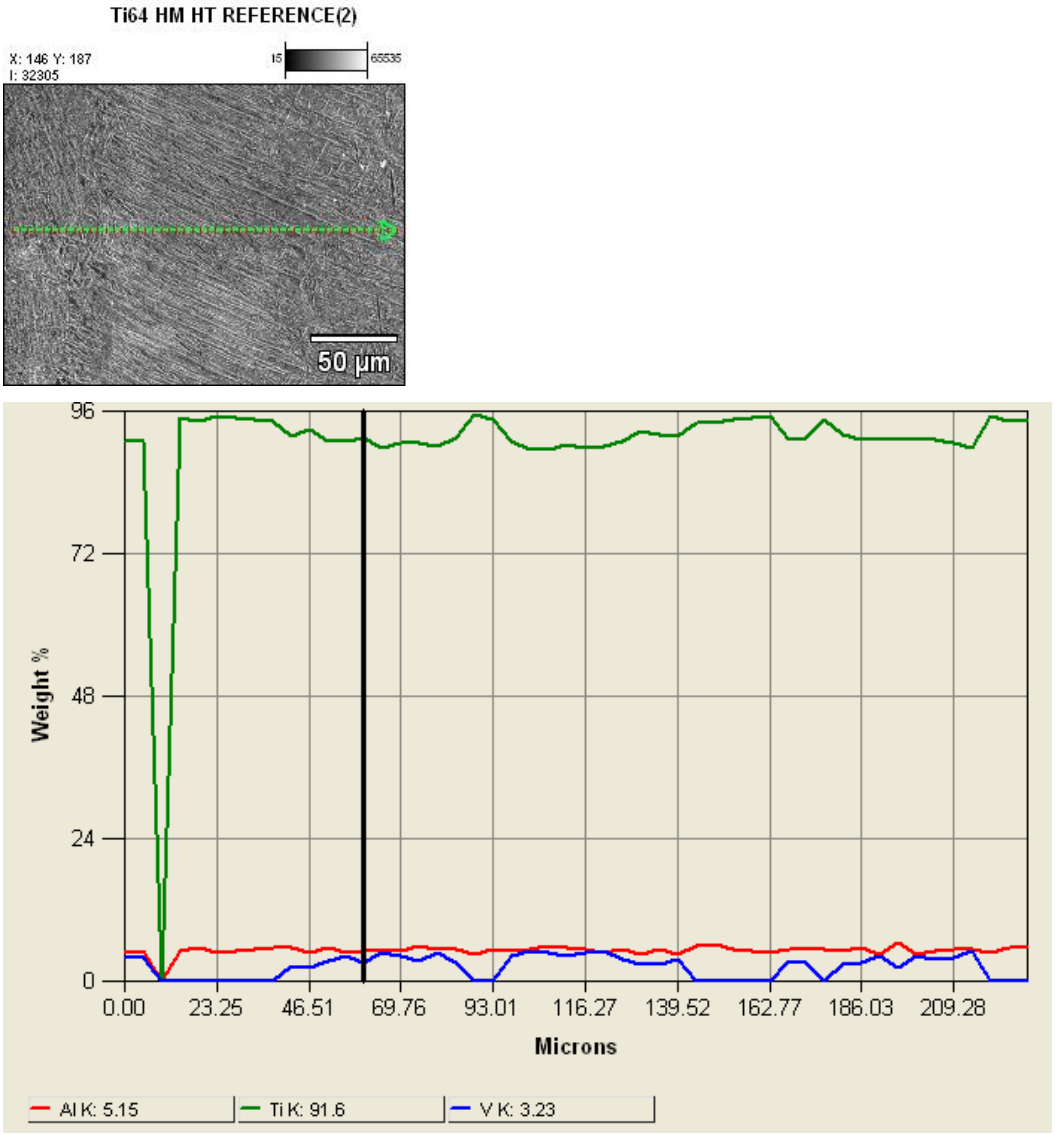

Figure 26. EDS line scanning analysis of the diffusion zone of the Ti6Al4V hybrid manufactured specimen

The hardness of IC, AM, wrought and HM Ti6Al4V is presented in Figure 27. The AM specimen with an α' martensitic Widmanstätten structure showed a higher hardness compared to the IC and wrought manufactured specimens with α/β lamellae colonies. The hybrid manufactured specimen showed respectively similar harnesses in the IC and HM region. The average hardness of the DZ is lastly higher than the IC region hardness but lower than the AM region hardness. The standard deviation in hardness was higher in lamellae colony microstructures than in martensitic morphologies.

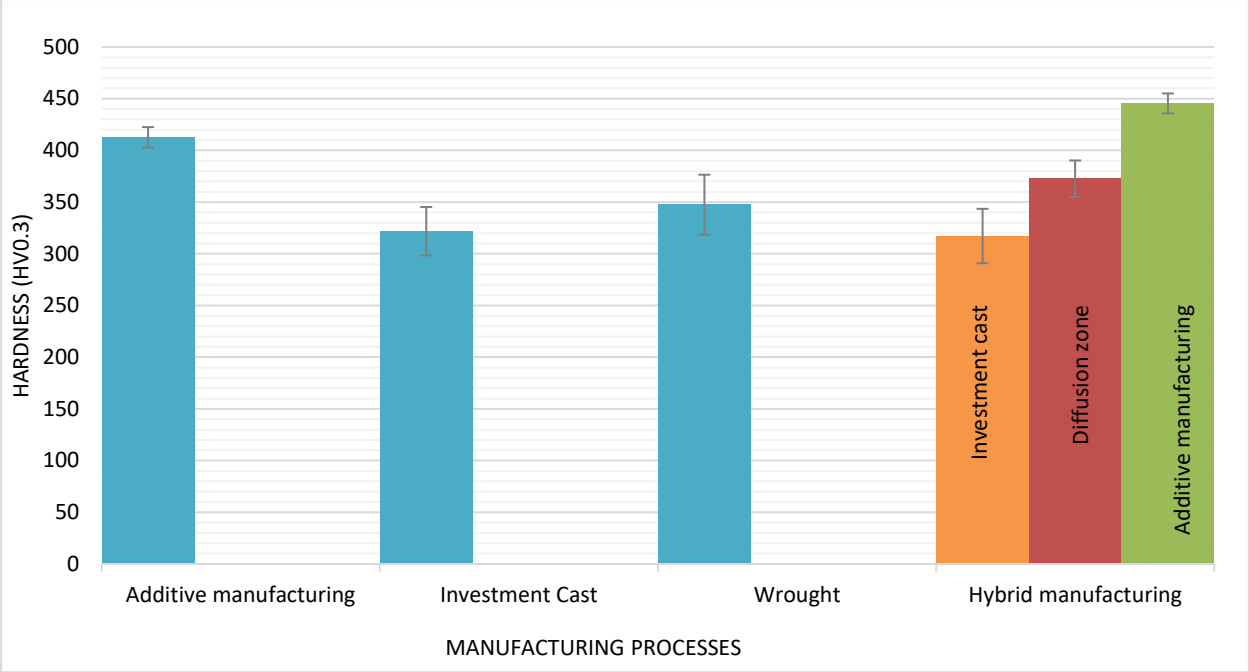

Figure 27. Average Vickers micro-hardness with standard deviation error bars of specimens manufactured with additive manufacturing, investment cast, wrought and hybrid manufacturing

The hardness profiles of the IC, wrought, AM and HM Ti6Al4V specimens are shown in Figure 28. The AM specimen with a martensitic microstructure showed a consistent hardness which is an indication of a homogenous structure. The HM specimen showed three different hardness values for the three different regions across the specimen. The hardness value in each region of the HM specimen was in agreement with the hardness measured in wrought and investment casting specimen.

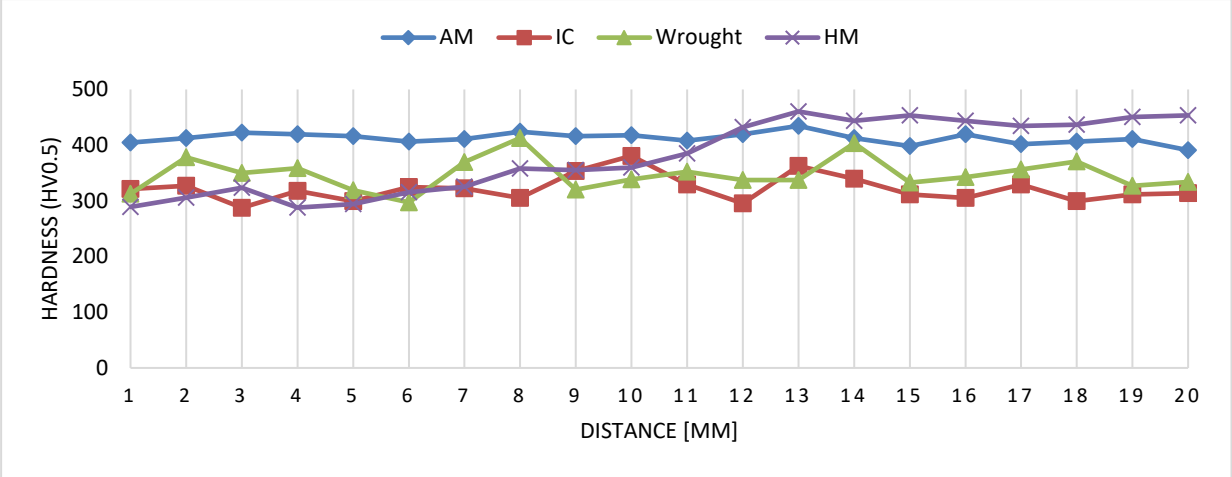

Figure 28. Hardness profiles of wrought, investment cast, additive manufactured and hybrid manufactured Ti6Al4V specimens.

4.1.5 Surface preparations

The surface of IC specimens was prepared prior to HM using several different preparation techniques as shown in Figure 29. Stereo microscopy revealed large equiaxed grains in the IC region, along with the layer bands and columnar grains in the AM region. The DZ, which is the dark layer between the IC and AM regions, is also observed. The DZ thickness appeared to be a function of the surface preparation technique as revealed in Figure 29 (a) – Figure 29 (f).

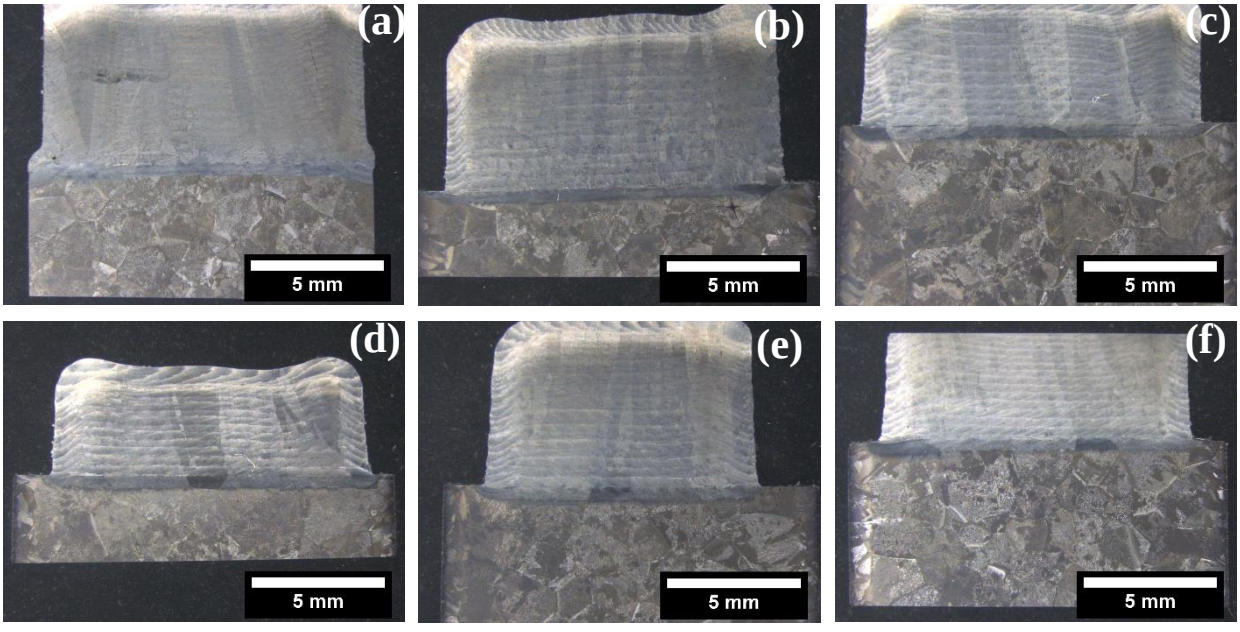

Figure 29. Hybrid manufactured Ti6Al4V using different surface preparation techniques; (a) ablation, (b) as-cast, (c) chemical milling, (d) just-cut, (e) polishing, (f) sandblasting.

The microstructures of the diffusion zone of the HM Ti6Al4V the obtained from different surface preparation techniques are shown in Figure 30 (a)-(f). The ablation, chemical milling, just-cut and polishing technique (Figure 30 (a), (c), (d) and (e) respectively) revealed similar acicular α'

martensitic morphology. The as-cast surface (Figure 30 (b)) showed a clear α-phase division line between the two processes, while the sandblasted (Figure 30 (f)) specimen's DZ showed small coarse α-phase grains.

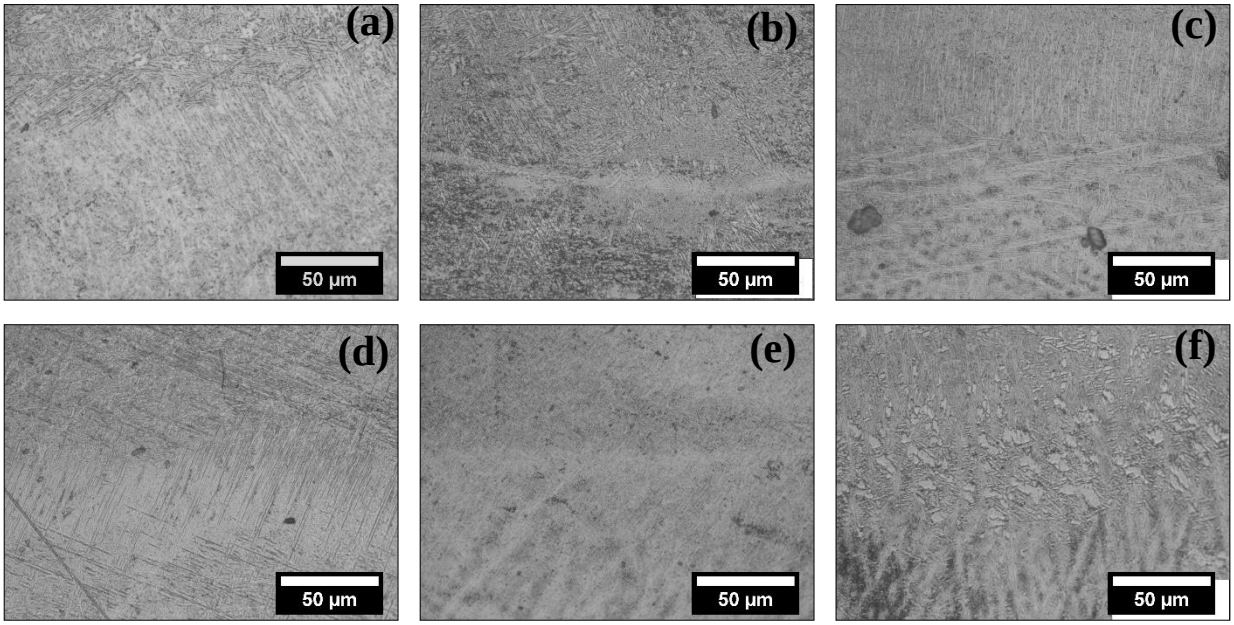

Figure 30. Optical micrographs of the diffusion zone of hybrid manufactured Ti6Al4V with different surface preparation techniques; (a) ablation, (b) as-cast, (c) chemical milling, (d) just-cut, (e) polishing, (f) sandblasting

The resulting DZ size from the ablation, chemical milling, polishing, sandblasting techniques and as-cast and the just-cut surface is presented in Figure 30. The average DZ thickness ranged from about 400 to 500 µm.

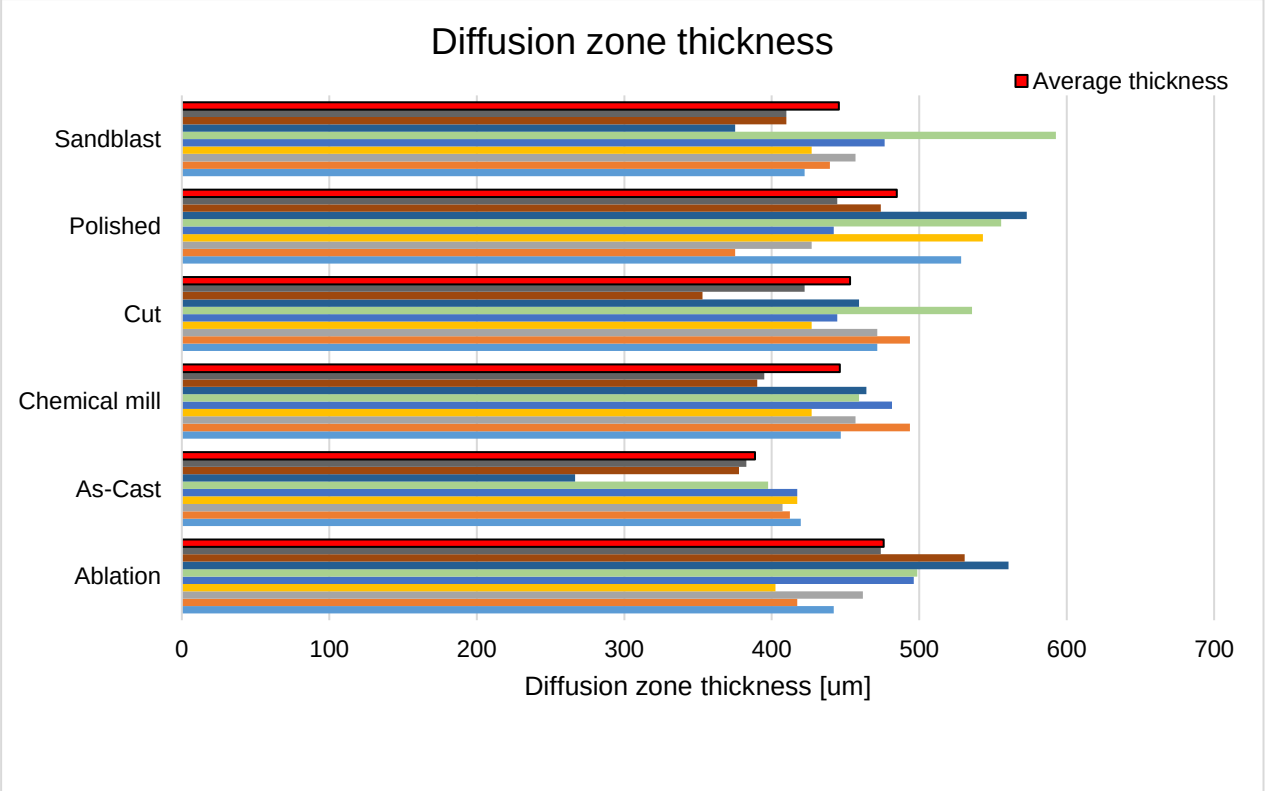

Figure 31. Diffusion zone thickness measurements of hybrid manufactured Ti6Al4V alloy specimens with different surface preparations

The defects in the DZ of HM Ti6Al4V specimens for different surface preparations are presented in Figure 32. The IC specimens with just-cut and polished surfaces prior to AM had no defects in the DZ. The as-cast surface preparation specimen has a lack of fusion defect identified by the long horizontal pore stretching over the DZ (Figure 32 (a)). The ablation and chemical mill indicate bigger pores with random shapes, caused by the AM process and is referred to as process-induced porosities. The sandblast surface preparation specimen shows an array of gas-induced porosities along the DZ.

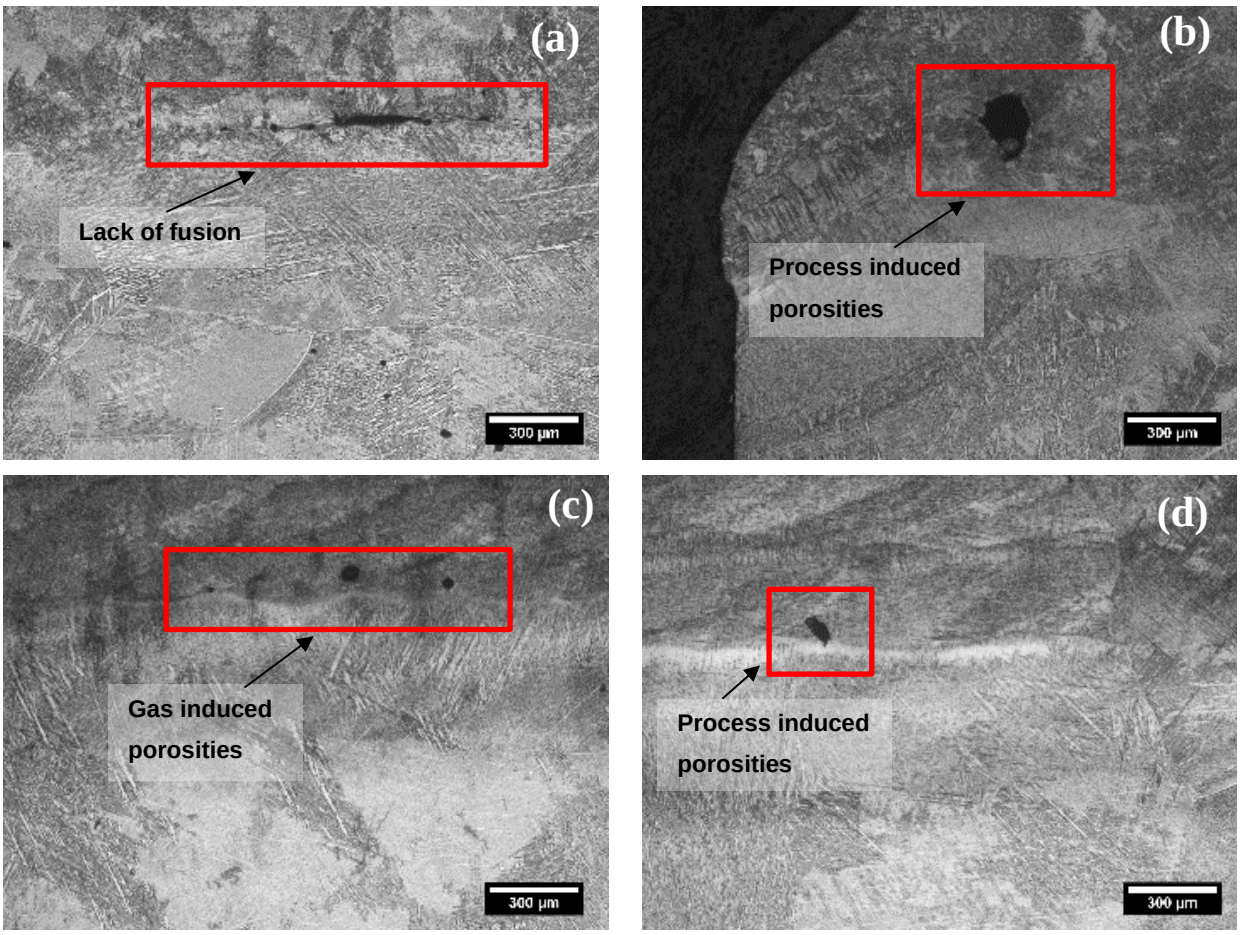

Figure 32. Defects, in the diffusion zone of HM specimens, resulting from (a) as-cast surface, (b) ablation, (c) sandblasting and (d) chemical milling techniques

The hardness profiles of HM Ti6Al4V specimens with different surface preparation techniques are presented in Figure 33. The IC and AM regions appeared unaffected by the type of surface preparation technique used. The DZ, however, showed a gradual change in hardness except for the surface prepared using sandblasting.

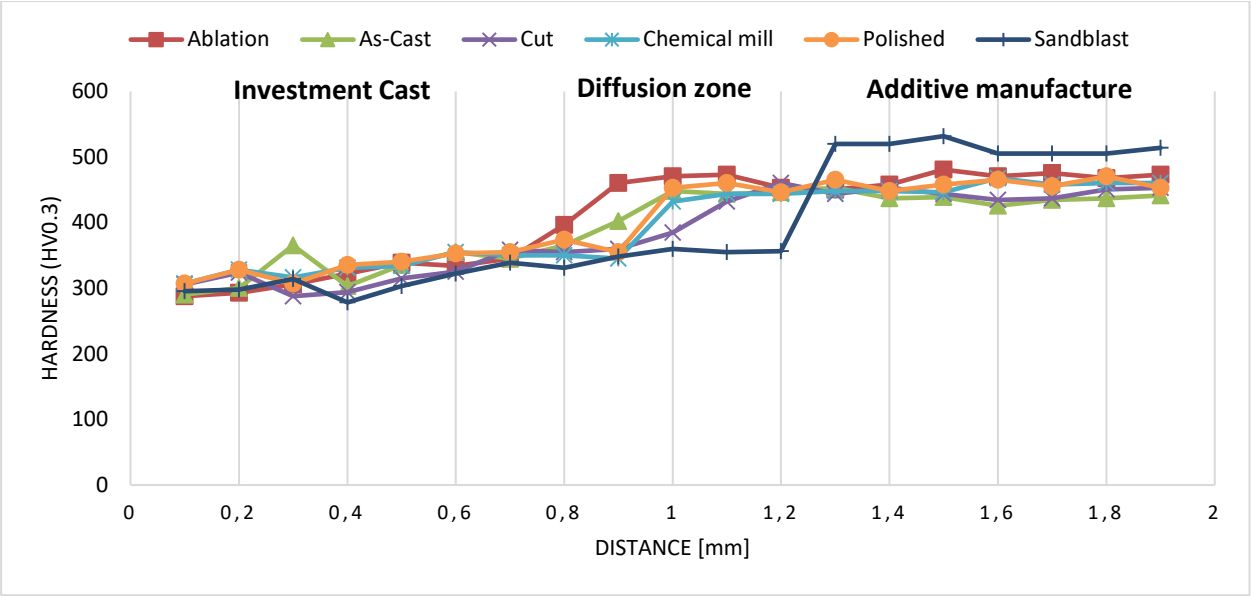

Figure 33. Vickers microhardness profile of HM Ti6Al4V showing the effect of ablation, chemical milling, sandblasting techniques, as cast and just-cut free surface

4.1.6 Heat-treatments of Ti6Al4V

The effect of different cooling rates after solution-treatment at 1050°C for 2 hours, on the DZ, is obvious; the DZ has almost completely disappeared from the solution heat-treated AC and FC specimens leaving a distinct boundary line between the IC and AM region. The WQ specimen showed a DZ with a more integrated structure, where some of the AM α' martensitic needles cross over to the IC side. Fine grains and coarser laths are revealed in the AM regions after heat treatment.

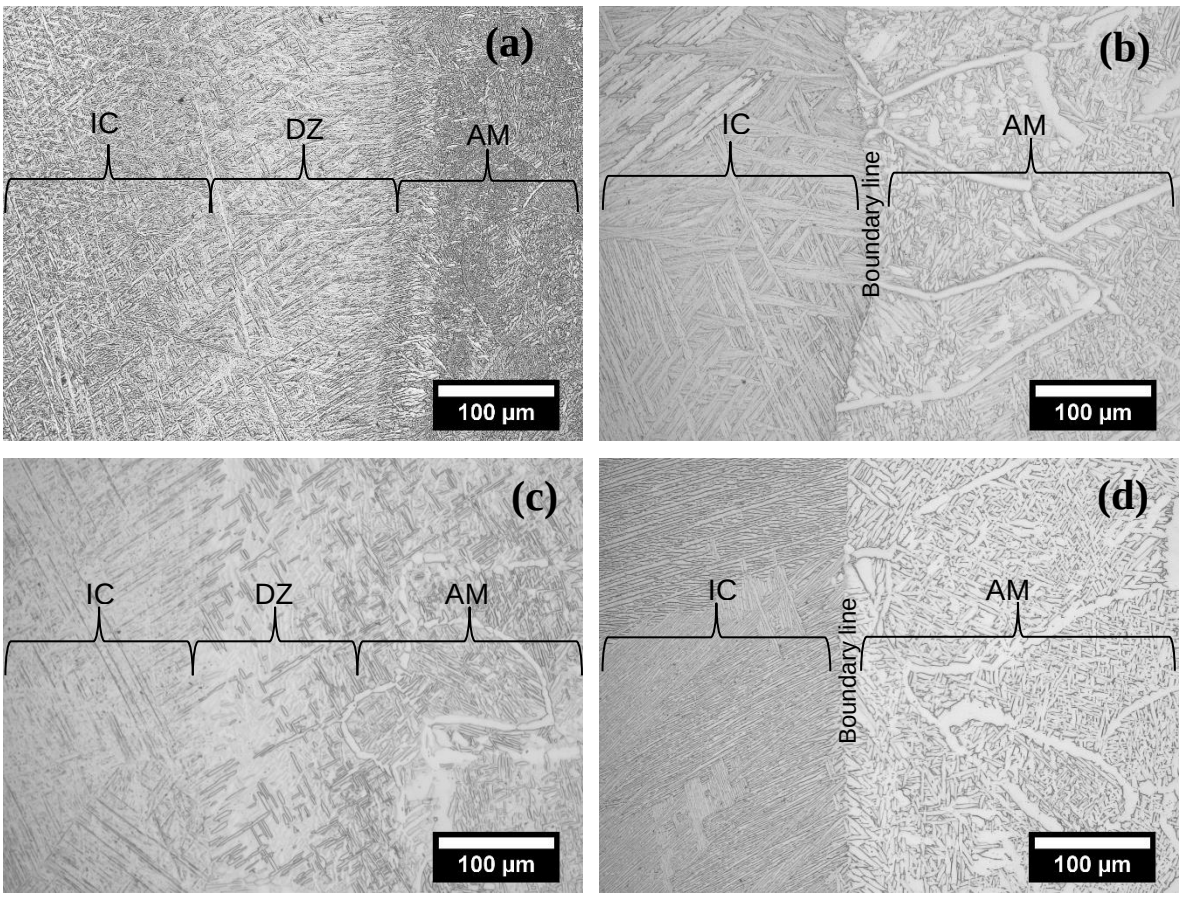

Figure 34. Diffusion zones of hybrid manufactured Ti6A4V specimens in (a) non-heat treated, (b) air-cooled, (c) water quenched, and (d) furnace cooled after solution treatment.

IC, DZ and AM regions of the hybrid manufactured Ti6Al4V after solution-treatment and air-cooled (AC), water quench (QW), and furnace cooled (FC) are shown in Figure 35 (a)-(c), (d)-(f), and (g)-(i) respectively. The AC produced a partial martensite structure with very fine α/β lamellae structure in the IC region (Figure 35 (a)), followed by transformed β, and some coarse α-laths in the AM region (Figure 35 (c)). The WQ led to a fully martensitic structure in the IC region (Figure 35 (d)) and a basketweave structure of α/β phase lamellae in the AM region (Figure 35 (f)). The FC produced a fine structure of α/β lamellae with colonies of α-laths in the IC region (Figure 35 (g)), and small colonies of relatively coarse α-laths with thin β-phase between them in AM region (Figure 35 (i)).

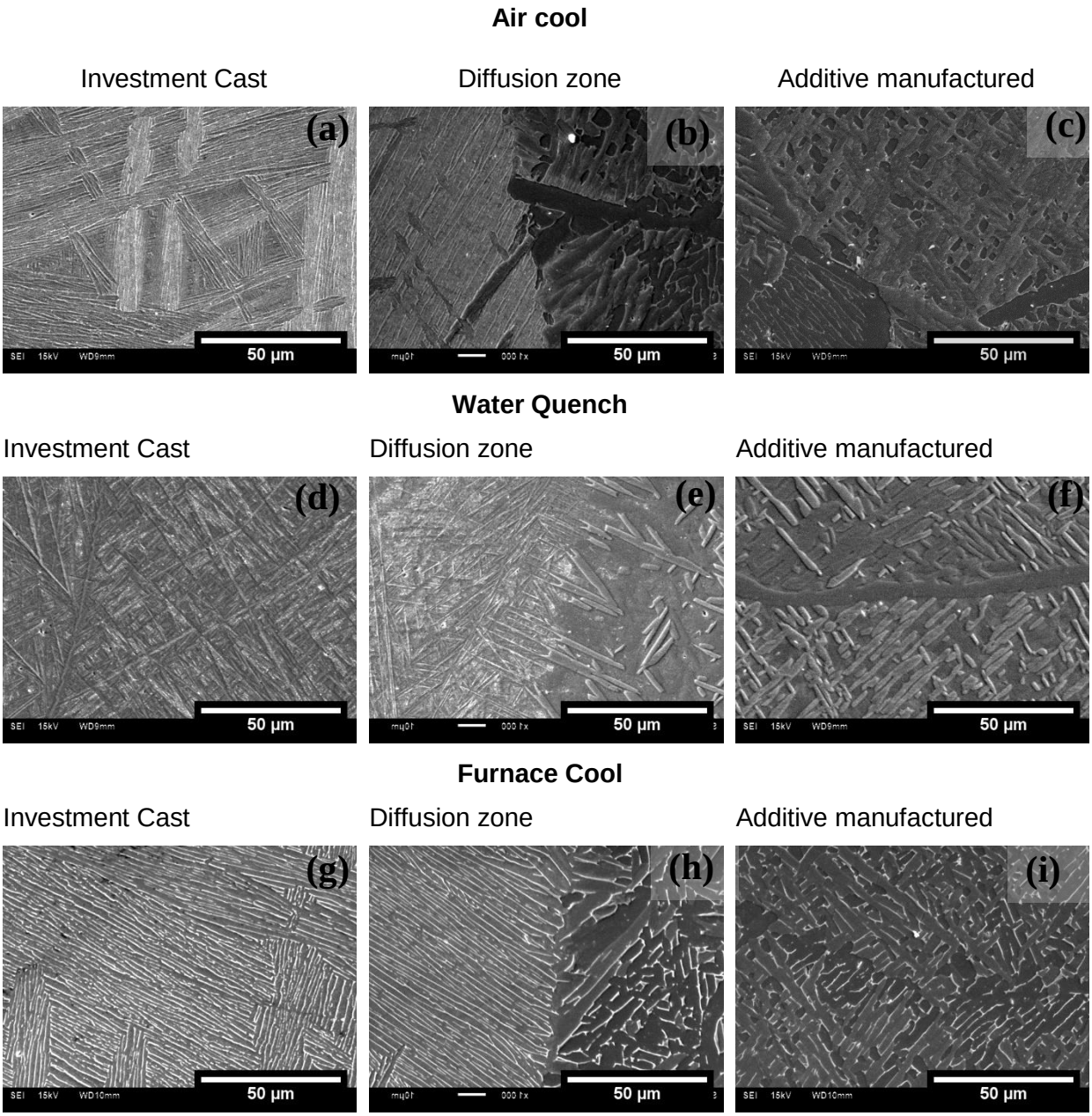

Figure 35. IC, DZ and AM regions of the hybrid manufactured Ti6Al4V after solution-treatment and (a)-(c) air-cooled, (d)-(f) water quench, and (g)-(i) furnace cooled.

Average Vickers microhardness with standard deviation error bars in the IC, DZ and AM regions for the non-heat treated, solution-treated and air-cooled (AC), water quenched (QW) and furnace cooled (FC) hybrid manufactured Ti6Al4V are shown in Figure 36. The AC IC region with partial martensite and very fine α/β lamellae structure gave the same average hardness as the IC region of the non-heat treated HM. Coarse α-laths in the AC AM region had a slight drop in hardness from the AM region of the non-heat treated HM. The fully martensitic structure in the WQ IC region gave the highest hardness than the AC and FC IC regions. The WQ specimen's AM region containing β-phase lamellae basketweave structure gave a hardness slightly lower than that of the non-heat treated HM specimen. The fine

structure of α/β lamellae with colonies of α-laths in the IC region of the FC specimen showed an increase in hardness compared to the non-heat treated HM specimen. And the AM region of the FC specimen with α-phase and α'-laths gave a hardness similar to the hardness of the non-heat treated HM specimen.

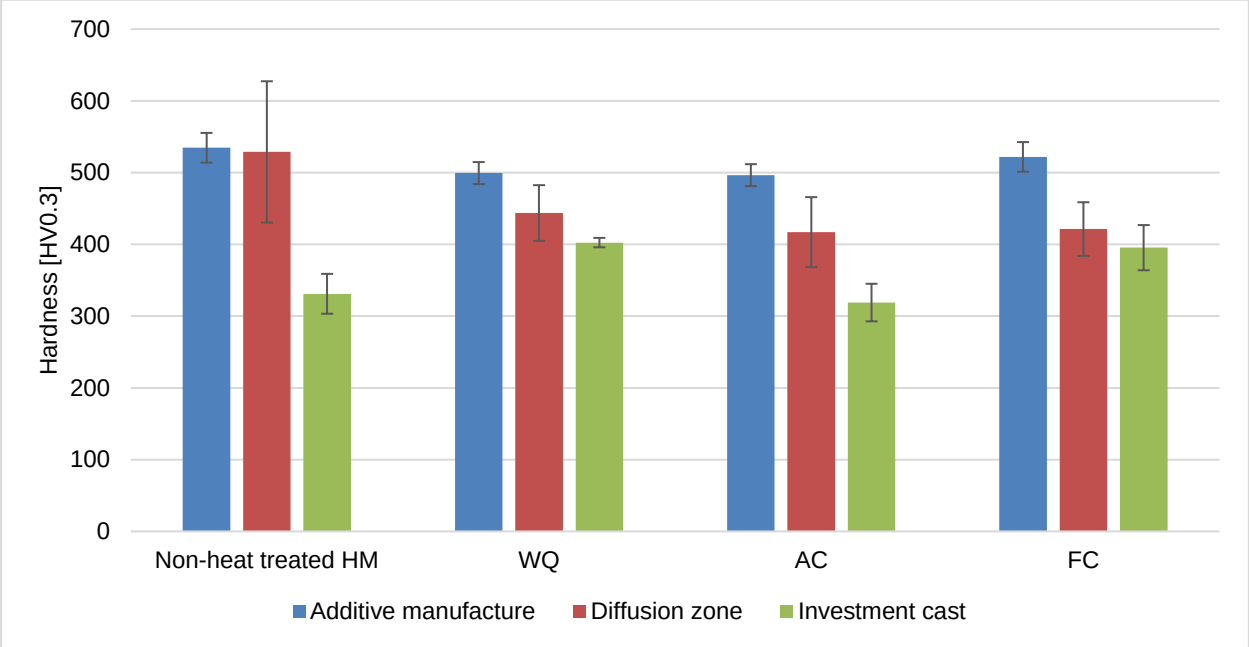

Figure 36. Average Vickers microhardness with standard deviation error bars of the non-heat treated, solution-treated and air-cooled (AC), water quenched (QW) and furnace cooled (FC) hybrid manufactured Ti6Al4V

The hardness profiles of Ti6Al4V hybrid manufactured in IC, DZ and AM regions after solution-treated and air-cooled, water quenched and furnace cooled are presented in Figure 37 The WQ specimen showed a more uniform hardness profile indicating a homogeneous structure, with the least outliers and lowest deviation in hardness from the IC to the AM region.

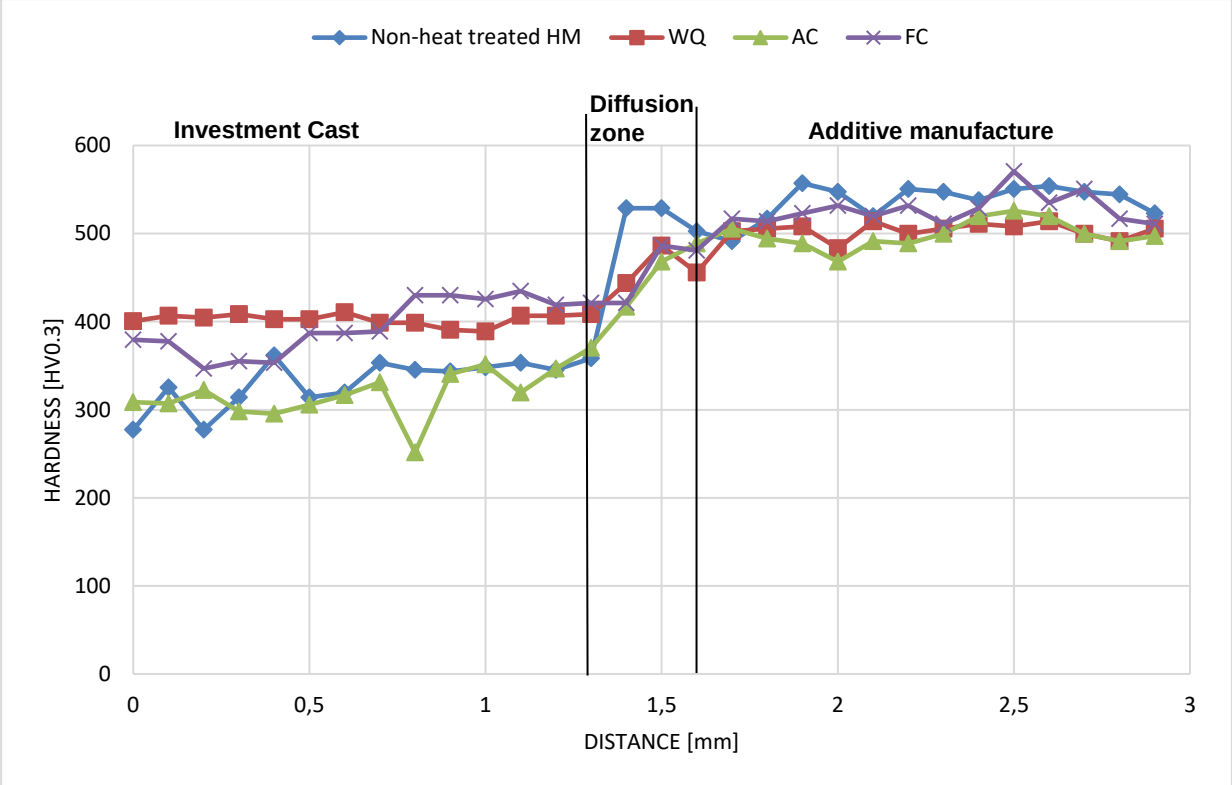

Figure 37. Hardness profiles of Ti6Al4V hybrid manufactured in IC, DZ and AM regions after solution-treated and air-cooled, water quenched and furnace cooled.

Vickers microhardness indents in the diffusion zone of hybrid manufactured specimens of non-heat treated HM, solution-treated and water quenched, solution-treated and air-cooled, solution-treated and furnace cooled are shown in Figure 38 respectively.

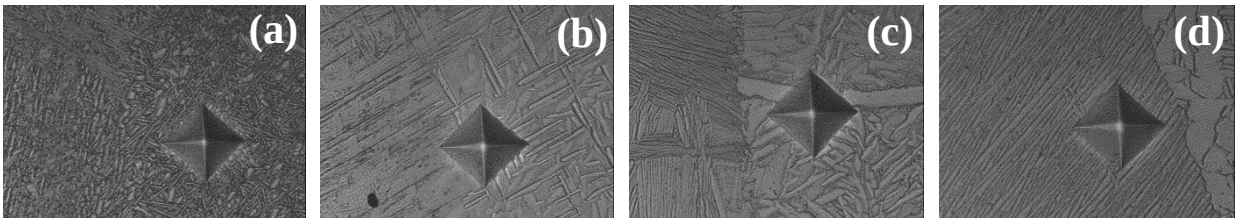

Figure 38. Vickers microhardness indents in the diffusion zone of hybrid manufactured specimens (a) Reference, (b) solution-treated and water quenched, (c) solution-treated and air-cooled, (d) solution-treated and furnace cooled

The grain size, lath size and volume fraction of α and β-phase in IC, DZ and FC regions for the solution-treated HM and AC, WQ and FC Ti6Al4V specimens are presented in Table 13. The IC region's equiaxed grains are much bigger compared to the AM columnar grains. While the WQ specimen showed the larges average grain size for the IC region. The grain sizes of the AM region appear to be unaffected by the cooling medium. The percentage of α-phase is relatively high in the AM regions.

Table 13. Grain size, lath size and volume fraction of α and β-phase in IC, DZ and FC regions for the solution-treated HM and AC, WQ and FC Ti6Al4V specimens

Quenching medium	HM region	Average Grain size (μm)	laths size (μm)	Volume fraction, %	
				α	β
	IC	1221.78	1.048	78.96	AC
AC	DZ	*	*	60.12	39.88
	AM	225.40	3.547	73.63	26.37
	IC	1699.45	*	66.13	WQ
WQ	DZ	*	*	75.78	24.22
	AM	234.35	2.464	82.24	17.76
	IC	1495.93	2.162	71.73	FC
FC	DZ	*	*	70.74	29.26
	AM	238.39	2.765	84.39	15.61

4.1.7 Furnace tensile tested

The room temperature and high temperature (400°C, 600°C, 800°C) HM Ti6Al4V tested specimens are shown in Figure 39. The temper colours of the titanium alloy specimens are observed. The room temperature tensile tested specimen had no change in colour. The specimen pulled at 400°C has a straw-yellow exterior colour, while the specimens pulled at 600°C has a dark blue outer appearance, and the specimen pulled at 800°C a brownish-black exterior.

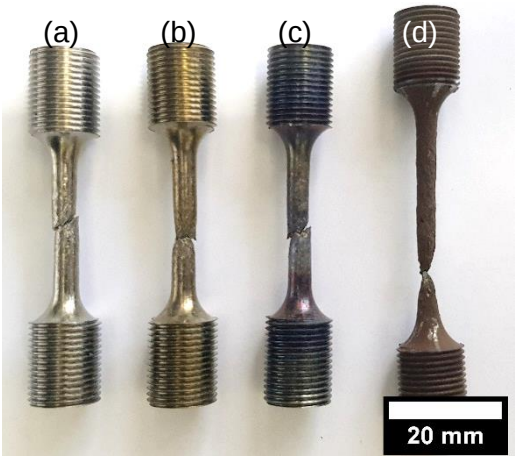

Figure 39. Tensile specimens of HM Ti6Al4V tested at (a) room temperature, (b) 400°C, (c) 600°C, and (d) 800°C

The microstructural changes in HM Ti6Al4V tensile tested specimens at 400, 600 and 800°C are presented in Figure 40 The microstructures in IC, DZ and AM regions of the HM tensile tested specimens are revealed. The specimens tested at 400°C revealed α-phase grain boundaries

with plate-like α-phase lamellae colonies in the IC region (Figure 40 (a)), however, parallel needle structure of α’ martensite is visible in the DZ (Figure 40 (b)). The AM region showed prior β columnar grain with a Widmanstätten structure of α' martensite laths (Figure 40 (c)). The specimens tested at 600°C generated α/β lamellae with thicker α-laths in the IC region (Figure 40 (d)), however, acicular α’ martensite morphology is revealed in the DZ, and the AM region showed an acicular α’ martensite basketweave structure. The IC region for the specimens tested at 800°C produced fine globular or spheroidized α-grains (Figure 40 (g)), fine spheroidized α-grains are observed in DZ (Figure 40 (h)) while the AM region showed coarser and elongated α-phase (Figure 40 (i)).

400 °C

Investment Cast | Diffusion zone | Additive manufactured

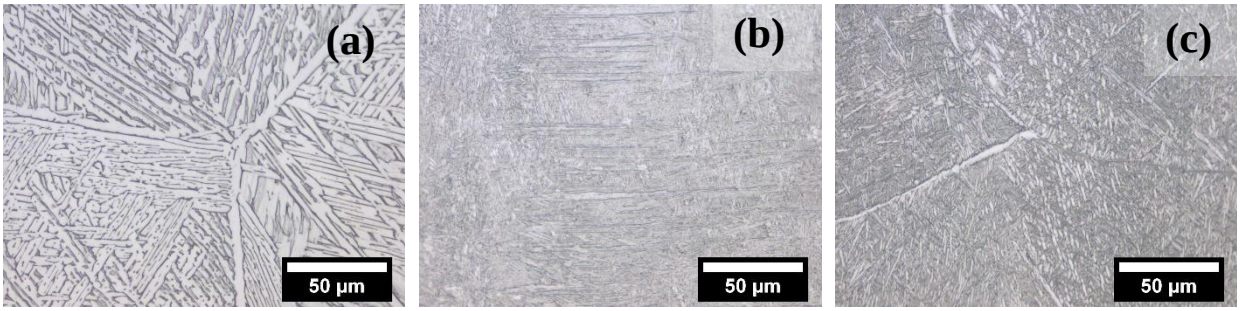

600 °C

Investment Cast | Diffusion zone | Additive manufactured

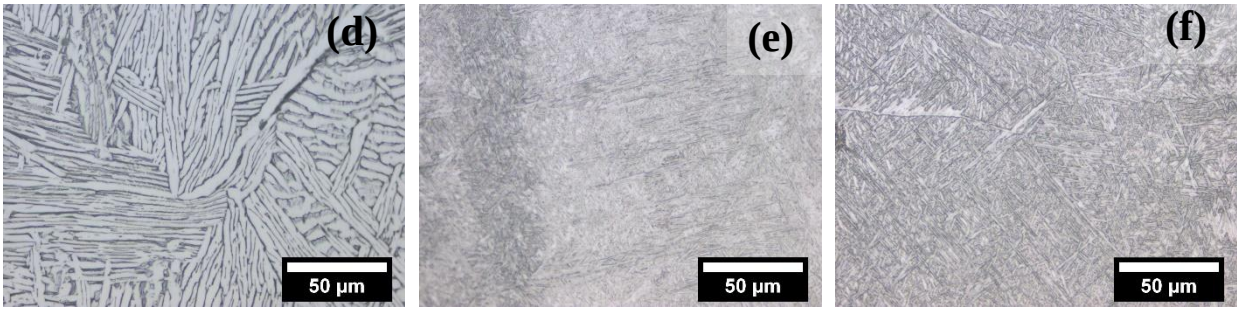

800 °C

Investment Cast | Diffusion zone | Additive manufactured

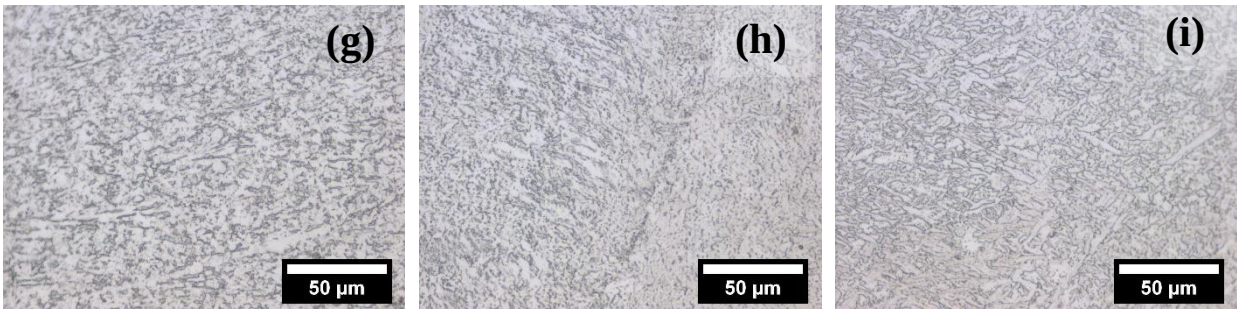

Figure 40. IC, DZ and AM regions of hybrid manufactured Ti6Al4V specimens tensile tested at (a)-(c) 400°C, (d)-(f) 600°C, and (g)-(i) 800°C.

The average Vickers microhardness for hybrid manufactured Ti6Al4V tensile specimens pulled at different elevated temperatures are presented in Figure 41. The standard deviation error bars of the IC, DZ and AM regions overlap each other, respectively for the different furnace temperatures.

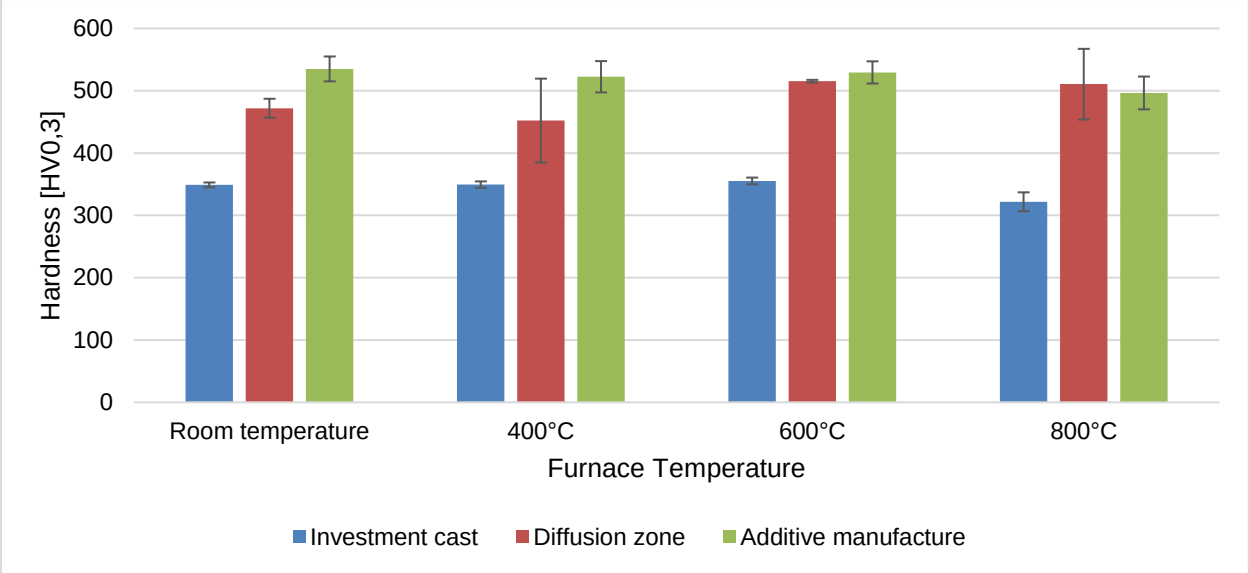

Figure 41. Average Vickers micro-hardness of fractured specimens tensile tested at different elevated temperatures with standard deviation error bars

The hardness profiles of HM Ti6Al4V alloy specimens are presented for furnace tensile tests at different temperatures in Figure 42. The graphs are very similar.

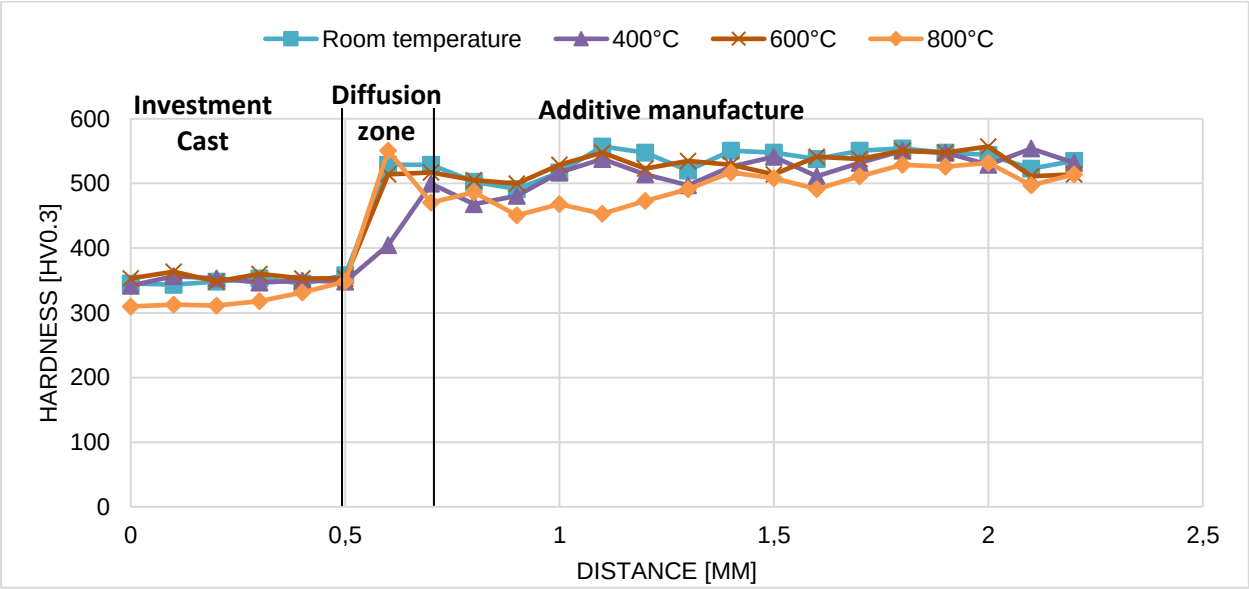

Figure 42. Hardness profiles of fractured Ti6Al4V alloy specimens tensile tested at different elevated temperatures

The microstructural quantification results for different furnace tensile testing temperatures of Ti6Al4V is presented in Table 14. The average grain size in the IC region is smaller in specimens pulled at 600°C compared to specimens pulled at lower temperatures.

Table 14. Grain size, lath size and volume fraction of α and β-phase for HM Ti6Al4V tensile tested at 400, 600 and 800°C

Furnace temperature	HM region	Average Grain size (μm)	laths size (μm)	Average %	
				α	β
	IC	1262.58	2.985	71.012	400°C
400°C	DZ	*		57.975	42.025
	AM			54.674	45.326
	IC	1035.83	3.164	71.982	600°C
600°C	DZ	*	*	62.101	37.899
	AM			56.185	43.815
	IC			68.31	800°C
800°C	DZ	*	*	71.09	28.91
	AM			67.052	32.948

4.2 Room temperature tensile properties

4.2.1 Wrought, Investment cast and Additive manufacturing

The tensile properties of specimens manufactured with different processes are presented via engineering stress-strain curves in Figure 43. The curves show Yield Strength (YS) and Ultimate Tensile Strength (UTS) for Ti6Al4V alloy specimens manufactured with AM, IC and wrought processes. The AM specimens with martensitic microstructure gave higher YS and UTS, compared to the lamellar structures of IC and wrought. The ductility of the different manufacturing processes are indicated by the slope of the stress-strain curve before YS, the AM specimens showed the lowest ductility, less than 10%, while IC and wrought specimens had higher ductility.

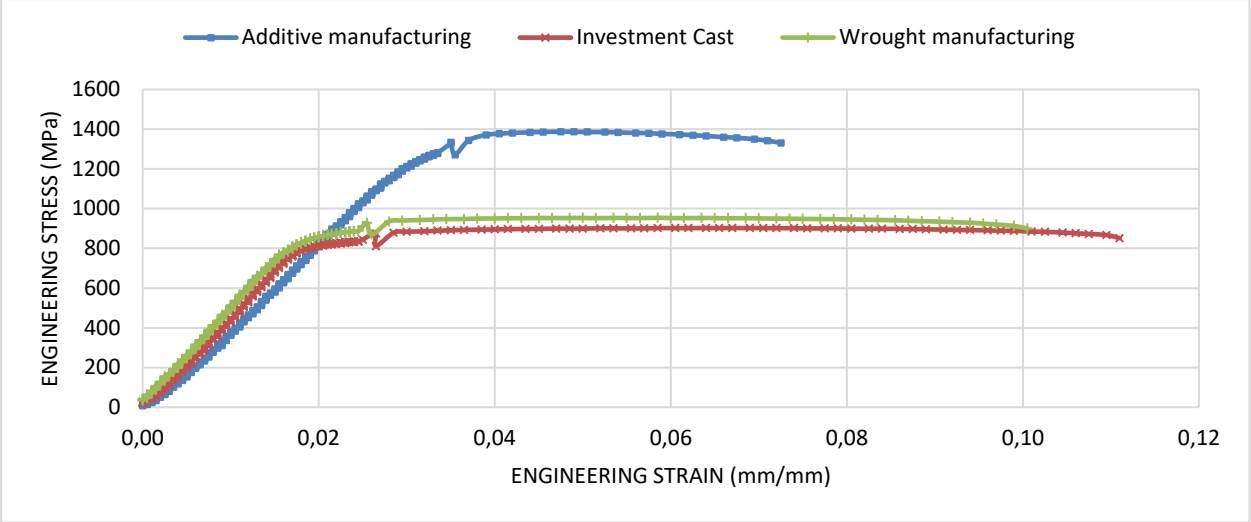

Figure 43. Engineering stress-strain curve for tensile tested Ti6Al4V alloy specimens manufactured with different processes

The strain hardening exponent (n) and strength coefficient (K) for Ti6Al4V alloy tensile specimens for different manufacturing processes are presented in Table 15. The strain-hardening exponent and strength coefficient was greater for additive manufactured tensile specimens

Table 15. Ti6Al4V strain hardening exponents and strength coefficients for various manufacturing processes

Manufacturing process	Strain-hardening exponent (n)	Strength coefficient (K) [MPa]
Wrought	0.0539	1175.3
Investment Cast	0.0737	1180
Additive manufactured	0.0842	1873

The strain hardening curve of Ti6Al4V specimens manufactured with various processes are shown in Figure 44. The strain hardening curves all indicate a decrease in strain hardening rate as the true strain increases. The martensitic microstructure of the AM specimen had the highest strain hardening rate, compared to the lamellar structures of IC and wrought specimens.

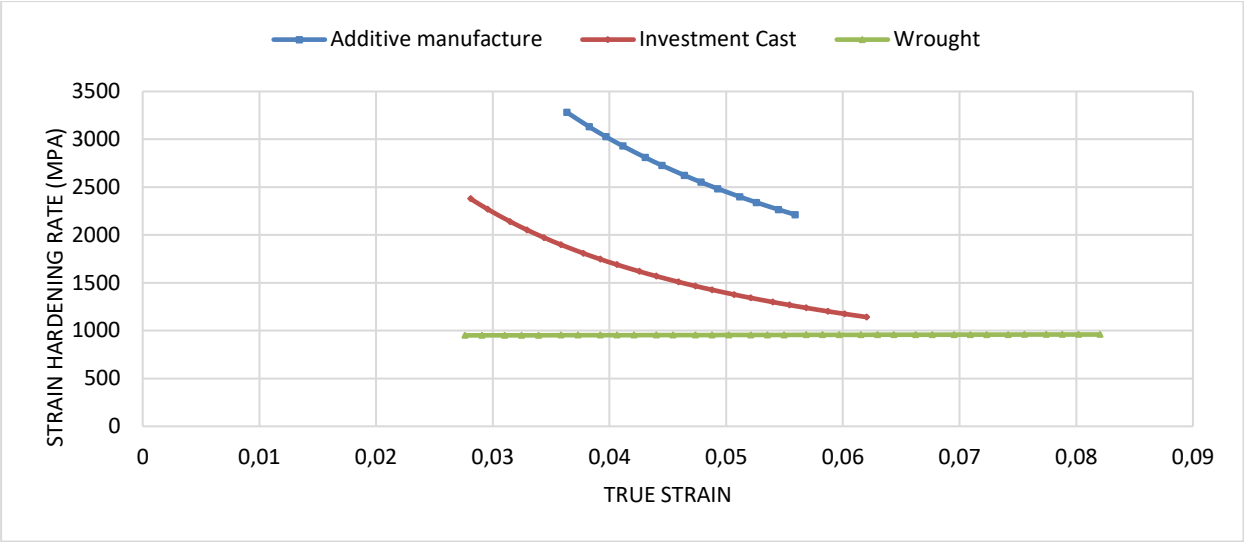

Figure 44. Hardening curves for tensile tested Ti6Al4V alloy specimens manufactured with different processes

4.2.2 Hybrid manufacture

Ti6Al4V HM specimens with the top two surface preparations, as determined in substudy 2 were tensile tested, the results are presented in Figure 43. Both specimens, prepared with ablation and just-cut surfaces, fractured in the IC region of the HM specimen. The tensile properties (YS and UTS) of specimens with ablation and just-cut surface preparations are very similar to each other and to the IC specimens in section 4.2.1. The slopes of the stress-strain curves indicating the percentage elongation are similar for both surface preparation techniques.

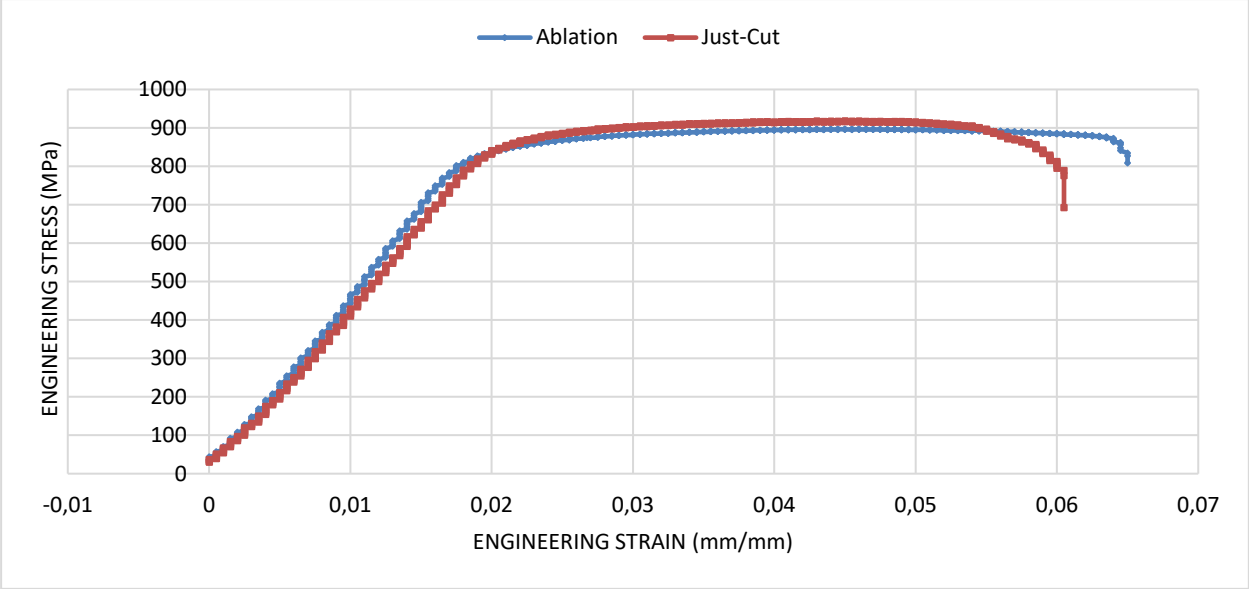

Figure 45. Engineering stress-strain curve for tensile tested hybrid manufactured Ti6Al4V alloy specimens with different surface preparations

The strain hardening exponent (n) and strength coefficient (K) for HM Ti6Al4V tensile specimens with different surface preparations applied to the IC side prior to AM are presented in Table 16. The strain-hardening exponents and strength coefficients for the two different surface preparations were alike.

Table 16. Hybrid manufactured Ti6Al4V strain hardening exponents and strength coefficients for various surface preparations

Manufacturing process	Strain-hardening exponent (n)	Strength coefficient (K) [MPa]
Ablation	0.1038	1302.9
Just-Cut	0.1069	1346.3

The strain hardening curves are given in Figure 46. The curves are comparable and indicate that the strain hardening rate lowers with an increased true strain.

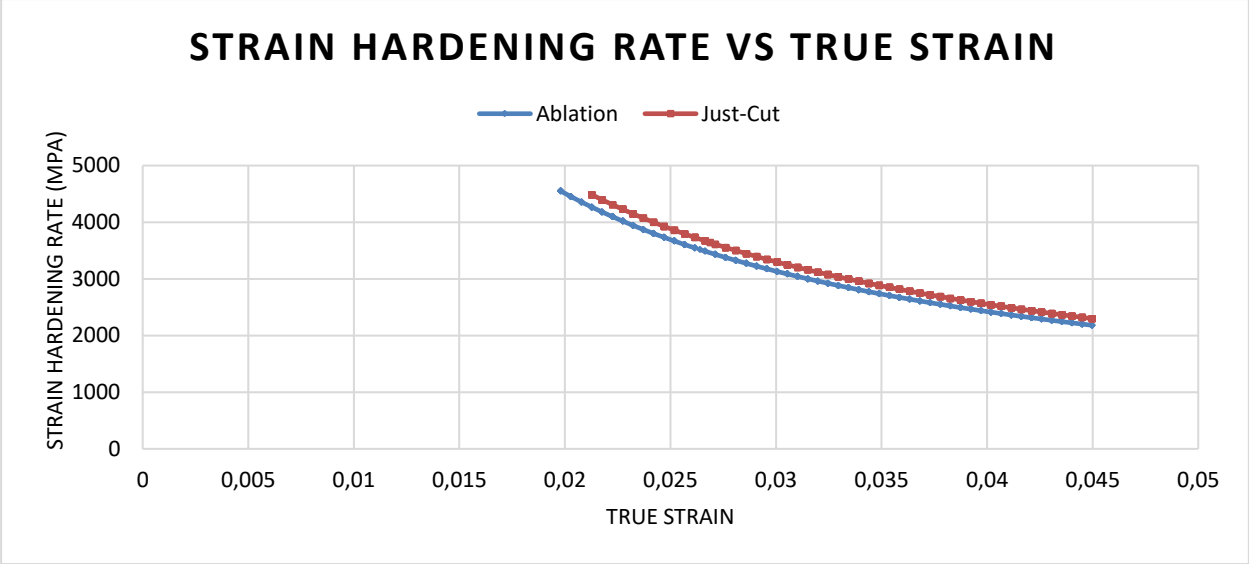

Figure 46. Hardening curves for tensile tested hybrid manufactured Ti6Al4V alloy specimens with different surface preparations

4.2.3 High-temperature tensile properties

The tensile properties of Ti6Al4V hybrid manufactured furnace tensile tested specimens at temperatures of 400°C, 600°C, and 800°C are presented in Figure 47. All specimens fractured in the IC region of the HM specimen during furnace tensile testing. There is a decrease in YS and UTS, from room temperature tensile testing to furnace tensile testing at elevated temperatures. As the furnace's temperature increases, the YS and UTS decrease. The HM specimens pulled at 800°C gave the lowest YS and UTS. The specimens tested at 400°C and 600°C, showed a similar ductility much lower than the specimens pulled at 800°C.

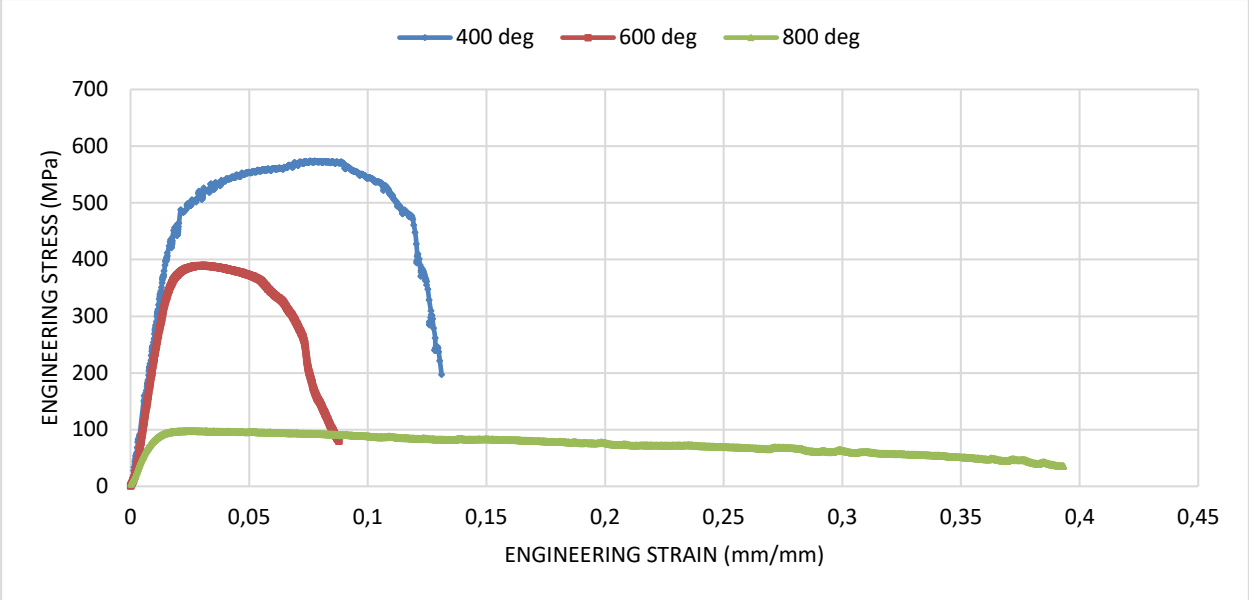

Figure 47. Engineering stress-strain curve for hybrid manufactured Ti6Al4V alloy specimens furnace tensile tested at different elevated temperatures

The strain hardening exponent and strength coefficient for HM furnace tensile tested specimens are given in Table 17. The strain hardening exponent and strength coefficient decreases with an increase in furnace temperatures.

Table 17. Hybrid manufactured Ti6Al4V strain hardening exponents and strength coefficients for various furnace tensile testing temperatures

Furnace temperature	Strain-hardening exponent (n)	Strength coefficient (K) [MPa]
400°C	0.1561	921.99
600°C	0.0993	569.75
800°C	0.0111	103.66

Figure 48 shows the hardening curve as the strain hardening rate over the true strain for furnace tensile tested specimens at different elevated temperatures. The specimen tested at 400°C had the highest strain hardening rate, however, it's much lower than the HM specimen pulled at room temperature.

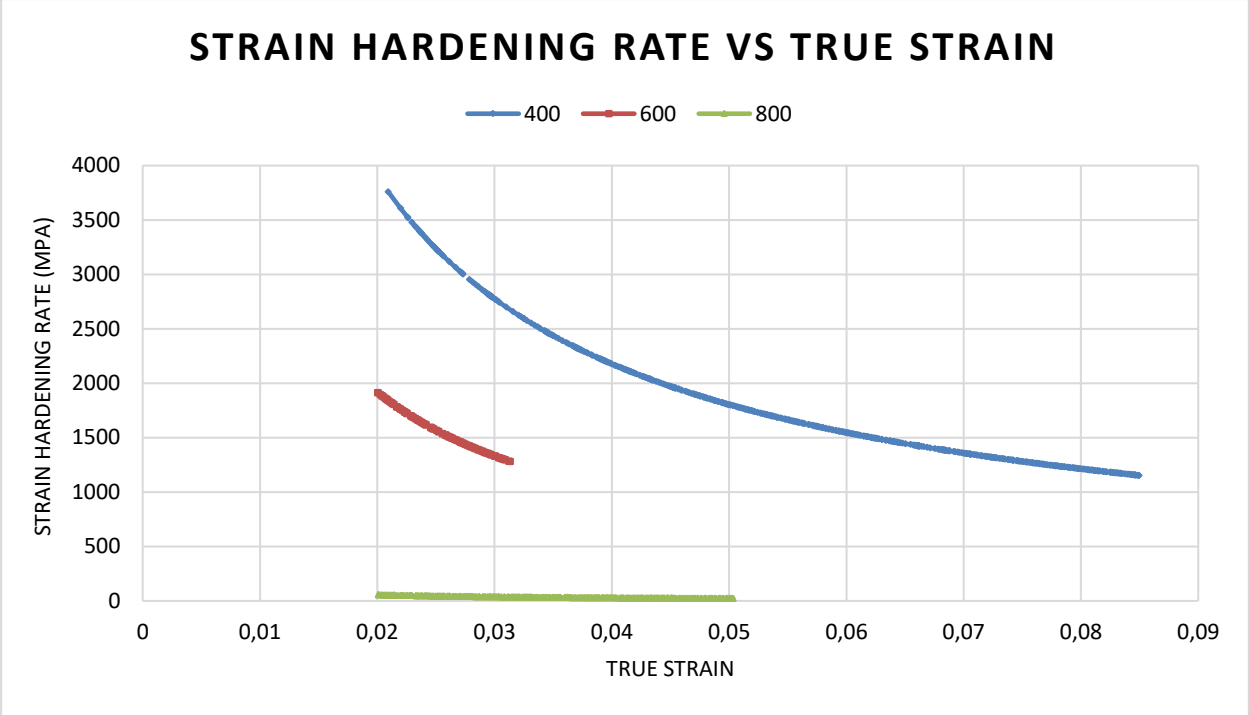

Figure 48. Hardening curves for hybrid manufactured Ti6Al4V alloy specimens furnace tensile tested at different elevated temperatures

4.3 Fractography

4.3.1 Wrought, Investment cast, Additive manufacture

The tensile fractures of wrought, IC and AM Ti6Al4V tested specimens are shown in Figure 49. The wrought and IC fractures have somewhat necking (Figure 49 (a), (b)), while the AM fracture has no necking (Figure 49 (c)).

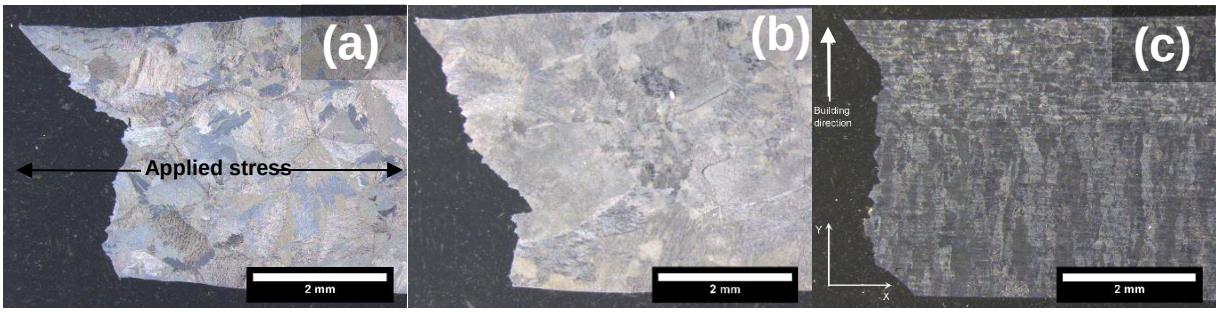

Figure 49. Stereo micrographs of cross-sectioned tensile tested specimens manufactured by (a) wrought, (b) IC, and (c) AM processes

Fracture cross-sections of the wrought, IC and AM Ti6Al4V are given in Figure 50. Figure 50 (a) and (b) show kinking of α/β lamellae, the lamellar lines tend to deflect towards a fractured edge, in the ductile IC and wrought structure especially in the necking region of the tensile specimens. Figure 50 (c) illustrated a coalescence of microcracks along α'-laths in the partial martensitic AM structure.

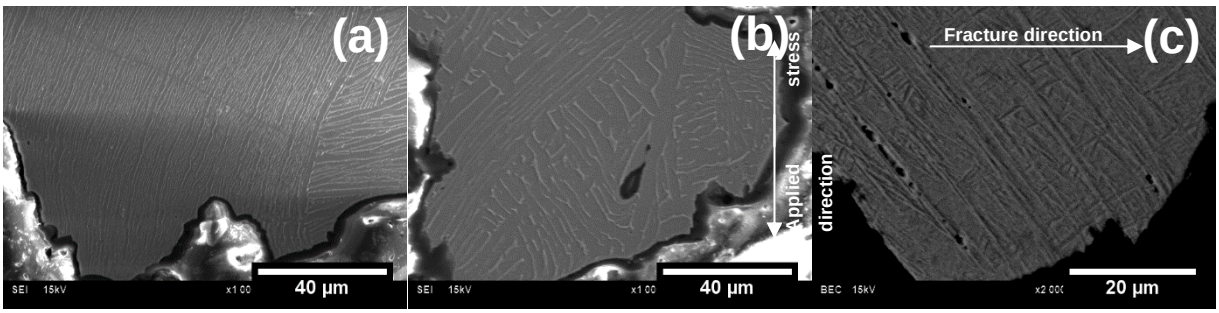

Figure 50. SEM micrographs showing cross-sectioned fracture regions of tensile tested specimens (a) wrought, (b) IC, and (c) AM tensile test specimens

The fracture surfaces of the wrought, IC and AM are shown in Figure 51. The wrought and AM fracture surfaces (Figure 51 (a) and (c), respectively) showed relatively rougher surfaces, while the IC fracture surface appeared to be almost flat (Figure 51 (b)).

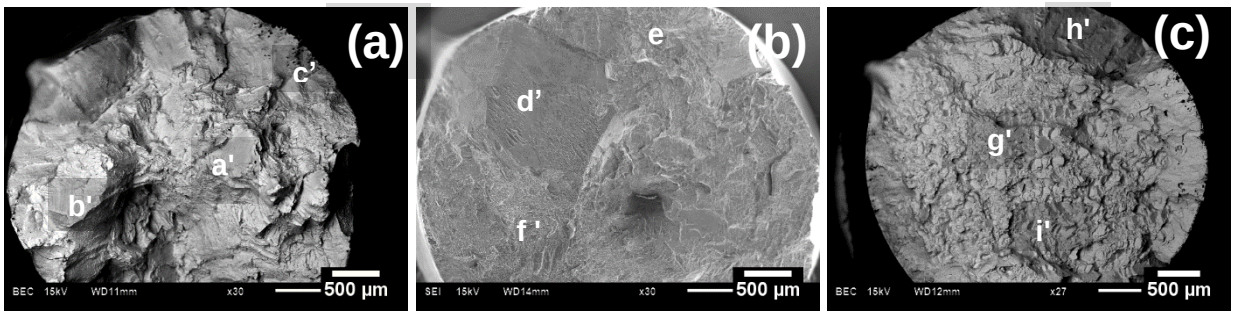

Figure 51. The fracture surfaces of (a) wrought, (b) IC, and (c) AM Ti6Al4V

Figure 52 gives a higher magnification of the numbered areas in Figure 51.

The fracture surfaces of a specific area as shown in Figure 51 of the wrought, IC and AM Ti6Al4V are given in Figure 52 (a)-(c), Figure 52 (e)-(f) and Figure 52 (g)-(i), respectively. The wrought and IC fracture surfaces revealed transgranular quasi-cleavage surface areas (larger in IC fracture) with ridges, microvoids and laths. However, transgranular quasi-cleavage surface areas were relatively small (size of grains) in the AM fracture surface.

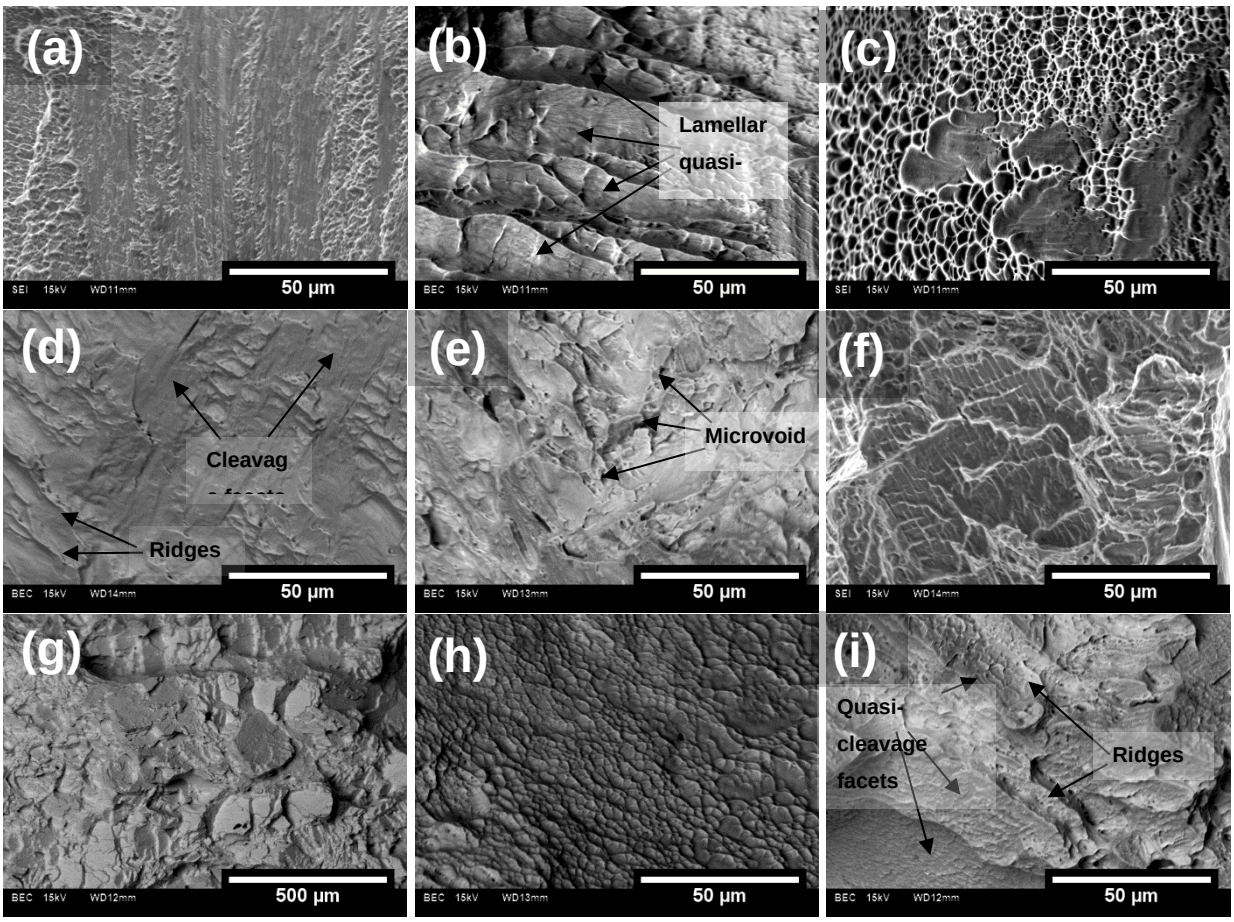

Figure 52. Fracture surfaces of a)-c) Wrought, d)-f) IC and g)-i) AM Ti6Al4V tensile specimens

4.3.2 Hybrid manufacture

The HM tensile test specimens were prepared with ablation and just-cut surface preparation techniques on the IC side, prior to AM. Three specimens received ablation treatments and three had the oxide layer cut-off (just-cut). Figure 53 shows the six HM tensile specimens after fracture. Specimens (a)-(c) received ablation treatment and resulted in; one fracturing in the AM region (Figure 53 (a)), one in the DZ (Figure 53 (b)), and one fracturing in the IC region (Figure 53 (c)). The HM specimens with just-cut surface preparations resulted in similar conditions, where each fracture occurred in a different region. Figure 53 (d) occurred in the IC region, Figure 53 (e) in the DZ and Figure 53 (f) in the AM region.

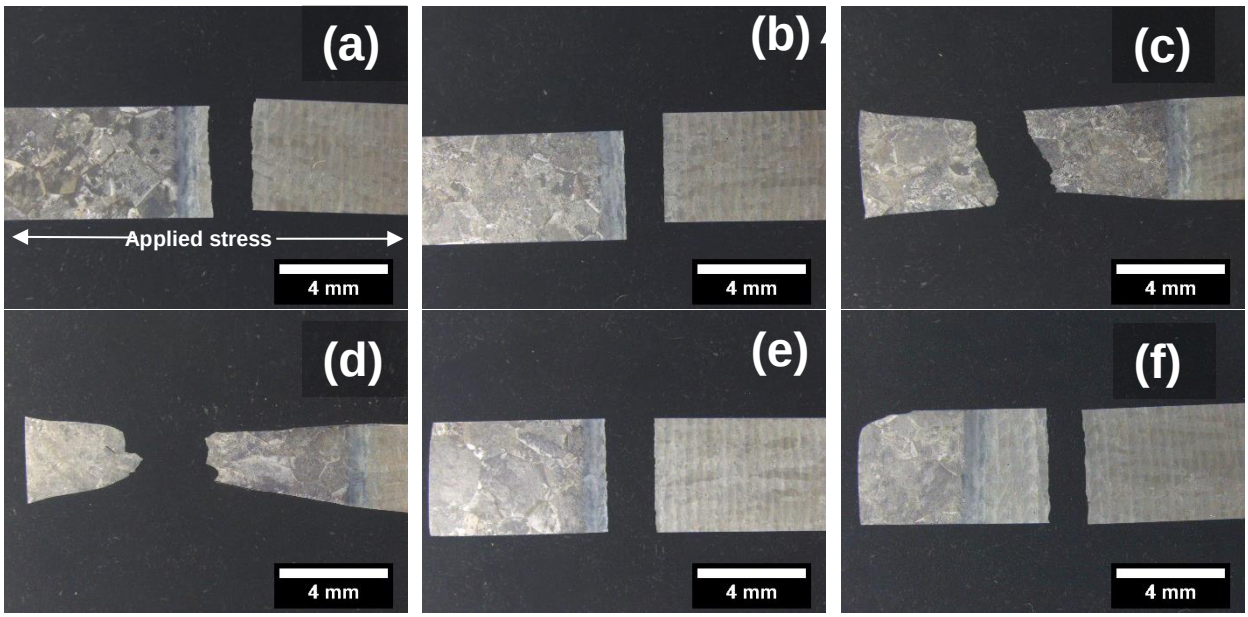

Figure 53. Stereo micrographs of cross-sectioned tensile tested specimens with surface preparations (a)-(c) Ablation, and (d)-(f) just-cut

Figure 54 shows the cross-section view of the fractures, the labelling agrees with the labelling in Figure 53, thus the fracture showed in Figure 54 (a) is of the specimen in Figure 53 (a). Fractures in Figure 54 (a) and (f) shows straight secondary cracks parallel to the fracture profile, cutting through grain boundaries. The fracture in Figure 54 (b) occurs on a grain boundary, while the fracture in Figure 54 (e) which is also in the DZ, looks similar to fractures in Figure 54 (a) and (f). These fractures are brittle granular fractures. Fractures in Figure 54 (c) and (d) occurred in the IC region and shows rougher fracture profiles, with the fractures propagating along the α-laths. The α-laths are also observed to kink towards the fracture, the fractures are ductile transgranular fracture.

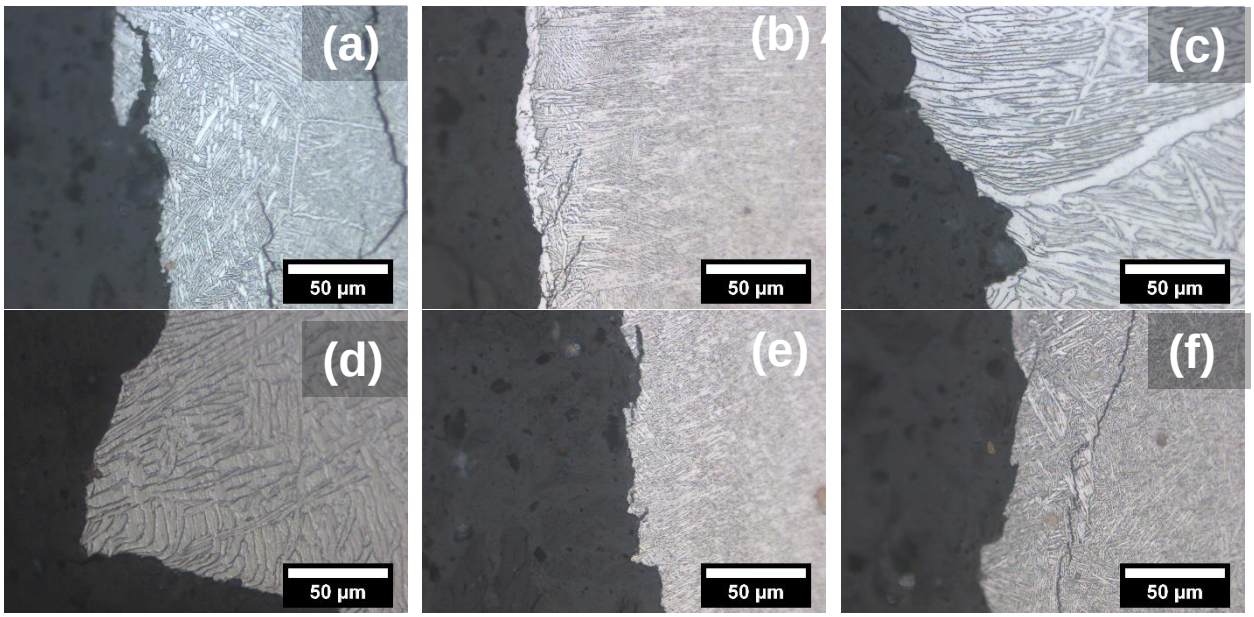

Figure 54. Stereo micrographs of cross-sectioned fracture regions of tensile tested specimens with surface preparations (a)-(c) Ablation, and (d)-(f) just-cut

The fractured surfaces of HM tensile specimens are presented in Figure 55. The labelling matches the previous figure's labelling, thus specimens in Figure 55 (a) to (c) received ablation surface preparations on the IC rod's surface prior to AM, and Figure 55 (d) to (f) was just-cut to remove the oxide layer. Figure 55 (a), (b), (e) and (f) has flat surfaces, with (b) showing alternating fracture modes of granular fractures and cleavage fractures. Figure 55 (c) and (d) shows a rougher surface for the fractures that occurred in the IC regions of the HM specimen.

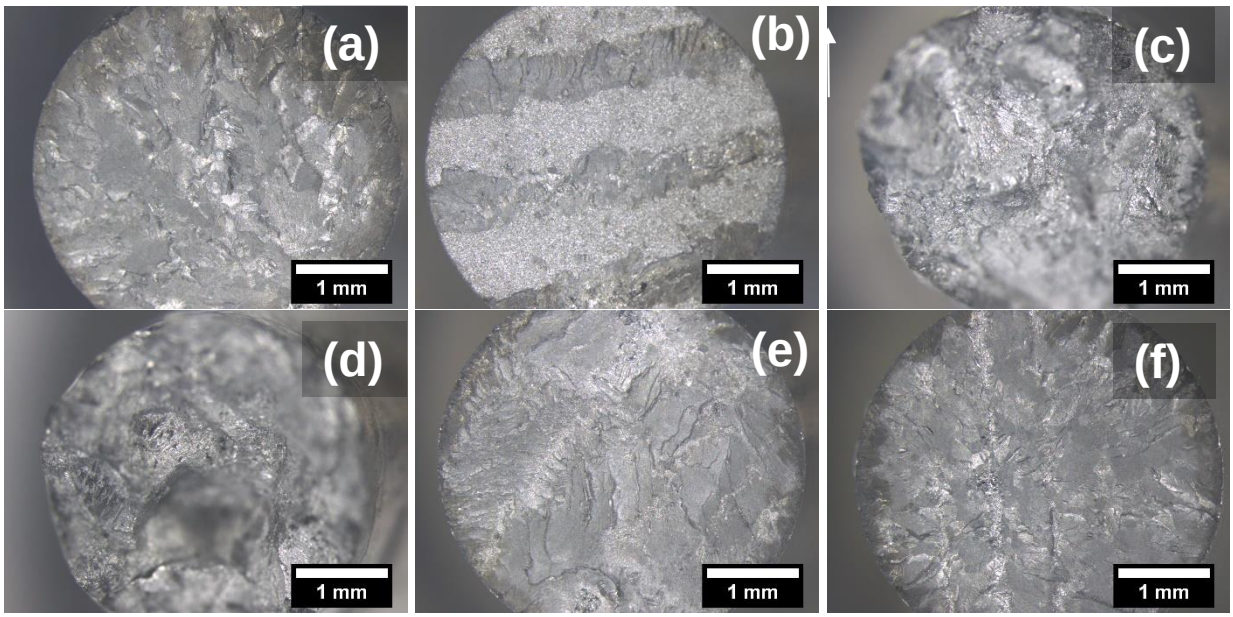

Figure 55. Stereo micrographs showing the fractured surfaces of hybrid manufactured and tensile tested specimens, the specimens were prepared with (a)-(c) Ablation, and (d)-(f) Just-cut, prior to additive manufacturing

SEM micrographs of fractured surfaces in Ti6Al4V HM specimens as seen in Figure 53-55 are presented in Figure 56. Figure 56 (a), (e) and (f) shows a similar crystallographic stage I-like crack propagation in α-martensite. Figure 56 (c) and (d) shows a typical ductile fracture of fine equiaxed dimples. While Figure 56 (b) shows two different fracture modes.

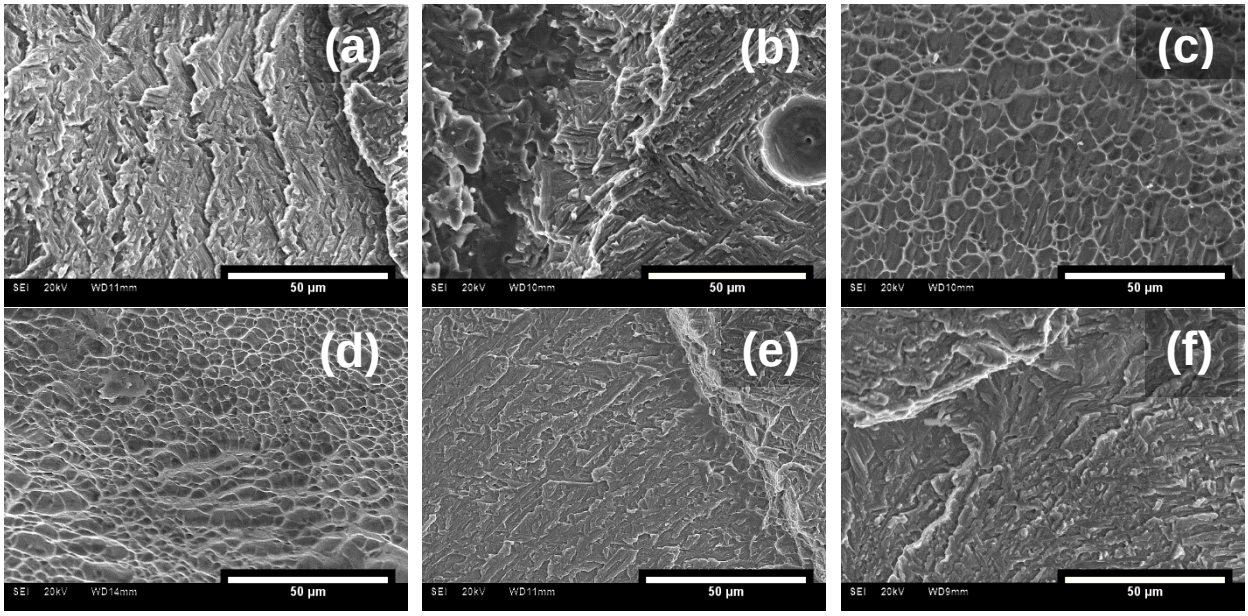

Figure 56. Fracture surfaces of Ti6Al4V hybrid manufactured specimens with (a)-(c) Ablation, and (d)-(f) just-cut surface preparations prior to additive manufacturing

Figure 57 shows higher magnifications of the two different fracture modes in Figure 56 (b). Figure 57 (a) shows an intergranular fracture, and Figure 57 (b) a crystallographic fracture in the α-martensite.

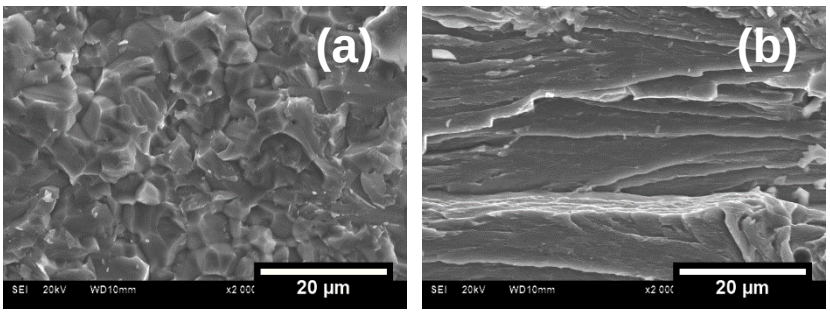

Figure 57. Two fracture modes found in a single specimen prepared with Ablation

The alternating regions in the tensile tested specimen prepared with ablation as seen in Figure 57, are analysed using EDS. The EDS results are presented in Figure 58 and Table 18. The results show no significant change in composition over the different regions.

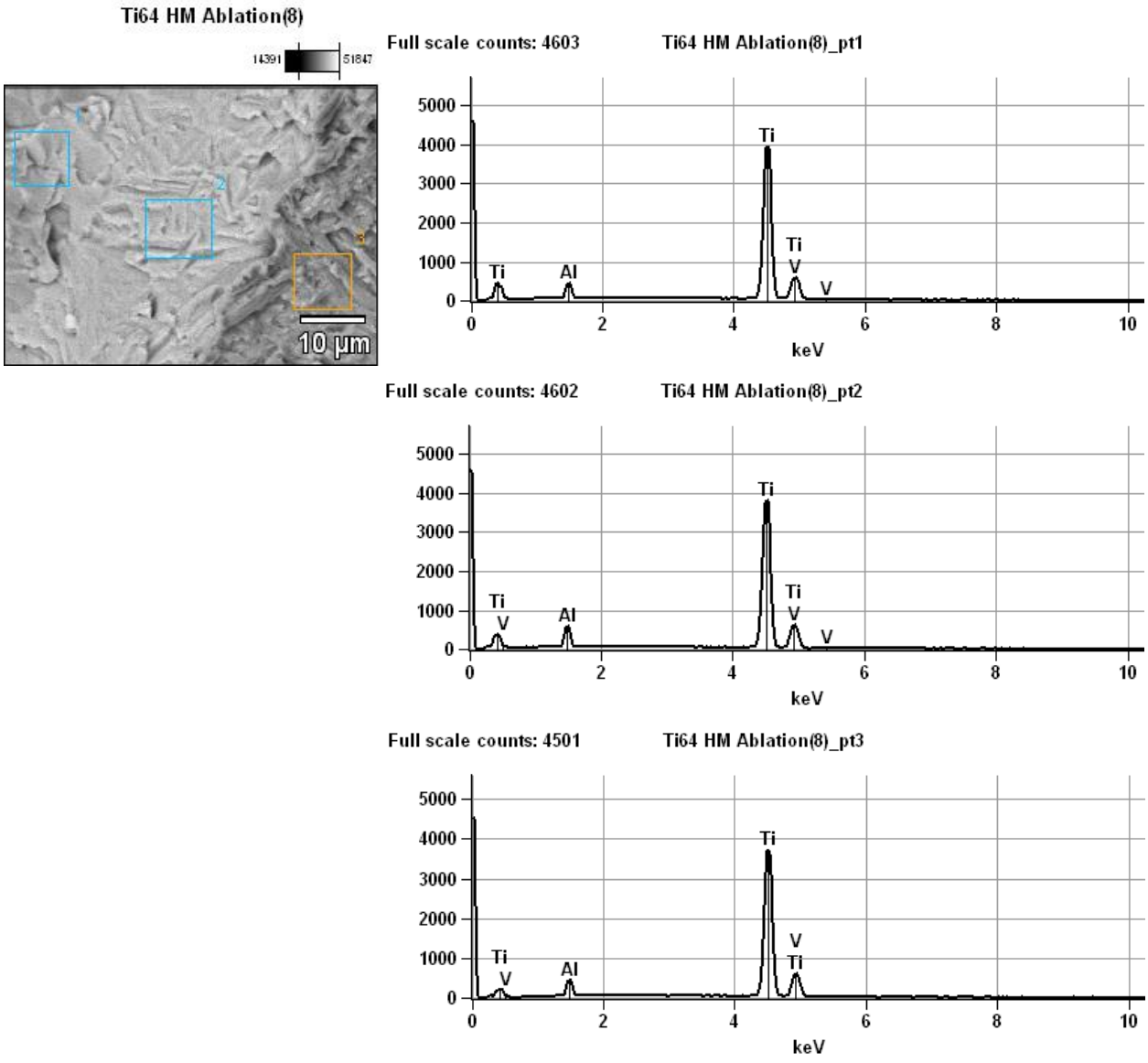

Figure 58. EDS analysis of different fracture modes in the same specimen

Table 18. EDS analysis of different fracture modes in the ablation 2 surface preparation HM Ti6Al4V tensile specimen

	Al-K	Ti-K	V-K
Ti6Al4V HM Ablation 2_pt1	4.23	92.75	3.02
Ti6Al4V HM Ablation 2_pt2	6.01	90.11	3.87
Ti6Al4V HM Ablation 2_pt3	4.96	91.22	3.83

4.3.3 Furnace tensile tested

The Ti6Al4V HM furnace tensile tested specimens after fracture are presented in Figure 59. The specimens pulled at 400°C shows some necking (Figure 59 (a)), specimens pulled at 600°C shows barley any necking (Figure 59 (b)), and specimens pulled at 800°C shows extreme necking

(Figure 59 (c)). In Figure 59 (d)-(e) the three different regions of the HM specimen can be seen. All of the specimens fractured in the IC region.

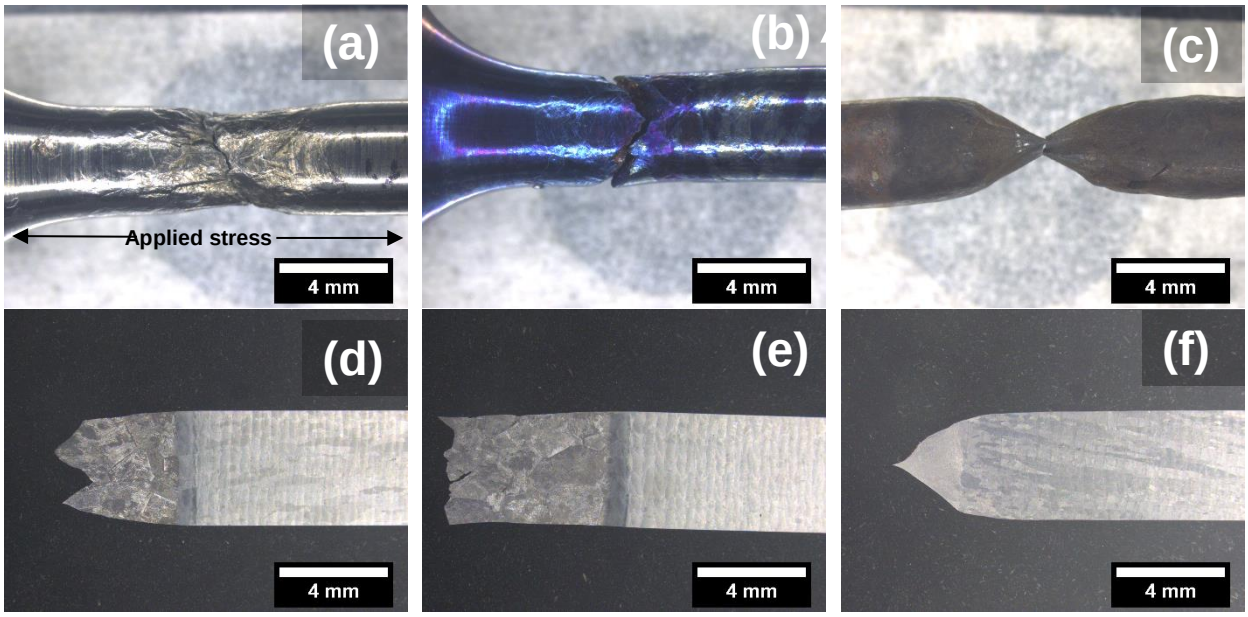

Figure 59. Stereo micrographs of furnace tensile tested specimens at (a) 400°C, (b) 600°C, and (c) 800°C. Cross-sectioned furnace tensile tested specimens at (d) 400°C, (e) 600°C, and (f) 800°C.

Fractures in Figure 60 (a) and (b) shows rougher fracture profiles, with the fractures propagating along the α-laths. The α-laths are also observed to kink towards the fracture, the fractures are ductile transgranular fracture. The fracture in Figure 60 (c) occurred at 800°C and shows a great area reduction, the fracture is observed as extremely ductile.

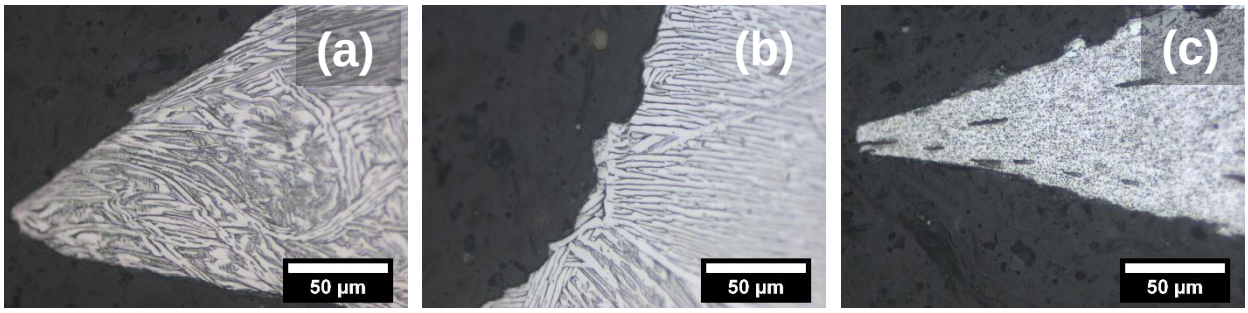

Figure 60. Optical micrographs of cross-sectioned fracture regions of furnace tensile tested specimens at (a) 400°C, (b) 600°C, and (c) 800°C.

The fractured surfaces of HM furnace tensile tested specimens are presented in Figure 61. The three fractures reveal three different fracture modes, Figure 61 (a) shows a rougher surface, and Figure 61 (b) shows an intergranular fracture with grain shapes reminiscent of the ideal grain, while in Figure 61 (c) no fracture mode can be observed, only a great reduction in area.

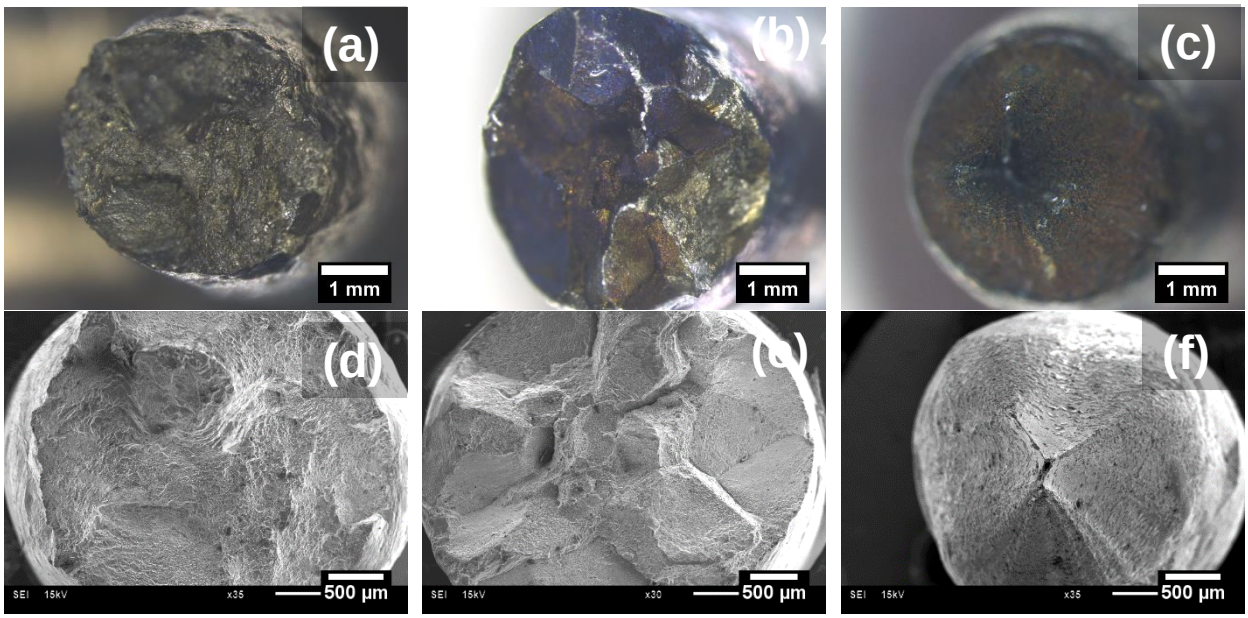

Figure 61. Stereo micrographs showing the fractured surfaces of hybrid manufactured and tensile tested specimens, the specimens were prepared with (a)-(c) Ablation, and (d)-(f) Just-cut, prior to additive manufacturing

SEM micrographs of fractured surfaces of Ti6Al4V HM furnace tensile tested specimens are presented in Figure 62. Figure 62 (a) and (b) shows quasi-cleavage facets while (c) indicates a small cross-sectional area fracture.

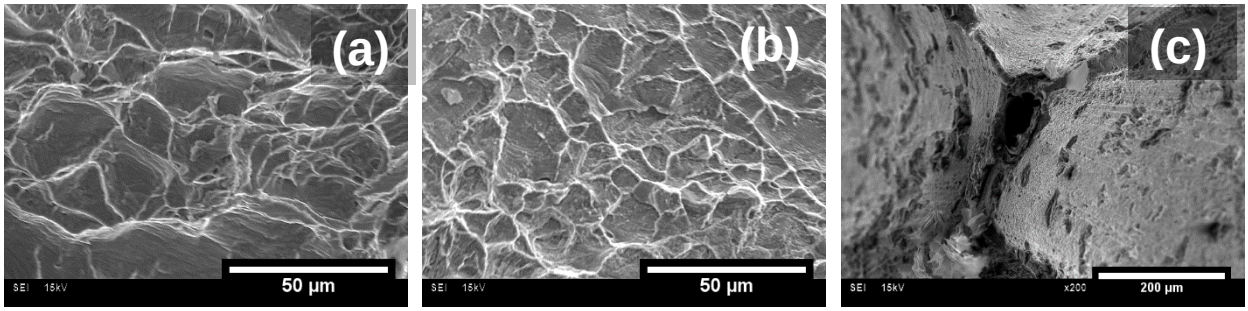

Figure 62. Fracture surfaces of Ti6Al4V hybrid manufactured specimens with (a)-(c) Ablation, and (d)-(f) just-cut surface preparations prior to additive manufacturing

CHAPTER 5. DISCUSSION

The evaluation of the results is discussed in this chapter. The discussion is based on the microstructural evolution, the tensile properties of various microstructures and the fractography analysis on how and why the tensile fracture occurred.

5.1 Microstructural evolution

Microstructural characterisation of the Ti6Al4V alloy material that is used was established via EDS analysis. The white areas showed higher vanadium content, while the darker areas had more Aluminium. Vanadium is a beta (β) stabiliser and Aluminium an alpha (α) stabiliser, therefore the white areas on the SEM micrographs are β-phase and the dark areas α-phase. The SEM uses inverted colours in contrast to the optical microscope and stereo microscope, thus on the optical and stereo microscope images the white areas are α-phase and the dark β-phase.

The transformed β and α -phase lamellae colonies in the wrought Ti6Al4V, formed as a consequence of the heat treatment above the β-transus (1050°C for 30 min). A very typical microstructure for the two-phase (α+β) titanium alloys [51]. The columnar grains of the additive manufactured (AM) microstructure were oriented in the building direction and crossing multiple-layer bands. The grain growth direction is counter to the heat flux. Since heat rapidly dissipates into the substrate (horizontally) when the process starts, forcing the grains to grow vertical [5]. The re-melting also allows for epitaxial grain growth [52], [53]. The smaller grains and lath thickness in the wrought microstructure led to a higher hardness compared to the IC microstructure's hardness [5],[41],[54]. This is in agreement with the Hall-Petch equation, stating that a finer structure leads to higher hardness. However, the AM Ti6Al4V with partial martensitic microstructures proved to be superior in hardness. The high hardness of AM specimens is attributed to the presence of partial martensitic structure due to the high cooling rate during the 3D printing process [55].

The hybrid manufacturing (HM) specimen's microstructure revealed no significant changes in the AM and IC regions from the reference AM and IC specimen's microstructures, the only difference was an additional diffusion zone (DZ). The acicular α' martensitic morphology in the DZ formed due to diffusion-less β to α' transformation [56]. The hardness of the DZ is the median of the IC and AM regions.

The influence of prior surface preparations on microstructural defects of HM Ti6Al4V components were evaluated based on the diffusion between the AM and IC. By comparing rough and smooth surfaces as obtained from the various surface preparation techniques. It can be concluded that a

smooth, clean surface on the IC rod prior to AM leads to a better diffusion. The uneven diffusion bonding of rough surfaces can be attributed to the presence of coarse peaks that result in smaller contact area and a concentrated melted pool [57]. The ablation, just-cut, and polished surface preparation techniques produced ideal results, however, to polish a component prior to completion would prove to be difficult and time-consuming and labour intensive. A CNC milling machine can be automated to remove the oxide layer on a component producing a *just-cut* surface. Ablation also uses an automated process. Thus, the top two surface preparation techniques were ablation and just-cut. These two surface preparations were used to further investigate the HM component, by preparing HM tensile testing specimens.

The solution-treatment (1050°C for 2 hours) of the HM specimens transformed the (α+β) –phase to a β-phase structure. The three different cooling rates that were used, air cooling (AC), water quenching (WQ) and furnace cooling (FC) transformed the β-phase back to the initial (α+β) –phase. However, the various cooling rates used changed the proportion, morphology, size and shape of α and β phases.

The Ti6Al4V HM alloy specimens that were solution-treated and AC, transformed α/β lamellae to β- phase, the relatively slow AC rate transformed the β- phase to very fine α/β lamellae. Colonies of very fine α/β lamellae were produced in the IC region, and a partial martensitic basketweave structure with thick α- grain boundaries were formed in the AM region. The WQ is almost instantaneous and reduces the transformation time of the β-phase and β-grains. The high cooling rate led to a fully martensitic phase in the IC region, a partial martensitic phase in the DZ, and an α' martensitic basketweave structure in the AM region. The slow FC rate produced very fine α/β lamellae colonies in the IC region and a partial martensitic basketweave structure in the AM region. FC leads to Ti_3Al being formed more easily as opposed to using AC, this could explain why FC produces a higher hardness than AC [9]. The lamellae morphologies in the IC regions of AC and FC showed a heterogeneous microstructure with many due to different sizes of colonies and α-laths. The fully martensitic structure found in the IC region of the WQ specimen gave the highest increase in hardness when compared to the non-heat treated specimen. The WQ specimen also had to lowest deviation in hardness over the different regions of the HM specimen and produced a stable hardness-profile. All specimens (non-heat treated, AC, WQ and FC) had similar partial martensitic basketweave structures in the AM regions which also led to similar hardness in the AM regions. The AM regions had the highest hardness compared to the IC region and DZ. In a HM component homogeneity is one of the key factors in determining a suitable cooling rate, thus the WQ cooling rate is a suitable cooling rate for HM components.

The furnace tensile tests produced different temper colours, the colours are associated with the testing temperature. The specimens pulled at 800 °C turned brownish-black. The colour change is linked to a thick and porous multilayer oxide casing. Accordingly, the colour change can be used to assess the quality of the specimen in terms of operating use. There is no real change in microstructure between the room temperature, 400 °C and 600 °C tensile specimens, which gave α/β lamellae colonies in the IC regions, acicular α' martensite in the DZ and Widmanstätten α-martensite in the AM region. However, at 800 °C the microstructure changes to spheroidezed α-grains in the IC and DZ regions, with coarse elongated α-phase in the AM region. There is no change in hardness based on the various furnace tensile test temperatures, this could be ascribed to the similar microstructures obtained from the furnace temperatures being below the β-transus and furnace cooled

5.2 Tensile properties

By comparing the wrought, IC and AM tensile properties, it is evident that the α' martensitic microstructure of the AM led to higher YS (Yield Strength) and UTS (Ultimate Tensile Strength) values. The coarse α-laths in the α/β lamellae morphology reduced the strength of the wrought and IC. However, the wrought had a slightly higher YS and UTS than IC due to its smaller α-laths and grain sizes. This agrees with the Hall-Petch equation indicating that smaller grain sizes promote higher YS and UTS [41]. Previous research also indicated higher YS and UTS for martensitic microstructures compared to lamellar microstructures [9], [10], [40]. The lamellar structures had higher ductility.

The strain hardening exponent (n) and strength coefficient (K) indicates higher values for the AM's α' martensitic microstructure, followed by IC and then wrought. The strain hardening curve is determined from the plastic deformation section of the stress-strain curve, thus it describes the stress needed to deform the material further. When plastic deformation occurs, dislocations form, move, piles up and becomes entangled. The entanglement results in less mobility and strengthening of the material, thus strengthening by deformation. However, while the strength is increasing the ductility is decreased. The strain-hardening exponent or n-value is a measurement of the materials ability to gain strength while deforming [58], a high strain-hardening exponent represents an elastic solid, while a low value refers to a plastic solid. The n increases with an increase in ductility, thus for higher ductility in the wrought specimens a lower n is achieved.

Much lower strain-hardening curves were obtained for the HM specimens with ablation and just-cut surface preparations, which followed the low percentage elongations obtained.

When the Ti6Al4V tensile specimens are pulled at elevated temperatures, the dislocation formed can rearrange a little, causing the material to strengthen. The strain-hardening exponent decreases with increasing furnace tensile test temperatures. The specimens pulled at 800 °C presented the lowest strain-hardening exponent and strength coefficient. This is in agreement with previous research, concluding that when the temperature increases the tensile properties decrease, due to an increase in the mobility of dislocations [59].

5.3 Fractography

The cross-section view of the wrought, IC and AM tensile tested specimens compares well with the microstructures observed. The AM specimen revealed microcracks along the α' needles, the crack typically propagated along these needles to create a large brittle fracture. The fracture mode is observed to have larger areas of cleavage facets, obtained along with the martensitic needles. The wrought and IC microstructures contained equiaxed grains. As grain sizes decrease the number of grains in the same area increased, which led to an increase in the number of grain boundaries. Grain boundaries act as obstacles for a fracture movement, an increase in grain boundaries causes entanglement and results in increased material strength [40][13]. The fractures of wrought and IC are observed to start with coalescence of microvoids, opening small pores between grain boundaries, or at any defect inside the specimen. The fracture propagates with increased applied stress. A 45° fracture deflection is evident towards the edge of the specimens at the maximum shear stress (shear lips), this fracture segment is transgranular. Transgranular fractures are usually caused by catastrophic failure. Catastrophic failure occurs when necking or fracture already started, and the remaining intact specimen's area is reduced, thus decreasing the applied stress required for failure. The failure is sudden, fast and complete, cutting directly through grains. The cross-sectional area reduction or necking describes the ductility of the specimens and agrees with the percentage elongation achieved. The wrought specimen showed the most necking and has the greatest elongation, as opposed to the AM specimen indicating almost no necking with less than 10% elongation. This compares well to the SEM micrographs of the cross-sectioned fractures which showed lamellar lines elongating and deflecting towards the fractured edges, while AM showed microvoids aligning with the martensitic needles. The wrought manufactured specimen's overall fractured surface resembles a partial inter-crystalline fracture, where some fractures occur between grains. The IC fracture showed cleavage facets, microvoids and ridges on cleavage facets, resulting in an overall quasi-cleavage fracture. The quasi-cleavage fracture is common in high strength materials [24].

The preliminary research on the wrought, IC and AM microstructures and tensile properties indicated that a hybrid manufactured specimen would fracture in the IC region. However, the HM tensile tested specimens showed divers fractures, with each surface preparation technique

resulting in different fractures for each specimen. Each surface preparation technique had one specimen fracturing in the AM region, one in the DZ region and one fracturing in the IC region. The specimens that fractured in the AM region, fractured between layer bands. The fractures indicate weak interlayer adhesion and secondary cracks were also observed parallel to the fracture. The fractures in the AM and DZ regions were due to process-induced defects, such as unmelted powder particle, residual stresses or cracking. The specimens fractured before a YS could be determined and fractured at a low UTS of 400 MPa. The fracture surfaces show brittle fractures, which are supported by the 0% elongation. The crack propagation and secondary cracks were observed to follow lamellae, the fracture surfaces also show patterns of lamellae. The fractures in the AM and DZ region showed cleavage fractures, apart from one specimen prepared with ablation, showing alternating fracture modes of granular fractures and cleavage fractures. A further investigation showed no significant change in composition over the alternating fracture modes. The specimens which fractured in the IC regions as predicted by the preliminary study indicated good diffusion between the IC and AM with sufficient AM interlayer adhesion. The equiaxed dimples observed in the fractured surfaces indicate that these specimens fractured by the initial formation of microvoids at grain boundaries, forming a coalescence until the cross-sectional area was reduced enough for the applied stress to cause failure. For comparisons based on the tensile properties, only the specimens that fractured in the IC regions were compared.

The HM specimens with just-cut surface preparations and tensile tested in the furnace at 400°C, 600°C, and 800°C all fractured in the IC region. The fact that the specimens all fractured in the IC region showed sufficient bonding between the IC and AM and interlayer bonding diffusion. The high temperature of the furnace could have aided in relieving some residual stresses caused by the AM process which could have been a cause of failure in the HM room temperature tensile testing. The high percentage elongation in specimens pulled at 400°C and 600°C was observed in the cross-sectional micrographs where the α/β lamellae morphology was deformed and the α-laths elongated towards the fracture surface. The α/β lamellae existed in colonies of various directions which led to often crack deflections producing uneven fracture surfaces. The specimens pulled at 800°C had microcracks along the necking of the specimen between the spheroidezed α-grains the extreme necking led to an area that was too small and fracture occurred.

CHAPTER 6. CONCLUSIONS

The conclusions made from the analysis of the microstructural characterization, tensile properties and fractography of the hybrid manufactured Ti6Al4V alloy are presented in this section.

6.1 Conclusion

Ti64Al4V components were machined from wrought rods and manufactured using investment casting, additive manufacturing and a combination of investment cast and additive manufacturing known as Hybrid manufacturing. The effect of surface preparation techniques and microstructural evolution during additive manufacturing and heat treatment of the Ti6Al4v hybrid manufactured components on the hardness and tensile properties at room elevated temperature were evaluated. The conclusions drawn are presented in this section.

The surface preparations on the investment cast rod's surface, prior to additive manufacturing showed no conclusive results on the sizes of the diffusion zones. The hardness of the investment cast and additive manufactured regions compared well with the hardness obtained for the individual manufacturing specimens of investment cast and additive manufacturing, respectively. Defects were found in the diffusion zone of as-cast surface (no surface preparation), sandblast and chemical milled prepared surface while the polished surface preparation technique was found to be impractical. The two best-suited surface preparation techniques for hybrid manufacturing proved to be ablation and just-cut surface.

The additive manufactured Ti6Al4V with long columnar grains, Widmanstätten α' martensitic laths and retained β-grain boundaries proved to have superior mechanical properties. The microstructure led to a greater hardness, yield strength, ultimate tensile strength and strain hardening exponent as compared to the wrought and investment cast α/β lamellae structures in equiaxed grains. However, additive manufactured Ti6Al4V tensile tested specimens gave the lowest percentage elongation.

The tensile tests of hybrid manufactured specimens prepared with ablation and just-cut surfaces, caused fractures in all three regions of the hybrid manufactured specimens, respectively. The tensile results concluded that the just-cut surface preparation technique gave superior ultimate tensile strength and strain hardening exponents.

The solution-treated hybrid manufactured specimens prepared with just-cut surface preparations and air cooled, water quenched or furnace cooled resulted in improved tensile properties. The solution-treated and water quenched specimen proved to be the cooling medium of choice for the hybrid manufacturing as it led to a fully martensitic phase in the investment cast region, a partial

martensitic phase in the diffusion zone, and an α' martensitic basketweave structure in the additive manufactured region. The hardness of the water quenched specimen indicated a more homogeneous structure across the different regions of the hybrid manufactured specimen while also producing a higher hardness compared to the non-heat treated specimen.

The additive manufactured specimen had micro-cracks along the α' needle like phase, with small quasi-cleavage facets. The Ti6Al4V wrought and IC fracture surfaces revealed transgranular quasi-cleavage surface areas.

The hybrid manufactured specimens prepared with a just-cut surface preparation gave no significant change in hardness for different high temperature tensile testing. The yield strength, ultimate tensile strength and strain hardening exponent showed a decrease with an increase in the high temperature tensile testing. The ductility was found to increase with temperature. The α/β lamellae morphology in specimens pulled at 400°C and 600°C was deformed and the α-laths elongated towards the fractured surface while the various directions of the colonies slowed the crack propagation leading to rougher surface fractures. The specimens pulled at 800°C had micro-cracks along the spheroidized α-grains with the highest ductility. Ductile fractures were observed for all high-temperature tensile testing. The ultimate tensile strength drops with factors of 1.6, 2.4 and 9.4 for tensile tests at 400°C, 600°C, and 800°C, respectively compared to the room temperature hybrid manufactured tensile test.

CHAPTER 7. FUTURE RESEARCH

To further investigate the effect of the surface preparations on hybrid manufacturing it is recommended to additive manufacture a single track of Ti6Al4V onto each of the investment cast rods prepared with the six different surface preparations. The diameter and contact angle of the single track on the investment cast rod should be measured and evaluated. Figure 63 illustrates a single track of additive manufactured material on an investment cast rod.

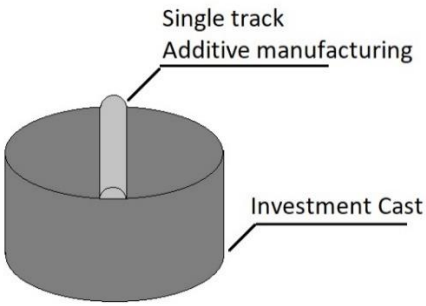

Figure 63. Single track of additive manufacturing onto an investment casted rod

The solution-treated and water quenched specimens showed an improvement in the homogeneity of the hybrid manufactured specimen and an increase in the hardness. To evaluate the full effect of the cooling rates, tensile tests should be performed.

BIBLIOGRAPHY

[1] K. A. Lorenz, J. B. Jones, D. I. Wimpenny, and M. R. Jackson, “A review of hybrid manufacturing,” in *Solid Freeform Fabrication Symposium (SFF), Austin, TX, Aug*, 2015, pp. 10–12.

[2] S. Liu and Y. C. Shin, “Additive manufacturing of Ti6Al4V alloy: A review,” *Mater. Des.*, vol. 164, p. 107552, Feb. 2019.

[3] P. A. Kobryn, A. W. Gunderson, and W. M. Griffith, *Casting Titanium Alloys: With Special Reference to Aerospace Applications*. Wexford Press, 2008.

[4] M. J. Donachie, *Titanium: A Technical Guide, 2nd Edition*. ASM International, 2000.

[5] A. Bagheri, N. Shamsaei, and S. Thompson, *Microstructure and Mechanical Properties of Ti-6Al-4V Parts Fabricated by Laser Engineered Net Shaping*. 2015.

[6] L. E. Murr *et al.*, “Metal Fabrication by Additive Manufacturing Using Laser and Electron Beam Melting Technologies,” *J. Mater. Sci. Technol.*, vol. 28, no. 1, pp. 1–14, Jan. 2012.

[7] Y. Zhu, J. Li, X. Tian, H. Wang, and D. Liu, “Microstructure and mechanical properties of hybrid fabricated Ti-6.5Al-3.5Mo-1.5Zr-0.3Si titanium alloy by laser additive manufacturing,” *Mater. Sci. Eng. A*, vol. 607, pp. 427–434, 2014.

[8] S. El-Hadad, M. Nady, W. Khalifa, and A. Shash, “Influence of heat treatment conditions on the mechanical properties of Ti–6Al–4V alloy,” *Can. Metall. Q.*, vol. 57, no. 2, pp. 186–193, Apr. 2018.

[9] M. J. Donachie and D. Mj, *Titanium : A Technical Guide*. Materials Park: A S M International, 2000.

[10] R. Reda, A.-H. Hussein, A. NOFAL, and E.-S. M. EL-BANNA, *OPTIMIZING THE MECHANICAL PROPERTIES OF TI-6AL-4V CASTINGS*, vol. 5. 2015.

[11] M. Qian, W. Xu, M. Brandt, and H. P. Tang, *Additive manufacturing and postprocessing of Ti-6Al-4V for superior mechanical properties*, vol. 41. 2016.

[12] Y. C. Lin, Y. Tang, X.-Y. Zhang, C. Chen, H. Yang, and K.-C. Zhou, “Effects of solution temperature and cooling rate on microstructure and micro-hardness of a hot compressed Ti-6Al-4V alloy,” *Vacuum*, vol. 159, pp. 191–199, Jan. 2019.

[13] C. Leyens and M. Peters, “Titanium and Titanium Alloys,” 2003.

[14] A. P. Singh, F. Yang, R. Torrens, and B. Gabbitas, “Solution treatment of Ti-6Al-4V alloy produced by consolidating blended powder mixture using a powder compact extrusion route,” *Mater. Sci. Eng. A*, vol. 712, pp. 157–165, Jan. 2018.

[15] A. P. Singh, F. Yang, R. Torrens, and B. Gabbitas, “Solution treatment of Ti-6Al-4V alloy produced by consolidating blended powder mixture using a powder compact extrusion route,” *Mater. Sci. Eng. A*, vol. 712, pp. 157–165, Jan. 2018.

[16] M. A. Imam and C. M. Gilmore, “Fatigue and microstructural properties of quenched Ti-6Al-4V,” *Metall. Trans. A*, vol. 14, no. 1, pp. 233–240, 1983.

[17] F. Yang and B. Gabbitas, “Effect of heat treatment on microstructures and mechanical properties of a Ti-6Al-4V alloy rod prepared by powder compact extrusion,” *Int. J. Mod. Phys. B*, vol. 29, no. 10n11, p. 1540004, 2015.

[18] S. Zhang, X. Lin, J. Chen, and W. Huang, “Effect of solution temperature and cooling rate on microstructure and mechanical properties of laser solid forming Ti-6Al-4V alloy,” *Chin. Opt. Lett.*, vol. 7, no. 6, pp. 498–501, Jun. 2009.

[19] A. Shaikh, S. Kumar, A. Dawari, S. Kirwai, A. Patil, and R. Singh, “Effect of Temperature and Cooling Rates on the α+β Morphology of Ti-6Al-4V Alloy,” *Procedia Struct. Integr.*, vol. 14, pp. 782–789, Jan. 2019.

[20] S.-C. Jeng and H. Chiou, “Effects of Cooling Rate on the Microstructure and Mechanical Properties of Ti-6Al-4V Alloy,” *Appl. Mech. Mater.*, vol. 284–287, pp. 103–107, Jan. 2013.

[21] W. Sha and S. Malinov, *Titanium Alloys: Modelling of Microstructure, Properties and Applications*. Elsevier Science, 2009.

[22] B. Hanson, *The Selection and Use of Titanium: A Design Guide*. Institute of Materials, 1995.

[23] M. Bermingham, S. D. McDonald, M. S. Dargusch, and D. H. StJohn, *MIcrostucture of cast titanium alloys*, vol. 31. 2007.

[24] V. A. Joshi, *Titanium alloys : an atlas of structures and fracture features*. Boca Raton: CRC Taylor & Francis, 2006.

[25] G. Lütjering and J. C. Williams, *Titanium*. Berlin, Heidelberg: Springer Berlin Heidelberg,

2007.

[26] P. A. Kobryn, “Casting of Titanium Alloys,” 1996.

[27] H.-P. Nicolai and C. Liesner, “Investment Casting of Titanium,” *Titanium and Titanium Alloys*. 28-Jan-2005.

[28] S. Kalpakjian, S. R. Schmid, and V. Sekar, *Manufacturing Engineering and Technology*. 2013.

[29] M. H. Bocanegra-Bernal, “Hot isostatic pressing (HIP) technology and its applications to metals and ceramics,” *Journal of Materials Science*, vol. 39, no. 21. pp. 6399–6420, 01-Nov-2004.

[30] J. Oh, N. J. Kim, S. Lee, and E. W. Lee, “Correlation of fatigue properties and microstructure in investment cast Ti-6Al-4V welds,” *Materials Science and Engineering: A*, vol. 340, no. 1. pp. 232–242, 2003.

[31] N. Arthur, M. Khodja, H. Moller, and & P. Rossouw, “PERFORMANCE EVALUATION AND CHARACTERISATION OF EIGA PRODUCED TITANIUM ALLOY POWDER FOR ADDITIVE MANUFACTURING PROCESSES.”

[32] B. Dutta and F. H. (Sam) Froes, “The Additive Manufacturing (AM) of titanium alloys,” *Metal Powder Report*, vol. 72, no. 2. pp. 96–106, 2017.

[33] H. Galarraga, Y. Zhai, and D. Lados, *Microstructure Evolution, Tensile Properties, and Fatigue Damage Mechanisms in Ti-6Al-4V Alloys Fabricated by Two Additive Manufacturing Techniques*, vol. 114. 2015.

[34] Z. Zhu, V. G. Dhokia, A. Nassehi, and S. T. Newman, “A Review of Hybrid manufacturing processes – state of the art and future perspectives,” *Int. J. Comput. Integr. Manuf.*, vol. 26, no. 7, p. 596.

[35] J. Ni, V. D. Majstorovic, and D. Djurdjanovic, *Proceedings of 3rd International Conference on the Industry 4.0 Model for Advanced Manufacturing: AMP 2018*. Springer International Publishing, 2018.

[36] “Elbow prosthesis: MedlinePlus Medical Encyclopedia Image,” vol. 2018, no. Jun 27,. 2018.

[37] S. Katayama, *Handbook of Laser Welding Technologies*, no. 41. Philadelphia, PA:

Woodhead Publishing, 2013.

[38] J. Sánchez-Amaya, M. R. Amaya Vázquez, L. Rovira, M. Botana Galvin, and J. Botana, *Influence of Surface Pre-treatments on Laser Welding of Ti6Al4V Alloy*, vol. 23. 2014.

[39] I. WATANABE, N. BABA, J. CHANG, and Y. CHIU, “Nd:YAG laser penetration into cast titanium and gold alloy with different surface preparations,” *J. Oral Rehabil.*, vol. 33, no. 6, pp. 443–446, Jun. 2006.

[40] J. Dong, F. Li, and C. Wang, “Micromechanical behavior study of α phase with different morphologies of Ti–6Al–4V alloy by microindentation,” *Mater. Sci. Eng. A*, vol. 580, pp. 105–113, Sep. 2013.

[41] M. Shunmugavel, A. Polishetty, and G. Littlefair, “Microstructure and mechanical properties of wrought and Additive manufactured Ti-6Al-4V cylindrical bars,” *Procedia Technol.*, vol. 20, pp. 231–236, 2015.

[42] K. Beyl, K. Mutombo, and C. P. Kloppers, “Tensile properties and microstructural characterization of additive manufactured, investment cast and wrought Ti6Al4V alloy,” *IOP Conf. Ser. Mater. Sci. Eng.*, vol. 655, p. 12023, 2019.

[43] W. D. Callister and D. G. Rethwisch, *Fundamentals of Materials Science and Engineering: An Integrated Approach, 5th Edition*. Wiley, 2016.

[44] G. E. Dieter, *Mechanical Metallurgy*. Createspace Independent Pub, 2014.

[45] M. G. Moletsane, P. Krakhmalev, N. Kazantseva, A. du Plessis, I. Yadroitsava, and I. Yadroitsev, “Tensile properties and microstructure of direct metal laser-sintered Ti6Al4V (ELI) alloy,” *South African J. Ind. Eng.*, vol. 27, no. 3SpecialIssue, pp. 110–121, 2016.

[46] S. Aleksandra *et al.*, *Identification of Mechanical Properties for Titanium Alloy Ti-6Al-4V Produced Using LENS Technology*, vol. 12. 2019.

[47] B. E. Carroll, T. A. Palmer, and A. M. Beese, “Anisotropic tensile behavior of Ti–6Al–4V components fabricated with directed energy deposition additive manufacturing,” *Acta Mater.*, vol. 87, pp. 309–320, Apr. 2015.

[48] S. Abiola Raji, A. Patricia Idowu Popoola, S. Leslie Pityana, O. Muhmmed Popoola, and F. Olufemi Aramide, “Laser Based Additive Manufacturing Technology for Fabrication of Titanium Aluminide-Based Composites in Aerospace Component Applications,” in *Environmental Impact of Aviation and Sustainable Solutions [Working Title]*, IntechOpen,

2019.

[49] D. Roylance, “STRESS-STRAIN CURVES,” 2001.

[50] J. Garcia and T. Morgeneyer, “Strength and fatigue strength of a similar Ti-6Al-2Sn-4Zr-2Mo-0.1Si linear friction welded joint,” *Fatigue Fract. Eng. Mater. Struct.*, Mar. 2019.

[51] J. Chrapoński and W. Szkliniarz, “Quantitative metallography of two-phase titanium alloys,” *Mater. Charact.*, vol. 46, pp. 149–154, Feb. 2001.

[52] G. Kühn, “W. Kurz, D. J. Fisher, Fundamentals of Solidification. Trans Tech Publications, Switzerland-Germany-UK-USA, 1986 (Erstauflage 1984), 242 Seiten, zahlreiche Abbildungen und Tabellen, Sachwortindex, SFr 54.00, ISBN 0-87849-523-3,” *Cryst. Res. Technol.*, vol. 21, no. 9, p. 1176, Sep. 1986.

[53] P. A. Kobryn and S. L. Semiatin, “The laser additive manufacture of Ti-6Al-4V,” *JOM*, vol. 53, no. 9, pp. 40–42, Sep. 2001.

[54] N. K. K. Arthur and S. Pityana, “Microstructure and material properties of LENS fabricated Ti-6Al-4V components ,” *R&D Journal* , vol. 34. scieloza , pp. 33–36, 2018.

[55] J. S. Zuback and T. DebRoy, “The Hardness of Additively Manufactured Alloys,” *Mater. (Basel, Switzerland)*, vol. 11, no. 11, p. 2070, Oct. 2018.

[56] T. Ahmed and H. J. Rack, “Phase transformations during cooling in α+β titanium alloys,” *Mater. Sci. Eng. A*, vol. 243, no. 1–2, pp. 206–211, Mar. 1998.

[57] J. Lin, S. Nambu, K. Pongmorakot, and T. Koseki, “Effect of surface roughness on bonding interface formation of steel and Ni by ultrasonic welding,” *Sci. Technol. Weld. Join.*, pp. 1–7, Aug. 2019.

[58] N. J. Den Uijl and L. J. Carless, “Advanced metal-forming technologies for automotive applications,” *Adv. Mater. Automot. Eng.*, pp. 28–56, Jan. 2012.

[59] J. Kim, K. H. Kim, and D. Kwon, “Evaluation of high-temperature tensile properties of Ti-6Al-4V using instrumented indentation testing,” *Met. Mater. Int.*, vol. 22, no. 2, pp. 209–215, Mar. 2016.